Information processing under physiological pulsatile stimulation in a G-protein coupled signaling pathway

by

Madhuresh Sumit

A dissertation submitted in partial fulfillment
of the requirements for the degree of
Doctor of Philosophy
(Biophysics)
at The University of Michigan
2016

Doctoral Committee:

Professor Jennifer J. Linderman, Co-Chair
Professor Shuichi Takayama, Co-Chair
Associate Professor Sunitha Nagrath
Professor Richard R. Neubig, Michigan State University
Assistant Professor Sarah Veatch
Assistant Professor Kevin Wood

DEDICATION

To all the *gurus,* the dispeller of darkness/ignorance, through whom we gain the quanta of light in this vastly illuminated universe.

ACKNOWLEDLEGEMENTS

I would like to express my deep appreciation and gratitude to my advisors, Professor Jennifer Linderman and Professor Shuichi Takayama. They have always conveyed a spirit of adventure and excitement for scientific research and scholarship that has immensely enthused me throughout my doctoral research. Both of them have been true *gurus* who would magically dispel the darkness surrounding my mind, and I would always feel assured and motivated after having a discussion with them. While the discussions with Professor Takayama encouraged me to think about big picture and broader applicability, the discussions with Professor Linderman encouraged me to dive deep to gain insights. Their continuous trust and support has gradually led me discover my own potentials as a researcher, and I am deeply grateful for their guidance.

I would also like to express my gratitude to Professor Richard Neubig for his guidance and insightful discussions. I would like to thank him for allowing me use the resources and facilities in his lab, and allowing me to participate in his lab group meetings that helped me in troubleshooting during my experiments. I would also like to thank Professor Sarah Veatch who has always been a very friendly mentor and teacher. Her courses during the initial years developed my excitement for biophysics, and her valuable inputs and suggestions during individual and committee meetings has been quite helpful. I would like to thank Professor Sunitha Nagrath who has been an excellent teacher, mentor and friend, and has also guided me for career and life in general. I would also like to thank Professor Kevin Wood for his valuable inputs and suggestions during individual and committee meetings.

As I write this, memories of past five years are replaying in my mind. I must thank members of the Takayama Lab and the Linderman Lab for these fond memories. They made all these years so colorful and worth treasuring for lifetime. With much gratitude, I thank previous members of the Takayama Lab; Dr. John Frampton, Dr. Sung Jin Kim, Dr. Chris Moraes, Dr. Toshiki Matsuoka, Dr. Joshua White, Dr. Steve Cavnar, Dr. Joseph Labuz and Dr. Taisuke Kojima for their support, friendship and conversations. Thanks to visiting researchers in the lab; Professor

Ryuji Yokokawa, Dr. Minsub Han, Chung Min Han, Chao Zhang and Dr. Cedric Bethany for interesting discussions on science, languages, culture and food. Special thanks to Dr. Brendan Leung, Dr. Arlyne Simon, Dr. David Lai, Dr. Byoung Choul Kim and Dr. Sasha Cai Lesher-Perez for being there whenever I needed them as a mentor and a friend. I would also like to thank current members of the lab; Dr. Nick Ginga, Dr. Ryan Oliver, Cameron Yamanishi, Joyce Chiu, Ge-Ah Kim, Priyan Weerappuli, Stephen Robinson, David Mertz and Kimberly Jen for their friendship and support. With much gratitude, I also thank previous members of the Linderman Lab; Dr. Nicholas Cilfone, Dr. Laura Chang, Dr. Cordelia Ziraldo and Danielle Trakimas for their fruitful inputs, discussions and friendship. I would also like to thank current members of the lab; Phillip Spinosa, Amy Oberlin, Joseph Cicchese and Bruna Menezes for their friendship and support. Special thanks to Dr. Elsje Pienaar for valuable suggestions and discussions. Being part of both the groups has given me so many sweet memories that I would cherish them my whole life. I would also like to thank previous and current members of the Neubig lab; Dr. Benita Sjogren, Dr. Andrew Storaska, Jeffrey Liepprandt, Erika Mathes Lisabeth, Behirda Karaj and Vincent Shaw for their valuable suggestions and helping with experimental resources.

Although not directly related to my thesis work, I would like to express my gratitude to Professor Mark Banaszak-Holl, Professor Bradford Orr, Professor Seok-Ki Choi and Professor Robert Kennedy for their mentorship and guidance during my PIBS rotations.

Finally, I would like to thank friends and family for their encouragement, love and support. I thank my parents for imparting the values of dedication and hard work in me, and always encouraging me during my doctoral training and research. I thank my wife for the incessant support and motivation during the last year of my thesis research. Thanks to my friends Prashanth KJ, Krishna Suddala, Carter Swanson, David Rowland, Sam Kotler, Julia Bourg, Abhishek Sunny, Srishti Gupta, Abhishek Singh and Swarn Lata Singh for their friendship and support.

TABLE OF CONTENTS

LIST OF FIGURES

Appendix Figures

LIST OF TABLES

LIST OF APPENDICES

ABSTRACT

Information processing under physiological pulsatile stimulation in a G-protein coupled signaling pathway

by

Madhuresh Sumit

Chairs: Jennifer J. Linderman and Shuichi Takayama

The cellular microenvironment is often dynamic, and several physiological ligands are released in pulsatile bursts. The main hypothesis driving this study is that cells are able to discern these time-varying dynamic inputs and must have evolved to exploit the temporal information available in their microenvironment to their advantage. Taking Muscarinic M3 (a G-protein coupled receptor)-mediated signaling as an example, this thesis explores how information is processed under pulsatile stimulation. Several experimental and computational approaches techniques including microfluidics, real-time multi-color fluorescence imaging of single cells, reaction kinetics modeling and information and noise analysis are implemented to gain mechanistic insights into the signaling circuit architecture.

A major finding of this thesis is that receptor-mediated signaling forms a low pass filter while downstream calcium-induced NFAT (Nuclear Factor of Activated T-Lymphocytes, a transcription factor) nuclear translocation forms a high pass filter. The combination acts as a band-pass filter optimized for intermediate frequencies of stimulation. Sensitivity analysis shows that receptor and downstream kinetics determine critical features of the band-pass and that the band-pass may be shifted for different receptors or NFAT dynamics. Another important finding in this thesis is that for weak physiological inputs, cells exhibit apparent stochastic responses that can be explained within a deterministic framework. Computational analysis suggests that cells may utilize

apparent stochasticity to enhance selectivity in downstream responses. This thesis also demonstrates that pulsatile inputs enhance information transfer downstream in noisy biochemical pathways. Finally, a microfluidic experimental method is developed to measure two microfluidic observables in the same cell, similar to a 'two-reporter' system, to estimate biochemical noise. Analysis with this method suggests that effect of drug action increases with increasing biochemical noise.

Although this thesis focuses on one particular receptor and ligand, the conclusions from this work may be applied to several signaling systems. Investigation of band-pass processing may lead to gaining mechanistic insights into hidden or unknown regulatory motifs in several signaling pathways that are poorly understood. Using pulsatility to modulate selectivity and sensitivity of signaling response amidst biochemical noise provides tools to synthetic biologists and pharmacologists for developing enhanced lab-on-chip devices and pharmaceutical interventions.

Chapter 1. Introduction

1.1. Motivation

Communication or transfer of interpretable information is essential for sustenance of every form of life. Cellular signal transduction is the chemical form of communication that is utilized by cells to access information from their extracellular microenvironment. This allows cells to adjust or respond according to a variety of external cues and to bring about physiological or phenotypic changes. Signal transduction is carried out through signaling networks. The structures of these signaling networks can be difficult to dissect for mammalian pathways due to spatial and temporal encoding (Purvis & Lahav, 2013). Often, the cellular microenvironment presents dynamic or time-varying inputs that need to be decoded downstream by cells to respond appropriately.

The main hypothesis driving this study is that cells must be able to discern time-varying inputs and must have evolved evolutionarily to exploit temporal information available in their microenvironment to their advantage. Several input signals are released in pulsatile bursts under physiological conditions, including acetylcholine (Dunant *et al*, 1974) (seconds to minute scale), glutamate (De Pittà *et al*, 2009) (millisecond to a few second scale) and GnRH (Chappell *et al*, 2003) (Gonadotropin releasing hormone) (a few hours). How such rhythmic processes and their appropriate timing influence downstream signaling outcomes is fundamentally important to biology. Conventional methods of investigating these pathways often fail to provide quantitative and mechanistic insights into dynamic nature of information processing in such signaling pathways. Despite several interrogations with novel tools such as microfluidics, have elucidated circuit architectures of such signaling pathways (Jovic *et al*, 2010, 2011, 2013; Ashall *et al*, 2009; Dhumpa *et al*, 2015), little is known about how nature utilizes physiological pulsatile bursts to its advantage for processes such as transcriptional activity and temporal selectivity. Taking muscarinic M3 receptor (a G-protein coupled receptor or GPCR)-mediated calcium signaling as an example, this thesis aims to explain how information is processed in such noisy signaling networks under physiological pulsatile stimulations.

In this chapter, we discuss how dynamic microenvironment may be able to expand the observability of a signaling system. We also discuss the sources of noise that such biochemical pathways often suffer from. We describe how microfluidic approach proves to be a great tool for not only expanding the observability, but also reducing the noise via synchronized cell responses. Taking examples from literature, we discuss how this approach has been implemented in gaining mechanistic insights into several signaling pathways. We then discuss our signaling system, and outline the goals of this thesis.

1.2. Dynamic microenvironment and observability space

The microenvironment surrounding cells in tissues of a multi-cellular organism may change rapidly due to various metabolic and signalling processes. Cells must be able to discern these dynamics to make appropriate decisions. In general, these dynamic patterns include changes in amplitude, duration of stimulation, gradients, or periodicity of the input signal (Fig. 1.1. A). However, to interpret these dynamic inputs, cells also require complex signaling pathways that may enable cells to process these inputs differently.

Understanding such complex signaling pathways primarily depends on robust discernment of signaling circuit architectures. This requires comparing and evaluating multiple response features. Ideally, one could observe every signaling node in the network, but this has practical limitations. However, we can exploit a cell's ability to discern these dynamics in our experiments, and use the information gathered to help understand the circuit architecture that may have a variety of network motifs (Uri Alon, 2007) (Fig. 1.1. B). To achieve this, we think about the "observability space" - the non-redundant and informative read-outs in the space-time domain. Often, cell signaling studies are limited to a single dimension in the observability space, i.e., variation in the input concentration and the corresponding downstream read-out. To expand the observability space, we need additional inputs that can provide distinct output (downstream) responses. Temporally varying stimulation provides this necessary expansion of observability space through additional input parameters such as duration of stimulation, rest period between the stimulations, input duty cycle etc. (Fig. 1.1. C). This space can be further expanded by introducing other time-dependent inputs such as positive and negative gradients, sinusoidal and saw-tooth waveforms. Thus, the same read-out can be measured distinctively for several input conditions. Increasing the number of read-outs further expands the space with the number of combinatorial investigations possible.

These many dynamic read-outs provide a wider window to compare and evaluate the response features and figure out the most appropriate circuit architecture, which is quite difficult to understand using conventional methods with limited observables under static inputs. Thus, multiple observables for the same read-out play an essential role in weeding out the non-conforming circuit architectures, as well as in gaining mechanistic insights into how temporal information is processed in a particular signaling circuit. This thesis is focused on pulsatile input because of its physiological relevance to the signaling pathways where input ligand is often released in intermittent pulsatile bursts.

1.3. Signal transduction and noise

Signal processing in temporally encoded networks often suffers from noisy transmission of information because of intrinsic and extrinsic factors (Cheong *et al*, 2011; Selimkhanov *et al*, 2014). These factors are broadly classified into two types of noise often present in a biochemical signaling network. First is stochastic noise, also termed intrinsic noise, attributed to stochasticity in molecular interactions, reactions involving low copy number species, and also to the measurement errors such as limited resolution of the measuring instruments. The second type of noise is biochemical noise, also termed extrinsic noise or cell-to-cell variability. Biochemical noise is attributed to the variability in the molecular abundance of signaling components and is therefore 'extrinsic' to the cell under study. Quantitative and mechanistic understanding of how cells process these noisy signals to facilitate reliable transmission of information is essential for developing target specific drug interventions, as well as for synthetic biology applications.

1.4. Microfluidic approach to investigation of cellular signaling architectures

Signaling circuit investigations at the single cell level with pulsed stimulation requires delivery of time-dependent ligand or drug molecule input. It is not possible to use macro-scale tools to precisely mimic and manipulate the cellular microenvironment. Large fluid volumes in macro-scale systems prevent rapid changes in concentrations, thus making these systems inaccurate and low throughput. To this end, several microsystems, in particular microfluidic devices, have recently been designed and developed that can handle microliter and sub-microliter volumes of fluids, and can mimic perturbations and measurements in both timescales as well as length scales (Duncombe *et al*, 2015). Depending upon the channel dimension along with the flow velocity,

microfluidic devices provide additional advantage of facilitating precise fluid control through laminar flow, wherein flow streams move as well-defined 'lamina' (or layers) without mixing (Takayama *et al*, 2003), thus allowing generation of precise temporal patterns of fluids.

Microfluidic devices for generating temporal input patterns

From the fabrication point-of-view, microfluidic devices can be broadly classified into solid-state devices and PDMS devices. Solid-state fabrication techniques include photolithography, glass etching and glass bonding, and the primary substrates include glass or silicon. While these techniques have been successful in several biophysical applications, such as capillary electrophoresis, cell trapping and cell separation, there are practical limitations with these devices in generating temporal microfluidic patterns. In contrast, poly-dimethylsiloxane (PDMS) based devices utilize the technique of soft lithography, wherein micron-sized patterns can be molded from a hard master template (Whitesides *et al*, 2001). PDMS is non-toxic, biocompatible and almost transparent in the wavelength regime typically used for fluorescence-based studies. Its elastic properties allow design of devices with micromechanical membrane valves to allow relatively easy control of fluid flow through the channels.

There are multiple approaches for generating temporal input patterns with PDMS based devices, including direct syringe pumping , pulse code modulation (PCM) (Zhang *et al*, 2010), fluidic membrane valves (Melin & Quake, 2007), Braille-pins based platform (Futai *et al*, 2006; Gu *et al*, 2004), elastomeric oscillators (Mosadegh *et al*, 2010) and others. While all these methods have advantages and disadvantages, the adoption of a method depends upon the requirements of the study. Since this thesis focuses on GPCR-mediated calcium signaling which occurs at a time scale of a few seconds to several minutes, it would require a microfluidic device that can deliver input ligands with temporal patterns in that time scale. To this end, Braille-pin based microfluidic devices provide a suitable platform to perform such experiments. A computer-controlled Braille pin-based platform was developed by Gu et al (Gu *et al*, 2004) that uses peristaltic pumping in alternate fashion to generate fluid flow. Futai et al (Futai *et al*, 2006) utilized this platform to develop a microfluidic device that allowed portable cell culture and long term monitoring of cells under microscope. Jovic et al (Jovic *et al*, 2010) modified the device design to have channels from two input reservoirs merging into a single outlet channel. Both the input channels could be controlled by the Braille platform to deliver alternate sequence of fluid from each of the channels

into the outlet channel (Fig. 1.2.). When one of the inlet reservoirs is filled with buffer and the other with ligand (dissolved in the buffer), the device can deliver pulsed stimulations with various durations (D) and rest periods (R) at a temporal resolution of a few seconds. This device has been used to investigate phase locked response in GPCR-mediated signaling pathway to elucidate circuit architecture and pathway recovery properties (Jovic *et al*, 2010, 2011, 2013). All the experimental data in this thesis are obtained with devices fabricated with the same design as Jovic et al (Jovic *et al*, 2010).

Advantages of microfluidic pulsatile stimulation

Conventionally, signaling responses are measured for step changes in the concentration of a stimulus. Yet, many physiologically relevant stimuli, including neurotransmitters, metabolic enzymes, hormones, and growth factors, are released in pulsatile bursts (Fig. 1.3. A) (De Pittà *et al*, 2009; Dyachok *et al*, 2006; Dunant *et al*, 1974; Bergendahl *et al*, 1998; Chappell *et al*, 2003). Time scales vary widely from milliseconds to several hours. Consequently, downstream activation of effector molecules may vary significantly for time varying inputs as compared to step changes (Sorre *et al*, 2014; Ryu *et al*, 2015). Complex time varying patterns such as pulsatile bursts can be delivered with high temporal resolution using microfluidic devices, thus mimicking the dynamic physiological microenvironment in a controlled fashion.

Pulsatile microfluidics also provide a tool for externally phase locking or synchronizing a cell population to study emergent population behavior *in vitro* (Fig. 1.3. B). Several physiological phenomena, such as hormonal secretion and heart contractions, are rhythmic or oscillatory at the tissue/organ scale. Such rhythmic activities indicate synchronization of millions of cells (Dhumpa *et al*, 2015, 2014). Microfluidics allows mimicking these tissue scale conditions *in vitro*. These features have also been explored to develop organ-on-chip and human-on-chip systems (Bhatia & Ingber, 2014).

As discussed in Section 1.3, *in vitro* cultures are prone to cell-to-cell variability (Snijder & Pelkmans, 2011; Ladbury & Arold, 2012; Hughey *et al*, 2014). Under step stimulation, these cells tend to vary widely in their signaling responses (Selimkhanov *et al*, 2014; Cheong *et al*, 2011; Zambrano *et al*, 2016). While some cells exhibit oscillatory responses, others may exhibit peak-and-plateau, single spike or no response (Fig. 1.3. C). Thus, biochemical noise leads to a wide range of responses, and makes it difficult to interpret how these responses affect the downstream

signal. Under external periodic stimulation, signaling systems may exhibit synchronized or phase locked responses (Jovic *et al*, 2010) that are easier to interpret, and also allow us to investigate how downstream responses depend on temporal modulation of the stimulation.

Several studies have shown that transcription factor activation and gene transcription vary significantly between continuous and pulsatile stimulation (Ryu *et al*, 2015; Tomida *et al*, 2012; Sorre *et al*, 2014). Rate constants for activation and deactivation of transcription factors, or nuclear translocation and back-translocation, may determine whether a continuous or a pulsatile stimulation leads to higher activity. Consequently, for two distinct transcription factors (say Z1 and Z2), the amount of activation may differ for different temporal inputs. This may lead to several combinations of gene activation, consequently determining the fate of the physiological or phenotypic response (Fig. 1.3. D).

1.5. Mathematical and computational modeling approaches to investigation of cellular signaling architectures

Mathematical and computational modeling have been used extensively to describe and predict dynamical systems in biology, including predator-prey dynamics (Alfred J. Lotka, 1925; Volterra, 1926), microbial growth (Monod, 1949), embryonic morphogenesis (Turing, 1952), cell cycle dynamics (Sible & Tyson, 2007) as well as several cell signaling pathways (Aldridge *et al*, 2006). Investigation of biochemical pathways is aided by quantitative predictions from mathematical and computational models that can be tested experimentally, with insights feeding back to improve the models. These models can be deterministic such as ordinary differential equations (ODEs), partial differential equations (PDEs), delayed differential equations (DDEs), or stochastic such as dynamic Monte Carlo method, Gillespie method, and Markov processes. Sometimes, a combination of deterministic and stochastic modeling is also used to explain certain phenomena observed experimentally (Tay *et al*, 2010). Other more abstract methods in modeling include fuzzy logic, Bayesian networks etc. Appropriate selection of modeling approach depends on the details available for that particular dynamical system. For modeling signaling pathways, details such as mechanisms, availability of experimentally determined kinetic parameters and capability of getting time-dependent read-outs are important (Aldridge *et al*, 2006). ODEs are frequently used to describe signaling pathways when such details are available. These ODEs can be solved to obtain time traces of individual signaling components. Modeling a dynamical system wherein spatial

dynamics is involved, PDEs with space and time derivatives are frequently used. Sometimes, signaling system under study involves compartmentalization of the signaling components. The component that translocates from one compartment to other exhibits a lag time before signaling in the other compartment. For such processes, DDEs are frequently used to describe the dynamics. Although deterministic models have an advantage in terms of the ease with which characteristic behaviors can be described and predicted (Scott *et al*, 2007), Stochastic models are often invoked to provide insights where deterministic models fail (Das *et al*, 2009; Ullah & Wolkenhauer, 2010; Tay *et al*, 2010; Turner *et al*, 2010). Signaling events that involve discrete and random waiting times (such as binding of a transcription factor to a gene sequence or low copy numbers of signaling molecules interacting with each other) are best described by stochastic processes.

In case of GPCR-mediated signaling, integrating modeling approaches with experiments has significantly enhanced our understanding of the GPCR-mediate signaling events leading to several cellular responses (Omann *et al*, 1987; Adams *et al*, 1998; Bhalla & Iyengar, 1999; Linderman & Lauffenburger, 1988; Mahama & Linderman, 1994c; Linderman, 2009). Several steps in the signaling pathway have been well characterized in terms of mechanistic insights as well as availability of kinetic parameters. For this reason, ODEs are frequently used to model GPCR-mediated pathways. Additionally, not all of the kinetic parameter values have been measured for these pathways. Other measured values may vary over several orders of magnitude. Techniques to efficiently sample the parameter space and to determine the correlation of the signaling response with each of the parameter varied are helpful (Blower & Dowlatabadi, 1994; Saltelli *et al*, 2002). Uncertainty and sensitivity analyses are an important aspect of mathematical and computational modeling (Marino *et al*, 2008; Zak *et al*, 2005; Saltelli *et al*, 2005).

With the advent of time-lapse microscopy with high spatio-temporal resolution, it has been possible to measure time traces of signaling components at single cell scale. However, as discussed earlier, *in vitro* cultures are prone to cell-to-cell variability (Snijder & Pelkmans, 2011; Ladbury & Arold, 2012; Hughey *et al*, 2014). Thus, the single cell traces obtained experimentally are often noisy and it is difficult to interpret the signaling dynamics. A deterministic model alone may not be able to provide the needed insights. For this reason, mathematical and computational models at single cell scale may also incorporate extrinsic noise and the signaling components are initialized in the model by choosing values from a distribution (Mahama & Linderman, 1994b). To interpret

single cell data, information theoretic analysis has recently been utilized to estimate the noise and information components in the signal (Cheong *et al*, 2011; Selimkhanov *et al*, 2014). This thesis aims to utilize these mathematical and computational approaches along with microfluidic interrogation of the signaling to obtain quantitative insights that can be validated experimentally.

1.6. Investigation of oscillatory signaling networks with microfluidics and computational modeling

Investigation of cellular signaling pathways with dynamic inputs using microfluidics is a research area that has grown significantly in the recent years. Several mammalian (Jovic *et al*, 2010, 2011, 2013; Sorre *et al*, 2014; Dhumpa *et al*, 2014; Tay *et al*, 2010; Kellogg & Tay, 2015; Zambrano *et al*, 2016; Ashall *et al*, 2009; Ryu *et al*, 2015; Dhumpa *et al*, 2015) as well as non-mammalian systems including bacteria (Prindle et al, 2014; Tsimring et al, 2010; Mondragón-Palomino et al, 2011), amoeba (Sgro et al, 2015), yeast (Hao *et al*, 2013; Mitchell *et al*, 2015), and nematodes (Tomida et al, 2012; Kato et al, 2014) have been investigated.

In mammalian systems, NFκB (nuclear factor κB) signaling is by far the pathway most studied using microfluidics and mathematical modeling. The intrinsic oscillatory dynamics of the pathway are on the time scale of minutes to hours and can be conveniently investigated for frequency modulated signaling (Tay *et al*, 2010; Zambrano *et al*, 2016; Kellogg & Tay, 2015; Ashall *et al*, 2009). Tumor Necrosis Factor – α (TNF-α) is an inflammatory signal that activates NFkB and induces its nuclear translocation via phosphorylation of the upstream IKKs kinases (Hoffmann *et al*, 2002). TNF-α is secreted in pulsatile bursts by cells neighboring to the T-cells, thus making the study using pulsatile microfluidics physiologically relevant (Ashall *et al*, 2009). Mimicking these physiological bursts, Ashall *et al* (Ashall *et al*, 2009) utilized pulsatile stimulation of TNF-α to show that a minimum 'reset time' is needed for complete recovery of NFκB amplitude peak. They found that the dampening is contributed not only by the negative feedback from NFκB-induced IκB expression, but also from A20 expression that inhibits the activation of an intermediate kinase, IKK-α. Thus, they utilized pulsing to figure out a hidden regulatory motif that was unknown prior to their investigation. Cells utilize pulsatile stimulation to determine the timing and specificity of NFκB dependent transcription. In particular, they showed that the four NFκB dependent transcripts *viz.* RANTES, IκBε, IκBα and MCP-1 are expressed in distinct fashion for the various TNF-α pulsatile stimulation patterns (Fig. 1.4. A).

Extracellular-regulated kinase (ERK) signaling plays an important role in cell fate regulation, including differentiation and cell proliferation. Stimulation by growth factors (GFs) like EGF (epidermal) and NGF (nerve) leads to the activation of GF receptors that activate a Ras-GTPase. This triggers the MAP kinase cascade that results in ERK activation (Avraham & Yarden, 2011; Marshall, 1995). The ligands EGF and NGF are known to have distinct ERK activation dynamics that lead to proliferation and differentiation, respectively (Avraham & Yarden, 2011; Marshall, 1995). Step stimulation of GFs leads to heterogeneous downstream ERK activation, thus complicating the understanding of the circuit architecture that differentiates the two input ligands. Ryu *et al* (Ryu *et al*, 2015) investigated this pathway in PC-12 cells for neurite growth (differentiation) by utilizing pulsatile stimulation to generate synchronized homogenous ERK signaling and probing the dynamics under several temporal conditions (Fig. 1.4. B). Sustained EGF stimulation led to an undifferentiated state while sustained NGF stimulation led to a differentiated state. Pulsatile stimulation of high concentration NGF also led to a differentiated state, except for slow stimulations (D = 3 min, R = 60 min). Since low NGF concentrations did not induce differentiation, they inferred that high NGF concentrations are required to trigger the pathways involved in differentiation other than ERK activation.

Transforming growth factor β (TGF-β) is a well-known mammalian morphogen that conveys positional information and determines cell fate during embryonic development (Massagué, 2012). TGF-β mediated signaling involves phosphorylation of a receptor-activated Smad (R-Smad) upon its binding to the TGF-β receptor. The phosphorylated R-Smad undergoes nuclear translocation, acts as a transcription factor and brings about transcriptional changes. These morphogen levels are not static and may present a dynamic (oscillatory or pulsatile) micro-environment to the developing embryo (Warmflash *et al*, 2012; Aulehla *et al*, 2009). To understand the implication of temporal encoding of such dynamic morphogenic signals in embryonic patterning, Sorre *et al* (Sorre *et al*, 2014) probed C2C12 cells using GFP-Smad4 fusion protein in a microfluidic cell culture device and live cell imaging. TGF-β stimulation leads to nuclear translocation of Smad4-GFP (Fig. 1.4. C), and subsequently to inhibition of myotube formation in myoblasts. While step changes in TGF-β concentration led to partial prevention of differentiation, pulsatile TGF-β stimulation was more potent in preventing differentiation (Fig. 1.4. C).

Another example where pulsatile stimulation has provided novel insights is insulin secretion from the islets of Langerhans. The islets are mainly composed of pancreatic β-cells. Upon

elevated glucose levels, the rate of glycolysis and consequently the ATP concentration increases in the β-cells, thus blocking the potassium channel and opening up of calcium channels. Positive feedback from calcium (calcium induced calcium release) raises its level and leads to the secretion of insulin granules via exocytosis. Sugar metabolism is oscillatory, and so is insulin secretion, both having a period of ~ 5 min. How these islets synchronize to generate oscillations in the insulin secretion has remained largely unknown. Dhumpa *et al* (Dhumpa *et al*, 2014) used a microfluidic device to investigate how step and oscillatory glucose input synchronizes the insulin secretion. They showed that under step elevation of glucose level, the calcium and insulin read-outs in the islet remained uncorrelated with no entrainment. In contrast, oscillatory glucose input led to oscillations in the calcium as well as insulin secretion in an entrained fashion (Fig. 1.4. D). The synchronization index increased with increasing periodic glucose amplitude. Mathematical modeling of the system revealed that an insulin-dependent negative feedback action of the liver on glucose level leads to synchronized oscillations in the islets. In a more recent work (Dhumpa *et al*, 2015), they determined the synchronization window by using a chirped waveform of glucose stimulation to find that the strongest resonance between the glucose input and calcium oscillations was within 2 min of the natural period of oscillation (~5 min) (Fig. 1.4. D). These studies reveal how feedback mechanisms may induce synchronized oscillations at tissue scale to give rise to emergent behaviors.

G-Protein Coupled Receptors (GPCR) are cell surface receptors that primarily signal through G-Protein coupling, resulting in various downstream signaling events through second messengers such as cytoplasmic calcium and ATP. These second messengers have oscillatory dynamics because of positive and negative feedback (Dyachok *et al*, 2006; Politi *et al*, 2006). The receptor itself may undergo dynamic uncoupling leading to oscillatory dynamics of G-protein activation (Dupont *et al*, 2011b). The oscillatory calcium response is widely studied to understand the temporal encoding of calcium-induced transcription factors (Dolmetsch, Ricardo; Lewis, Richard; Goodnow, Christopher; Healy, 1997; Tomida *et al*, 2003; Carcich & Joseph, 2001; Dolmetsch *et al*, 1998). To elucidate signaling circuit architecture, Jovic et al utilized pulsatile stimulation of HEK 293 cells stably expressing muscarinic M3 receptor (a GPCR) with carbachol, a chemical analog of acetylcholine (a neurotransmitter and physiological ligand for M3 receptor) (Jovic *et al*, 2010, 2011). A measure of response fidelity, defined as the phase locking ratio (PLR, ratio of number of calcium responses above a threshold value to the number of input ligand pulse)

was shown to change with the stimulation parameters concentration (C), duration (D) and rest period (R). The phase-locking analysis provided an expanded observability space to compare several models and examine the differences in activation and recovery properties between the models, which would otherwise not be possible through conventional methods. Utilizing these microfluidic results, several existing models were compared with distinct signaling motifs (positive and negative feedbacks) to discover the circuit architecture that best explained the data (Fig. 1.5. A). The analysis also revealed the importance of basal levels of PLC in generating subthreshold peaks. Pulsatile stimulation was also utilized to understand the pathway recovery properties in multiple concentration regimes (Jovic *et al*, 2013). In particular, the reduction in phase-locking at low values of C and D and the reduction in signal amplitude at high values of C and D for a fixed R was utilized to dissect the recovery properties of cytoplasmic calcium and receptor phosphorylation respectively (Fig. 1.5. B).

Several non-mammalian systems have also been investigated through temporal modulation of input signals using microfluidics and mathematical modeling to elucidate specific signaling features. A synthetic oscillatory network inducible with arabinose has been studied in the bacterial system using oscillatory arabinose input to quantitatively understand the entrainment of biological clocks (Mondragón-Palomino *et al*, 2011). These bacterial oscillators displayed a wide range of tunable frequencies and higher-order resonance. Computational simulation of this system indicated that the entrainment robustness of biological clocks may be attributed to the presence of a positive-feedback loop. In another work, a social amoeba, *Dictyostelium discoideim*, was studied to understand its coordinated and synchronized cAMP oscillations at population scale under starving conditions (Sgro *et al*, 2015). Using pulsatile microfluidic stimulations and mathematical modelling, they showed that the intracellular noise (stochastic heterogeneity) is the key driver of the population level behavior and that the biochemical noise (cell-to-cell variability) alone was unable to reproduce the results. Hao *et al* (Hao *et al*, 2013) studied how transcription factors (TFs) process dynamic input to generate diverse range of dynamic responses. Using yeast (*Saccharomyces cerevisiae*) as their model system, they showed that the stress-responsive TF Msn2 is able to distinguish various dynamic stress inputs based on upstream kinetics and may process it differently as a tracker, as a filter or as a signal integrator. Another group showed that the oscillatory stress stimulation in yeast cells results in an intermediate frequency regime for which the growth is slowed down significantly (Mitchell *et al*, 2015). Another model system

studied widely with microfluidics is a nematode (*Caenorhabditis elegans*). Tomida *et al* (Tomida *et al*, 2012) measured calcium and MAPK activity in sensory neurons of *C. elegans* under pulsatile stimulation of changes in NaCl concentration. The study showed that the stimulation parameters (C, D and R) determine the extent of MAPK-1 activation in a non-linear fashion attributed to the calcium dynamics, which showed dampening at rapid stimulations.

1.7. Brief description of muscarinic M3-calcium-NFAT signaling

Muscarinic M3 acetylcholine receptor is a GPCR expressed in many locations including beta cells of the pancreas, and is considered a potential target for Type 2 diabetes as well as neurodegenerative diseases (Kruse *et al*, 2014). Physiological ligand for this receptor is acetylcholine, a neurotransmitter that has been observed to be released in pulsatile bursts (Fig.1.3. A), thus making this signaling pathway ideal for our investigation. Ligand-induced activation of the receptor signals through the common G-protein-PLC-IP3 pathway that couples to the calcium-calcineurin pathway to induce NFAT (Nuclear Factor of Activated T-Lymphocytes) nuclear translocation. Calcium-dependent calcineurin-NFAT signaling plays key roles in T-cell activation, in insulin secretion (Rodriguez-Diaz *et al*, 2011; Nilsson *et al*, 2007) and in regulating neonatal beta cell development (Kragl & Lammert, 2012).

Current understanding of GPCR-calcium signaling model comes from recently published studies that are based on a combined experimental and modeling approaches (Jovic *et al*, 2013; Politi *et al*, 2006). Briefly, carbachol (CCh) binds to M3 muscarinic receptors, promoting G-protein coupling. Following the exchange of GDP for GTP on the alpha-subunit (Gα), Gα dissociates from the receptor and binds to PLC, initiating downstream signaling. GTP on activated Gα is rapidly hydrolyzed to GDP, forming inactive Gα-GDP. If Gα is bound to PLC, then this hydrolysis reforms inactive PLC as well as inactive Gα. The ligand-receptor complex (L-R) is reversibly phosphorylated to form inactive L-R-P state. Gα binding to PLC increases IP3 production; IP3 binds to the inositol triphosphate receptor (IP3R) on the endoplasmic reticulum (ER), triggering the release of Ca^{2+} from ER into the cytosol. Cytosolic Ca^{2+} acts both to stimulate and to inhibit its release from the ER through multiple pathways. The oscillatory release of Ca^{2+} from the ER is achieved by the SERCA pump, which pumps cytosolic Ca^{2+} back into the ER. Ca^{2+} can also enter or leave the cell through the plasma membrane (Fig. 1.6.). Calcium release in the cytoplasm leads to activation of several downstream calcium-dependent signaling components.

One such example is the calcium-mediated NFAT signaling (Tomida *et al*, 2003; Dolmetsch *et al*, 1998). Briefly, the rise in cytoplasmic Ca^{2+} activates calcineurin, which binds to cytoplasmic phosphorylated NFAT ($NFAT_{cyto}$-Pi) and leads to dephosphorylation ($NFAT_{cyto}$). The complex can either form inactive calcineurin and cytoplasmic $NFAT_{cyto}$-Pi upon rephosphorylation, or the calcineurin-dephosphorylated NFAT complex may translocate to the nucleus because of the exposure of the nuclear localization signal domain upon dephosphorylation. Nuclear dephosphorylated NFAT ($NFAT_{nuc}$) is the active form for NFAT that binds with DNA at specific sites and, along with other transcription factors, brings about a variety of physiological responses. $NFAT_{nuc}$ may then undergo phosphorylation to form inactive nuclear phosphorylated NFAT ($NFAT_{nuc}$-Pi) which then translocates back to the cytoplasm (Fig. 1.6.).

1.8. Overview of thesis

The ability to stimulate cells with temporally varying inputs has provided insight into how cells process and interpret these signals. As discussed in the previous section, several signaling pathways have been investigated using this approach in past couple of decades. The approach becomes even more relevant in mimicking physiological conditions with pulsatile inputs. With growing capabilities of measuring multiple read-outs in single cells, it is becoming increasingly evident that individual cells may not behave as expected from their population-averaged responses. Often, these signaling networks are non-linear and lead to bifurcation in the response which is not evident from population scale measurements (Altschuler & Wu, 2010; Spencer *et al*, 2009, 2013). Now that technology has advanced and is capable of addressing such questions, with the use of microfluidics and computational modeling, this is an exciting time to study how the dynamic cellular micro-environment is utilized by nature to process information at single cell level, how information processing is affected by unavoidable noise in the signaling system, whether nature utilizes noise to enhance selectivity, and what pharmacological implications pulsatile stimulation and noise might have. The results from such studies will take our understanding of temporal modulation of signals to a new and detailed level. It will enhance our understanding of cellular physiology as well as shed light on the effects of cellular noise and variability in dynamic signaling and selectivity. Although this thesis focuses on one particular receptor (viz. muscarinic M3 receptor), it endeavors to develop a general understanding about temporal information processing that may be applicable to many signaling pathways. These

understandings possess immense potential for therapeutic advantages and drug development as well as for advanced synthetic biology applications.

Within the above contexts, this thesis takes muscarinic M3 (GPCR)-mediated calcium signaling as a model signaling system and explores the following questions:

1. *How do pulsatile inputs affect downstream signaling and transcriptional activity, and is there a specific circuit architecture to process such signals? (Chapter 2)*

   Real-time assessment of cellular calcium levels and nuclear translocation of the calcium-regulated transcription factors NFAT1 and 4 is done under various pulsatile conditions. We obtain counterintuitive results, wherein an intermediate pulsing rate (less overall stimulation) elicits a larger response than is obtained by continuous exposure or frequent pulsing (which both provide greater overall ligand exposure). Furthermore, different stimulation frequency windows favor activation of the two different transcription factor isoforms. The frequency-dependence of the responses is consistent with the concept of a band pass filter. Based on computational modeling of the experimental data, band pass processing is expected to be a general theme that applies to multiple signaling pathways.

2. *Do physiologically relevant pulsatile bursts encode information as a deterministic strategy to guide cell fate or just lead to random stochastic signaling events? (Chapter 3)*

   Physiologically relevant stimulations that are transitory and weak often result in responses that appear stochastic. In this chapter, we show that such cases may be well described by deterministic processes in which there is a high Hill coefficient step and cell-to-cell variability. Additionally, we describe a tractable, rest period-based, two-pulse experimental test that can confirm that an apparently stochastic response may have a deterministic basis.

3. *How is information transfer capacity of such signaling pathways affected by the presence of biochemical noise? (Chapter 3)*

   We use pulsed ligand inputs and measure single cell response to quantify information transfer via M3 receptor to calcium and NFAT response under step and pulsed conditions. We show that the mutual information transfer under pulsed stimulation is not only greater than the step changes alone, but also exceeds the maximum information transfer possible under non-

pulsatile conditions. Focusing on a deterministic model, we show that the extent of biochemical noise critically determines the amount of information that can be transferred downstream. We also show that the two isoforms of NFAT with different band-pass windows also exhibit different levels of information transfer and their mutual information transfer is greater than their information transfer capacities alone.

4. *What are the implications of biochemical noise in determining drug action at single cell level? (Chapter 4)*

   In this chapter, we ask how biochemical noise may affect the drug action at single cell level. We developed a microfluidic experiment to measure two observables in the same cell, similar to a 'two-reporter' system to estimate biochemical noise in the system. Our analysis with microfluidic experiments and mathematical modeling suggests, counterintuitively, that the drug action on rescuing perturbed cells increases with increasing noise.

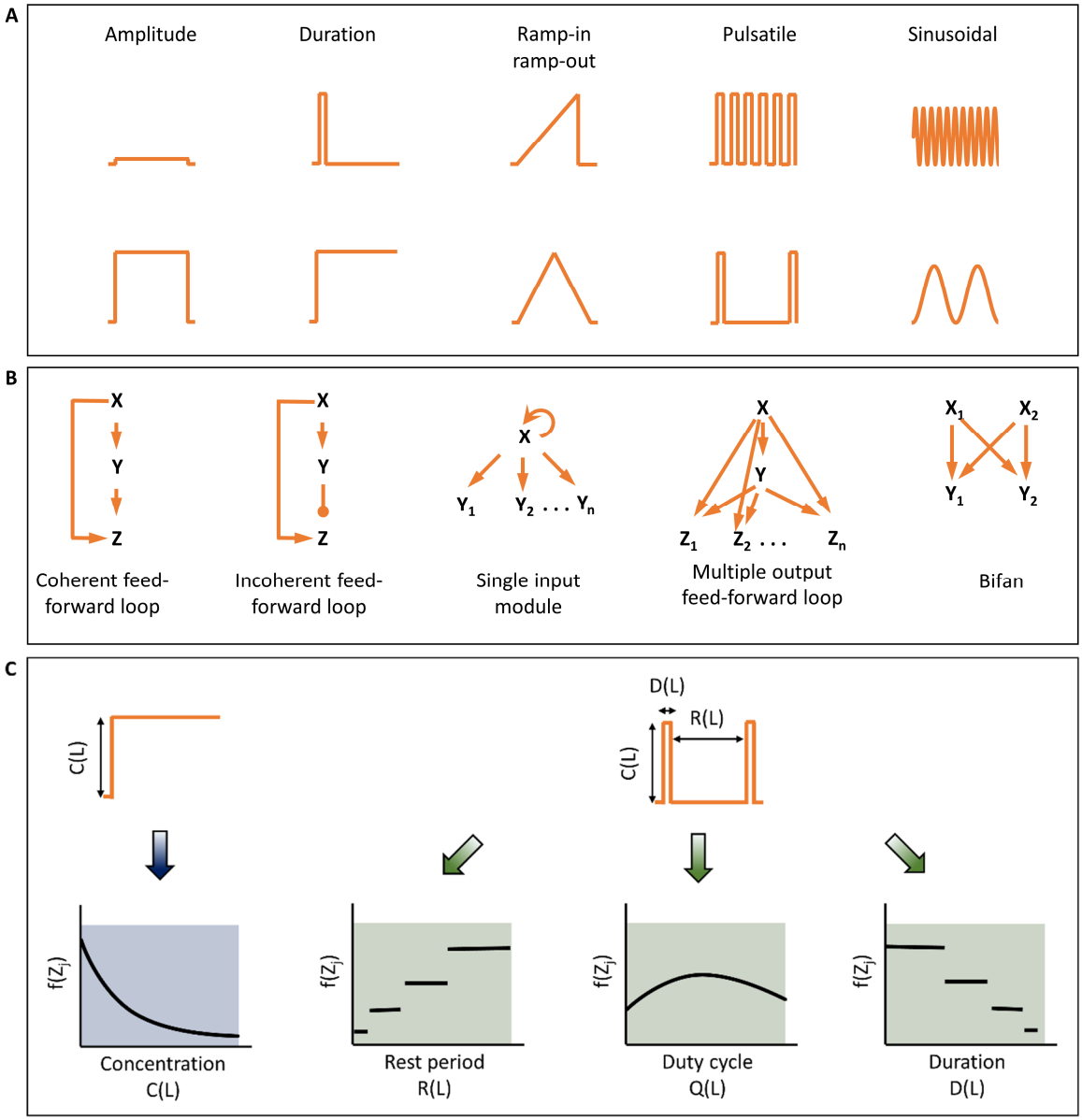

Fig. 1.1. **Dynamic microenvironment expands the observability space to investigate complex network structures.** A. Several dynamic modulations of signaling input observed in biological systems that includes modulation in amplitude, duration, gradient, pulsatile frequency, and sinusoidal rhythms. B. Examples of network motifs present in transcription networks that can sense temporal inputs. C. Temporal modulation expands the observability space by providing additional input-output responses and aids in distinguishing the network motifs.

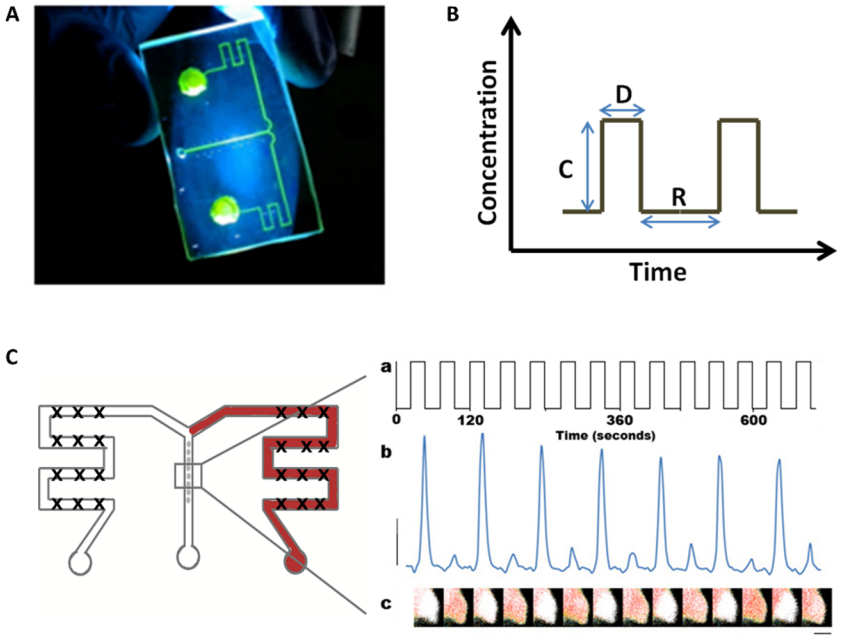

Fig. 1.2. Braille-pin based pulsatile microfluidic device allows delivery of temporally controlled ligand inputs. A. Braille-pin actuator based PDMS microfluidic device used to deliver time varying pulsatile ligand input to cells seeded in the microfluidic channel; image obtained from (Jovic *et al*, 2011). B. The ligand delivery (input) can be controlled in terms of C (concentration), D (duration of stimulation) and R (rest period between two consecutive stimulations). C. Peristaltic pumping using a Braille-pin based platform (Gu *et al,* 2004) in alternate fashion generates fluid flow. Channels from two input reservoirs merge into a single outlet channel to deliver alternate sequence of fluid from each of the channels into the outlet channel through the computer-controlled system (left). Pulsatile delivery of input ligand results in phase-locked calcium response (right). Image and data from (Jovic *et al*, 2011).

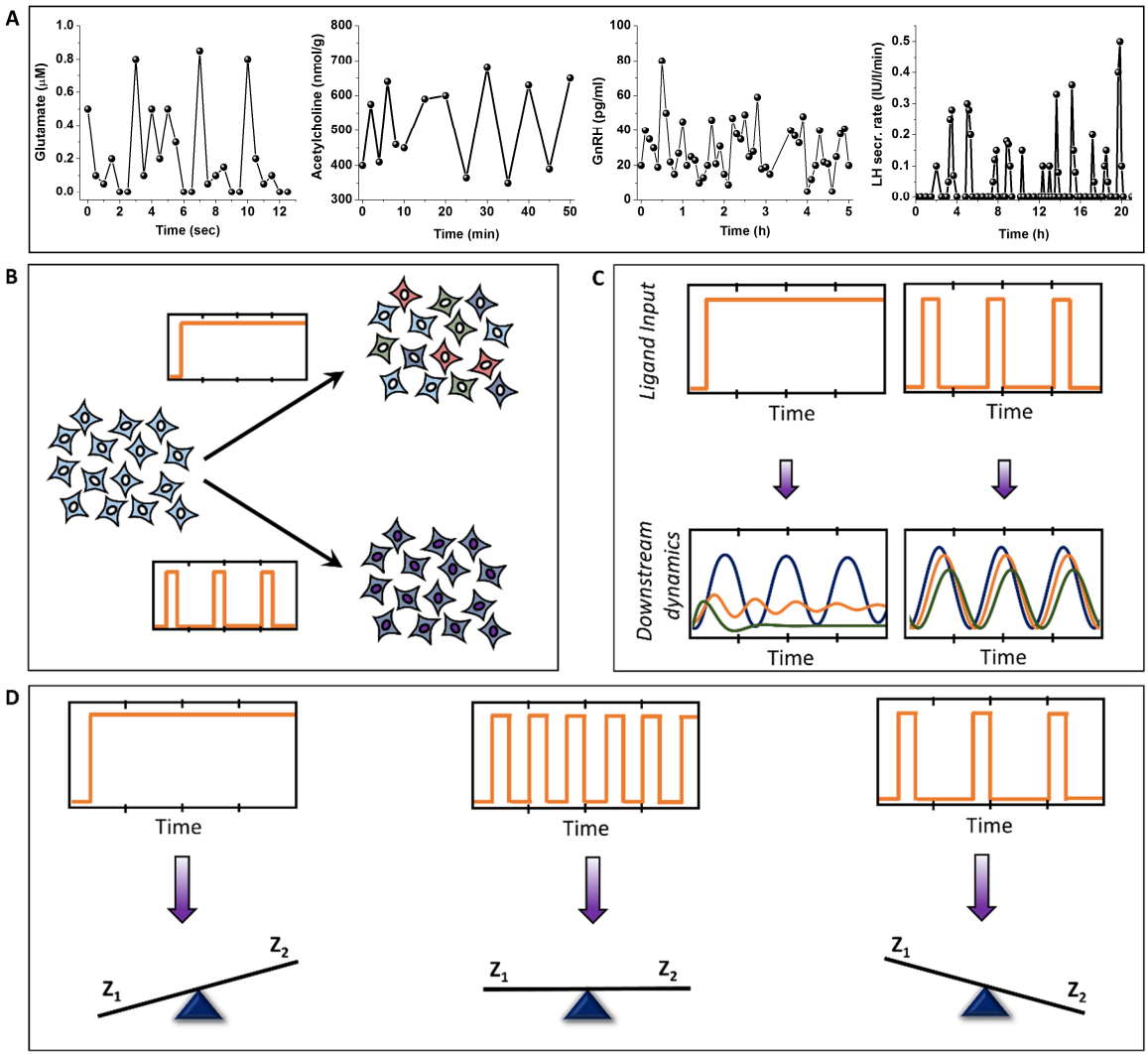

Fig. 1.3. Advantages of pulsatile stimulation over conventional methods. A. Pulsatile stimulation can mimic several time-varying ligand secretions that are physiologically more relevant e.g. glutamate, acetylcholine, Gonadotropin releasing hormone (GnRH) and Luteinizing Hormone (LH) are all known to be secreted in pulsatile fashion. Data adapted from several literature sources. B. Pulsatile stimulation results in phase-locking or entrainment in several non-linear systems thus filters out the temporal variations because of biochemical noise or cell-to-cell variability. C. Pulsatile stimulation may also lead to distinct downstream responses, thus regulating different fates through the same input. D. Using microfluidics to study behavior of entrained/phase-locked cells also provides a platform to study collective population behavior often observed physiologically.

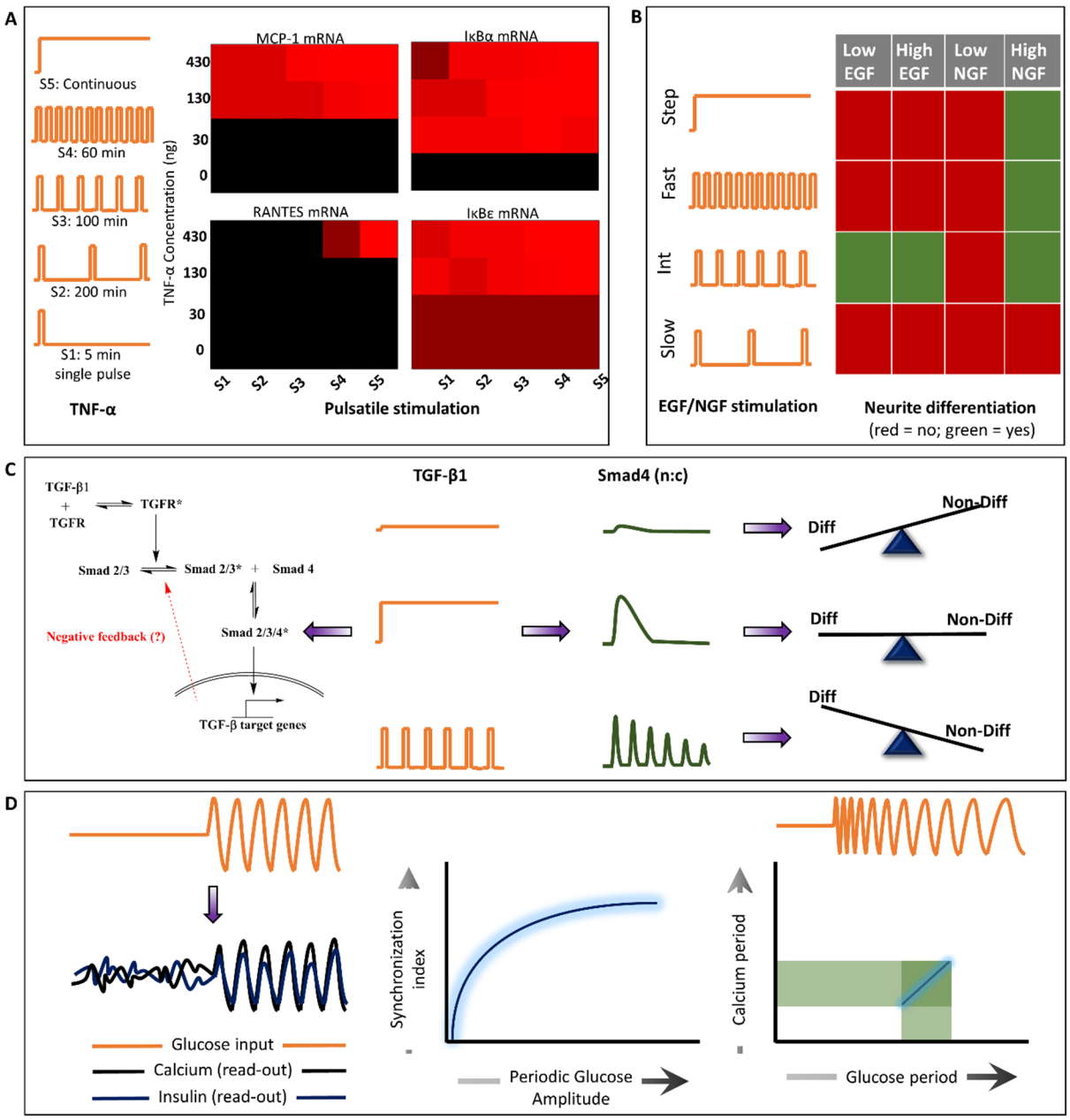

Fig. 1.4. Investigation of oscillatory signaling networks with microfluidics and computational modeling. A. TNFα-NFκB signaling. TNF-α induced NFkB oscillations show differential sensitivities of mRNA transcripts towards time-varying inputs. B. Growth factor mediated neurite differentiation. Temporally modulated growth factor stimulations, epidermal (EGF) and nerve (NGF), lead to distinct fates of neurite differentiation based on temporal regimes. C. TGF-β mediated Smad4 activation. Temporally varying inputs show no memory of stimulation and adapts to the external pulsing, suggesting an existence of negative feedback (adaptive mechanism). Pulsatile stimulation is more efficient is preventing differentiation of myocytes as compared to step changes in ligand concentration. D. RTK-Insulin pathway. Calcium and insulin secretion show entrainment to synchronize at tissue scale upon periodic glucose stimulation and the extent of synchronization increases with increase in periodic glucose amplitude. All figures and data are adapted from the articles referenced at appropriate places.

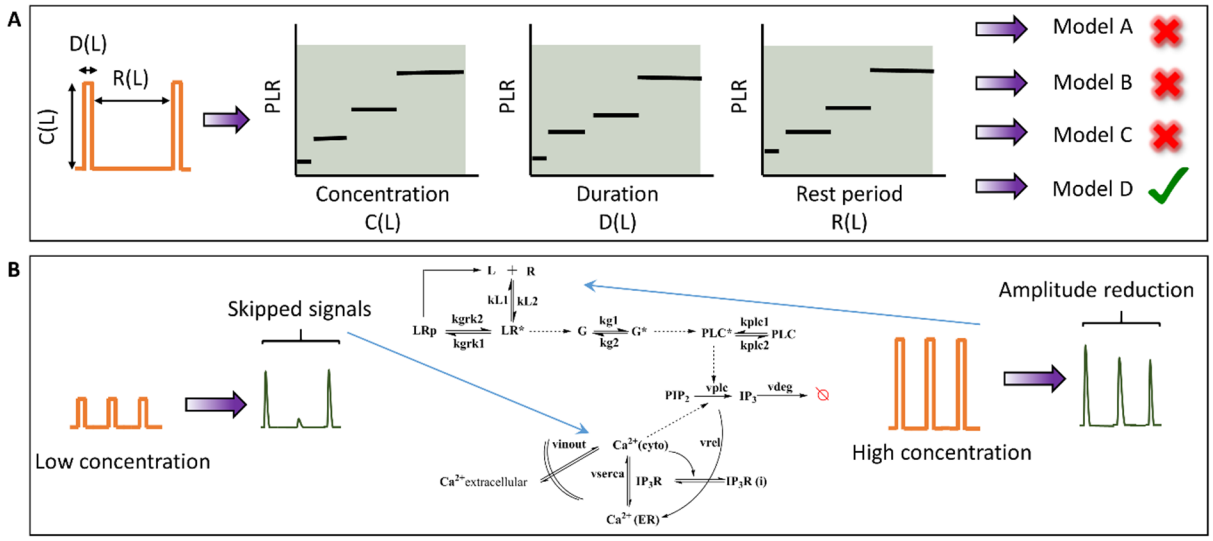

Fig. 1.5. Microfluidic phase locking analysis of GPCR-calcium signaling to dissect circuit architecture and pathway recovery properties. A. Phase locking properties upon pulsatile stimulation vary with stimulation parameters such as input concentration (C), pulse duration (D) and rest period between the pulses (R). Existing models, when compared for the phase locking properties, lead to identify circuit architecture that can best explain these properties. B. Pulsatile stimulations in low and high concentration regimes lead to characteristic signal/beat skipping (in low concentration regime) and amplitude reduction (in high concentration regime). These observations help understand the pathway recovery properties of the signaling, thus leading to model improvisation (Jovic *et al*, 2010, 2011, 2013).

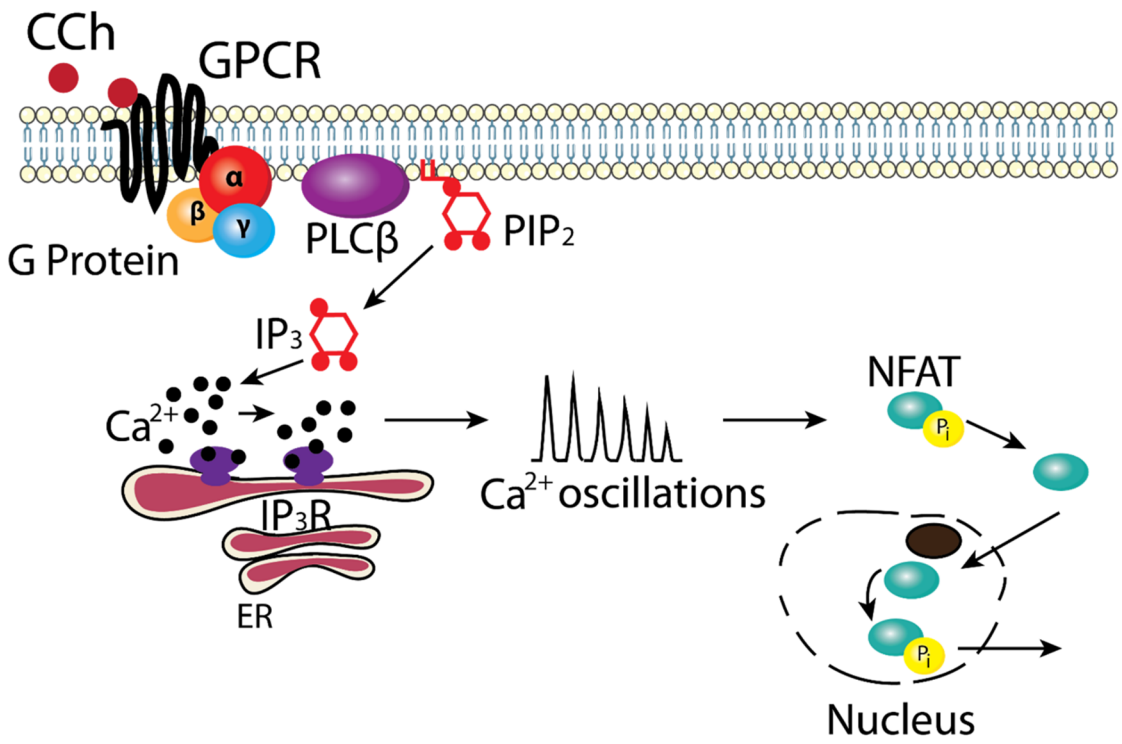

Fig. 1.6. Schematic of GPCR (muscarinic M_3)-calcium-NFAT signaling. Receptor-ligand binding leads to G-protein activation and the cascade eventually leads to release of intracellular calcium. Calcium mediates dephosphorylation of the cytoplasmic NFAT, which then translocates into the nucleus to bring about transcriptional activation. Phosphorylated NFAT translocates back into the cytoplasm.

Chapter 2. Band-pass processing in a GPCR signaling pathway selects for NFAT transcription factor activation

2.1. Introduction

Appropriate timing is crucial for proper development and maintenance of physiological functions (Purvis & Lahav, 2013; Toettcher *et al*, 2013; Paliwal *et al*, 2008; Fujita *et al*, 2010; Ashall *et al*, 2009). Timing information is relayed through modular interaction of signaling motifs in complex signaling pathways (Lim *et al*, 2013; Sneppen *et al*, 2010; Hao *et al*, 2013). Cellular responses are typically studied for step changes in ligand concentrations, although in nature stimuli are often periodic or fluctuate over frequencies ranging from milliseconds to days (Goldbeter, 1996; Aladjalova, 1957; Walker *et al*, 2010; Armstrong *et al*, 2009; Tengholm & Gylfe, 2009). A majority of these rhythmic as well as arrhythmic stimuli lead to oscillations in second messengers (e.g. calcium, cAMP, PKA, MAPK) (Dupont *et al*, 2011a; Ni *et al*, 2011; Cheong *et al*, 2010; Hilioti *et al*, 2008; Dyachok *et al*, 2006). Among these, the effect of frequency modulation of calcium oscillations on downstream transcription factor activation has been extensively studied using calcium-clamped cells (Tomida *et al*, 2003; Dolmetsch *et al*, 1998). However, the more physiologically relevant ligand-induced calcium oscillations and downstream signaling are less well-understood. Using pulsatile ligand stimulation of a G-Protein coupled receptor (GPCR), we provide new insights into how cell surface receptor activation leads to calcium signaling and activation of a downstream transcription factor, NFAT (Nuclear Factor of Activated T-Lymphocytes).

The M3 muscarinic acetylcholine receptor is a GPCR expressed in many locations (Kruse *et al*, 2014). Ligand-induced activation of the receptor signals through the common G-protein-PLC-IP3 pathway that couples to the calcium-calcineurin pathway to induce NFAT nuclear translocation (Fig. 2.1. A). Calcium-dependent calcineurin-NFAT signaling plays key roles in T-cell activation, in insulin secretion (Rodriguez-Diaz *et al*, 2011; Nilsson *et al*, 2007) and in regulating neonatal beta cell development (Kragl & Lammert, 2012). In this chapter, we employ

pulsatile stimulation of M3 receptors and simultaneous measurement of cytoplasmic calcium and NFAT nuclear translocation in single cells using a computer-controlled microfluidic device (Gu *et al*, 2004). Using computational modeling, we delineate the temporal modulation of GPCR (M3 receptor)-induced calcium oscillations and calcium-induced NFAT nuclear localization. Microfluidic experiments and mathematical modeling are used in combination to determine the model parameters that control the temporal coding of downstream signaling.

A common expectation in receptor-mediated signaling is that greater agonist stimulation will lead to greater activation of downstream signals until saturation of processes occurs. Indeed, ligand stimulation of M3 muscarinic receptor with higher ligand concentrations leads to faster calcium oscillations and overall larger calcium release. Here, we demonstrate, however, that reduced overall ligand exposure, if delivered as pulses of ligand, can give more efficient transcription factor activation. The optimal stimulation timing is achieved when the rest period between stimulations is sufficiently long to allow receptors to recover from stimulus-triggered desensitization, while being sufficiently short that downstream signaling cascades can be actively maintained. We also show that when using pulsatile stimulation, receptor desensitization and the dynamics of downstream signaling combine to form a band-pass regime of frequencies for which the signaling is significantly enhanced as compared to a step change in ligand stimulation. Critical factors that determine this optimal stimulation frequency are the rate constants for receptor desensitization and NFAT translocation. As an example, we show that the two NFAT isoforms (NFAT4 and NFAT1) have distinguishable band-pass windows for the same receptor.

2.2. Results

2.2.1. Simultaneous observation of calcium and NFAT4 dynamics in single cells under step and pulsatile ligand stimulation

We measured calcium and NFAT4 responses simultaneously in single HEK293 cells for a step change or pulsatile ligand stimulation using microfluidics (Fig. 1.2. A) (Jovic *et al*, 2011). Oscillatory cell signaling circuits under external periodic stimulation get entrained to the stimulatory input, a phenomenon commonly described as phase locking (Jovic *et al*, 2011, 2010). Using pulsatile ligand inputs with varying concentration (C), pulse duration (D) and pulse rest period (R) (Fig. 1.2. B), we tested the hypothesis that different pulsing patterns will alter intracellular calcium release and the amount of NFAT4 nuclear translocation. Cytoplasmic

calcium was quantified with RGECO1 sensor transiently transfected in stable M3 receptor expressing HEK293 cells and responses were induced by the cholinergic agonist carbachol (CCh) (Appendix 2 Fig. 2B.1). NFAT4 nuclear localization was quantified in the same cells by measuring the ratio of nuclear to cytoplasmic intensities of transiently transfected NFAT4-GFP (Appendix 2 Fig. 2B.2). Simultaneous observation of calcium and NFAT4 dynamics under step and pulsatile stimulation was performed at the single cell level in microfluidic device that can provide time-varying ligand stimulation (Fig. 2.1. B).

A step change in ligand stimulation leads to a concentration-dependent calcium frequency response in cells exhibiting calcium oscillations, with high cell-to-cell variability (Fig. 2.1. C and Appendix 2 Fig. 2B.1). Pulsatile stimulation results in calcium oscillations that are phase-locked at the specific frequency of ligand stimulation (Fig. 2.1. C, bottom panel) and are more sustained than those elicited by step stimulation. For each of the cells under step or pulsatile stimulation, NFAT4 nuclear translocation was observed and quantified amidst cell-to-cell variability (Fig. 2.1. C, right panels). Thus our experimental set-up can measure time-resolved phase-locked calcium response and corresponding NFAT4 nuclear translocation in single cells.

2.2.2. Experiments and simulations show distinct GPCR-calcium-NFAT4 pathway dynamics in response to step and pulsatile ligand stimulation

We performed a frequency response analysis of GPCR-calcium-NFAT4 signaling with varying ligand concentration (C) and rest period (R) values and developed our mathematical model to capture the characteristic features elicited by both step and pulsatile stimulation (Fig. 2.2.). The time-dependent responses for cytoplasmic calcium and NFAT4 nuclear translocation were generated for step stimulation and for three different pulse stimulation conditions, i.e., fast (corresponding to R = 24 s), intermediate (R = 72 s) and slow (R = 144 s) (Fig. 2.2. A). Distinct responses were observed for step and various pulsatile stimulations for calcium and NFAT4 (Fig. 2.2. B). Step simulation with CCh produced strong calcium response at the outset of stimulation, resulting in either oscillations (at lower concentrations) or peak-and-plateau responses (at higher concentrations), but also resulted in rapid decay of the peak amplitude and/or frequency over time. Pulsatile stimulation produced phase-locked calcium responses as expected (Jovic *et al*, 2011, 2010). However, calcium oscillations elicited by faster ligand pulses decayed rapidly over time, whereas oscillations elicited by slower ligand pulses were more sustained. The

corresponding NFAT4 responses exhibited a sustained time course reaching their maxima at different time points for step and various pulse conditions. A step change in ligand concentration stimulation led to a rapid (~ 500 s) attainment of the maximum NFAT response, followed by a slow decay. In contrast, slow pulsatile ligand stimulations led to a gradual accumulation of nuclear NFAT4.

For a quantitative and mechanistic understanding of the distinct frequency responses of calcium and NFAT4 under step and pulsatile conditions, we developed a mathematical model based on both literature data and our own microfluidic experiments. Our mathematical model is comprised of two modules: GPCR-induced calcium oscillations and calcium-induced NFAT4 nuclear translocation (Fig. 2.1. A, Appendix 2 Text 2A.1.). Most calcium mathematical models exhibit continuous oscillations without decay in frequency or amplitude when subjected to step ligand stimulation, in contrast to our own experimental observations and literature data (Kupzig *et al*, 2005; Li *et al*, 1998; Song *et al*, 2012). One model that does offer an explanation for frequency and amplitude decay (Giri *et al*, 2014) doesn't explain the phase locking behavior we observe. Building upon Jovic et al (Jovic *et al*, 2013), we incorporated receptor phosphorylation and receptor internalization followed by receptor recycling or degradation to reproduce our observed calcium response at various frequencies and concentrations of stimulation (Appendix 2 Text 2A.2.). Our mathematical model captures characteristic features of the calcium-NFAT4 signaling under step and pulsatile ligand stimulation (Fig 2.2. C).

2.2.3. Slower ligand pulses lead to more sustained calcium response, but intermediate frequency pulses lead to a maximum NFAT4 response

The sustained calcium oscillations and distinct NFAT4 responses that we observed under pulsatile ligand input allowed us to determine how calcium and NFAT4 dynamics depend upon the input ligand concentration and pulse frequency. We find that fast ligand pulses (R = 24 s) lead to less sustained calcium signaling as evident from a faster decay of the calcium duty cycle ratio (n), defined here as the ratio of the 'area under the curve' (AUC) of the nth calcium pulse to that of the first pulse. In contrast, slow ligand pulses lead to more sustained calcium signaling (higher duty cycle ratio) (Fig. 2.3. A, Appendix 2 Fig. 2B.3.). Our mathematical model also captures this characteristic feature of the calcium response for all ligand concentrations and pulse frequencies tested. The measured NFAT4 responses were compared by determining the maximum of the

normalized NFAT4 curve of nuclear to cytoplasmic ratio (NFAT4max) that each cell attained under various step and pulsatile ligand stimulation conditions. Surprisingly, NFAT4max was greater for stimulation at intermediate ligand pulse frequency (R = 72 s) than for a step change in ligand concentration for each of the ligand concentrations tested, in experiments and in the model (Fig. 2.3. B). Further, NFAT4max for intermediate ligand pulse frequencies was greater than for the slow or fast ligand pulse frequencies (Appendix 2 Fig. 2B.4. A).

The non-monotonic dependence of NFAT4 translocation on ligand pulse frequency was further explored by calculating NFAT4-AUC for each cell. For a ligand concentration of 40 nM, we find that the NFAT4-AUC is maximum for intermediate rest period (R = 72 s) as compared to both a shorter and longer rest period (Fig. 2.3. C). When the rest period is fixed and only the ligand concentration is varied, we find the NFAT4-AUC significantly increases at high concentrations (Appendix 2 Fig. 2B.4. B). The common notion that calcium oscillations are frequency modulated leads to the hypothesis that at the same calcium oscillation frequency, NFAT4 output should be the same regardless of concentration of ligand used to elicit that response. Our results suggest that both the frequency of calcium oscillations and the ligand-concentration dependent calcium duty cycle play important roles in signal transduction, and hence the GPCR-calcium-NFAT4 signaling is both frequency and amplitude modulated. We also determined a "ligand efficiency", or total NFAT4-AUC per unit ligand at intermediate ligand pulse frequency. The ligand efficiency decreases with increasing concentrations of ligand (Fig. 2.3. D). Taken together, our experiments and model support that although slower ligand pulses lead to a high fidelity calcium response, an intermediate frequency range for ligand pulses results in maximum NFAT4 activation.

2.2.4. A modular combination of high-pass and low-pass filter works as a band pass filter in GPCR-Calcium-NFAT signalling

When NFAT4max is calculated for a range of concentration (C) and rest period (R) values using the mathematical model, the greatest value is found for ligand pulses with R values in the range of ~ 50 s – 100 s (Fig. 2.4. A). A qualitative approach to delineate this feature is to calculate the response fidelity of various signaling modules (output response versus various frequencies or rest periods tested, normalized to the maximum of the output), a method adapted from dynamic system analysis (Isermann & Münchhof, 2011). Shutting down the receptor desensitization

module (by imposing parameter values to be zero) results in sustained and non-decaying calcium oscillations, i.e., the mean calcium duty cycle ratio remains ~ 1 for all R. Under such conditions, NFAT4 localization (output) correlates with the input ligand frequencies (Fig 2.4.B, black curve and Appendix 2 Fig. 2B.5.). Calcium-NFAT4 signaling thus works as a high pass filter that allows faster pulsatile stimulations to be transmitted with high fidelity. In contrast, when the receptor dynamics of desensitization, internalization and degradation are included in the mathematical model, we observe amplitude and frequency decay of calcium oscillations leading to rapid calcium duty cycle decay (output) with fast pulse stimulation (Fig. 2.4. B, red curve). Thus, receptor dynamics act as a low-pass filter that allows low frequency ligand pulses to be transmitted to NFAT4 responses with higher fidelity. The combination of low pass (receptor dynamics) and a high pass (calcium-NFAT signaling) filters acts as a band-pass filter (Fig. 2.4. B). The overall fidelity of GPCR-calcium-NFAT4 signaling is estimated by multiplying the impact of both low pass and high pass filters (Fig. 2.4. B, blue curve). The signal fidelity is maximum at intermediate frequencies of ligand stimulation, as we observe for NFAT4max in our experiments. Taken together, our experimentally-validated mathematical model demonstrates that the band-pass regime is a result of coupling of a low pass filter imposed by receptor dynamics with the high pass filter imposed by calcium-dependent NFAT4 translocation.

2.2.5. Receptor desensitization and NFAT translocation dynamics are key to the specificity of downstream signalling and specific temporal modulation

The band-pass nature of signal processing raises questions: can the peak location, height, or width of the band-pass curve be modulated? Might different receptors elicit maximal NFAT4 responses at different frequencies of ligand stimulation? To address these questions, we performed a sensitivity analysis on the mathematical model. Partial-rank correlation coefficients (PRCCs) with strong positive or negative correlations were determined for various curve characteristics such as peak-shift and height of the band-pass and steepness of the low-pass and high-pass filters (Appendix 2 Table 2C.1.). The phosphorylation rate constant of the receptor-ligand complex strongly correlates with peak-shift (negative, $P < 10^{-9}$) and also with peak-height (positive, $P < 10^{-9}$). The rate constant for recycling of the internalized receptor-ligand complex also contributes significantly to the peak-shift (positive, $P < 10^{-6}$). Among the parameters linked with calcium-NFAT signaling, the rate constants for NFAT nuclear translocation and for dissociation of the activated nuclear complex contribute significantly to the peak-shift, suggesting

that the characteristics of the band-pass regime are determined by both receptor kinetics and NFAT kinetics. Thus the band-pass regime could vary with receptor identity due to different phosphorylation and recycling rate constants and also with calcium-dependent transcriptional factor identity due to different translocation and dissociation rate constants (Fig. 2.4. C, Appendix 2 Table 2C.1.). For example, a rapidly translocating transcription factor will require faster ligand pulses to sustain the signal as it can move in and move out of the nucleus rapidly, while a slowly translocating transcription factor will require slower ligand pulses (Fig. 2.4. D). As an experimental demonstration of this concept, we measured NFATmax for another isoform of NFAT viz. NFAT1, which is known to have slower nuclear translocation and back-translocation rate constants than NFAT4 (Yissachar *et al*, 2013). When compared (for [CCh] = 80 nM), we find that the optimum pulse frequency for NFAT1 shifts towards slower pulsatile stimulation (Fig. 2.4. E). Taken together, our model sensitivity analysis and pulsatile experiments with NFAT4 and NFAT1 demonstrate that both receptor and NFAT dynamics play a significant role in downstream signal processing.

2.3. Discussion

A better understanding of how rhythmic processes and their appropriate timing enhances and selects for cellular functions is a fundamental problem in biology as well as a practical issue for cell culture application. Here we show that the most efficient NFAT nuclear translocation with muscarinic M3 receptor stimulation is obtained with "just right" timing of ligand pulses – not too slow or too fast. Time-varying ligand stimulation leads to different downstream responses for different stimulation conditions via band-pass processing of the signal (Fig. 2.4. D). GPCR-calcium-NFAT signaling forms a modular combination of low pass (GPCR signaling) and high pass (calcium-NFAT signaling) filters. Although GPCR kinetics are well-documented, only a few have explored their role as a low pass filter and how they contribute to downstream (Toettcher *et al*, 2013; Fujita *et al*, 2010; Hersen *et al*, 2008; Shankaran *et al*, 2007). Our work provides an experimental demonstration of how receptor down-regulation/desensitization may enhance information processing ability of the cells, consistent with the theoretical predictions made by Shankaran *et al* (Shankaran *et al*, 2007).

Infra-slow rhythms in the body which take place in the seconds to minutes time scale are an emerging area of interest for understanding physiological receptor-mediated signal processing

(Aladjalova, 1957; Collin *et al*, 2009; Ruskin *et al*, 1999; Linkenkaer-Hansen *et al*, 2001). The natural analog of CCh, acetylcholine (ACh), has been observed to have sustained oscillations in the range of ~ 0.2 min – 6 min during nerve stimulation (Dunant *et al*, 1974). In addition, other neurotransmitters like glutamate and dopamine have been shown to have sustained oscillatory release (De Pittà *et al*, 2009; Plaçais *et al*, 2012). Our work provides an experimental demonstration of how such periodic inputs might have an optimum frequency range for maximized target cell responsiveness, consistent with the theoretical predictions made by Li and Goldbeter (Li & Goldbeter, 1992). An understanding of how such biological rhythms affect cellular signal processing may facilitate the design of interventions to rationally modulate signaling and may also enable design and use of signaling modules in synthetic biology applications. Most studies focus on either longer or shorter timescales(Goldbeter, 1996). Our work may motivate investigation into biorhythms at such intermediate timescales.

Our work shows that variations in receptor kinetics (i.e., desensitization, internalization, degradation and recycling) are capable of generating different features for the low-pass filter and thereby affecting the band-pass regime. According to the recent 'barcode hypothesis', differences in phosphorylation and arrestin binding may encode for different desensitization, internalization, and recycling kinetics (Nobles *et al*, 2011; Lohse & Hoffmann, 2014); different receptors may also have different kinetics. The band-pass concept can be extended to non-GPCR receptors that mediate calcium-dependent transcription factor activation. The low pass filter formed by the receptor motif can determine whether slow ligand pulses would be most efficient (for rapidly down-regulated receptors) or whether fast pulses or a step change of ligand is most efficient (for slowly down-regulated receptors). Thus, T-cell receptors, which are slowly internalized and rapidly recycled (Liu *et al*, 2000), may not require ligand pulses for efficient signaling; a step change in ligand concentration could be sufficient. In contrast, pulsed stimulation can be more efficient than step changes for GPCRs. The band-pass concept might further be applied other second messenger systems, such as cyclic AMP, which undergoes oscillations via GPCR-Gs signaling and activates PKA that leads to phosphorylation of several downstream transcription factors (Ni *et al*, 2011). Overall, pulsatile microfluidic analyses add temporal dimensions in the observability space that, when coupled with computational modeling, can delineate the underlying band-pass characteristics of such network motifs. These band-pass characteristics

determine ligand pulse frequencies for efficient downstream signaling, and can potentially select for particular downstream responses as well.

2.4. Conclusions

Many biological processes are rhythmic and proper timing is increasingly appreciated as critical for development and maintenance of physiological functions. Temporal signal processing in receptor mediated pathways is increasingly appreciated as a tool that cells utilize to achieve enhanced activity and selectivity, and to distinguish signal from noise. Despite a few experimental evidences of such signal processing, proper mechanistic understanding based on the underlying kinetics remains largely unknown. To understand how temporal modulation of an input signal influences downstream responses, we employ microfluidic pulsatile stimulation of a G-Protein coupled receptor, the muscarinic M3 receptor, in single cells with simultaneous real-time imaging of both intracellular calcium and NFAT nuclear localization. Interestingly, we find that reduced stimulation with pulses of ligand can give more efficient transcription factor activation, if stimuli are timed appropriately. Our experiments and computational analyses show that M3 receptor-induced calcium oscillations form a low pass filter while calcium-induced NFAT translocation forms a high pass filter. The combination acts as a band-pass filter optimized for intermediate frequencies of stimulation. We demonstrate that receptor desensitization and NFAT translocation rates determine critical features of the band-pass filter and that the band-pass may be shifted for different receptors or NFAT dynamics. As an example, we show that the two NFAT isoforms (NFAT4 and NFAT1) have shifted band-pass windows for the same receptor. While we focus specifically on the M3 muscarinic receptor and NFAT translocation, band-pass processing is expected to be a general theme that applies to multiple signaling pathways.

2.5. Materials and Methods

Materials

Materials used for experiments in this Chapter are detailed in Appendix 1.

Methods

Methods description about cell culture, seeding cells in microfluidic device and time lapse image and analysis are detailed in Appendix 1.

Mathematical model development and computational analysis. We developed a mathematical model that links step or pulsatile ligand stimulation, receptor/ligand binding, calcium signaling, and NFAT translocation illustrated in Fig. 2.1. A. The model description, reactions and parameter table are provided in Appendix 2 Text 2A.2. A system of ordinary differential equations (ODEs) was generated for the model and solved in MATLAB (MathWorks Incorp) with the ode15s stiff solver.

Characterization of Ca^{2+} signaling and NFAT4 translocation. Intracellular calcium responses were characterized in terms of the varying ligand pulse parameters (Concentration (C) and Rest periods (R)). The ligand pulse duration (D) for which each pulse translates into a single calcium spike, i.e. without resulting in either no response at all or in multiple peaks, lies in the range ~ 16 s to ~ 32 s (Jovic *et al*, 2011). D was kept constant at 24 s in this study. We quantify the oscillation decay by defining calcium duty cycle ratio, which is the AUC of each calcium spike relative to the first spike and is thus an indicator of how the calcium response decays over time upon various pulsatile conditions.

$$Calcium\ Duty\ Cycle\ Ratio\ (n) = \frac{Calcium - AUC\ of\ nth\ pulse}{Calcium - AUC\ of\ the\ first\ pulse}$$

Extent of NFAT nuclear translocation was characterized using a standard procedure described in literature35 by determining the maximum of NFAT nuc/cyto ratio (NFATmax) attained under a pulsatile condition. MATLAB codes were written to determine the values of CDR(n) and NFATmax for both experimental and in silico data. AUC values for the time-course was determined for single cell traces by integrating the NFAT nuc/cyto ratio over time as follows:

$$NFAT - AUC = \int_{t=0\ s}^{t=tmax\ s} NFAT(t)dt$$

Here, tmax is the time when NFAT nuc/cyto attains its maximum. Nuclear export of NFAT (back-translocation) follows a first order decay kinetics, consistent with other studies (Yissachar *et al*, 2013; Tomida *et al*, 2003). Therefore, total NFAT-AUC is approximately proportional to the AUC calculated up to t_{max}. Time integrals were determined for the data sets using trapezoidal function in MATLAB. Statistical tests for determining the significance of the experimental data was performed with t-test for comparison of NFATmax for different pulse conditions.

Sensitivity analysis of the model. We used Latin Hypercube Sampling (LHS) and Partial-Ranked Correlation Coefficients (PRCC) to explore the mathematical model parameter space and identify those parameters which significantly contribute to the particular characteristics of the temporal signal processing in GPCR-calcium-NFAT signaling. MATLAB code for LHS-PRCC analysis was taken from Marino et al (Marino *et al*, 2008). Parameters related to GPCR-ligand binding kinetics and calcium-NFAT kinetics were varied over two logs by sampling from a uniform distribution using LHS. PRCC along with significance value was determined for each parameter against particular curve characteristics (Appendix 2 Table 2C.1.).

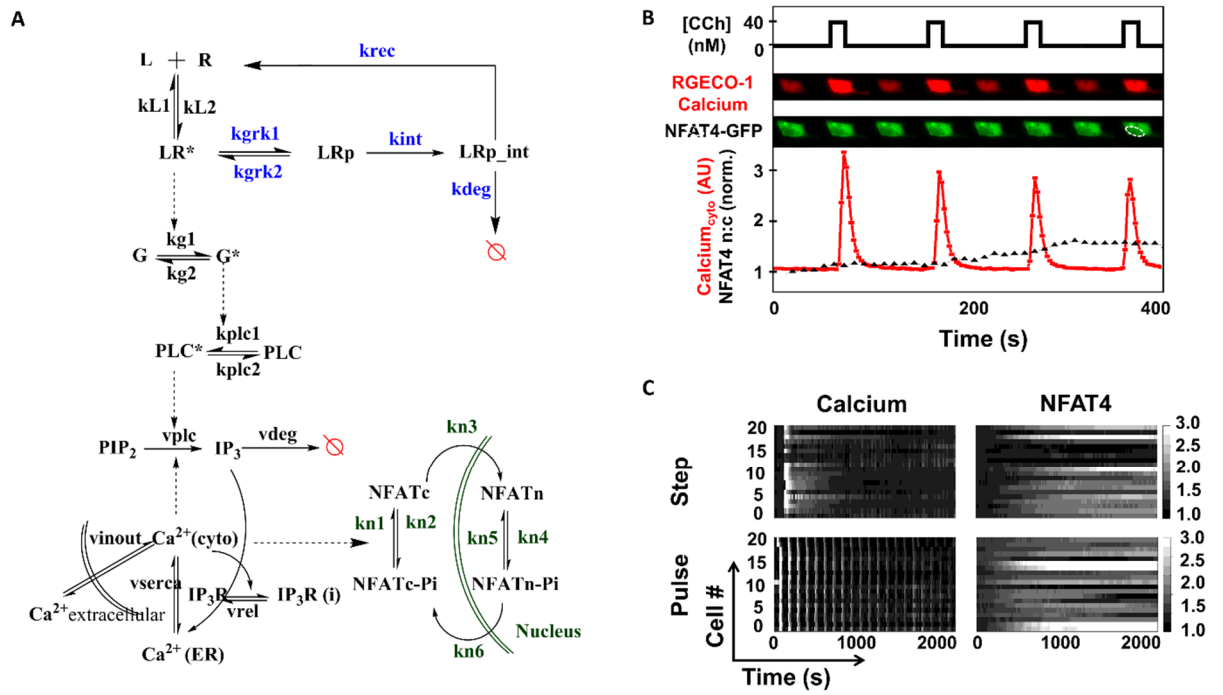

Fig. 2.1. Simultaneous observation of calcium and NFAT4 dynamics in single cells under step and pulsatile ligand stimulation. A. GPCR (Muscarinic M_3)-calcium-NFAT pathway showing calcium oscillations leading to NFAT nuclear localization, as shown in schematic in Fig. 1.6. The mathematical model incorporates receptor (R) – ligand (L) binding; phosphorylated (LRp) and active (LR*) complexes; receptor internalization, recycling and degradation; G-protein-PLC-IP3 pathway leading to the release of intracellular calcium; and calcium-calcineurin pathway for NFAT4 nuclear translocation. Red circle with a line indicates degradation. Some important rate constants are shown. Model equations and parameter values are available in the Appendix 2 Text 2A.2. B. Simultaneous observation of intracellular calcium concentration and NFAT4 in single cells under pulsatile ligand stimulation. C. Calcium and NFAT4 dynamics for a population of cells (20 cells) under step and pulsatile ligand stimulation shows signalling amid cell-to-cell variability.

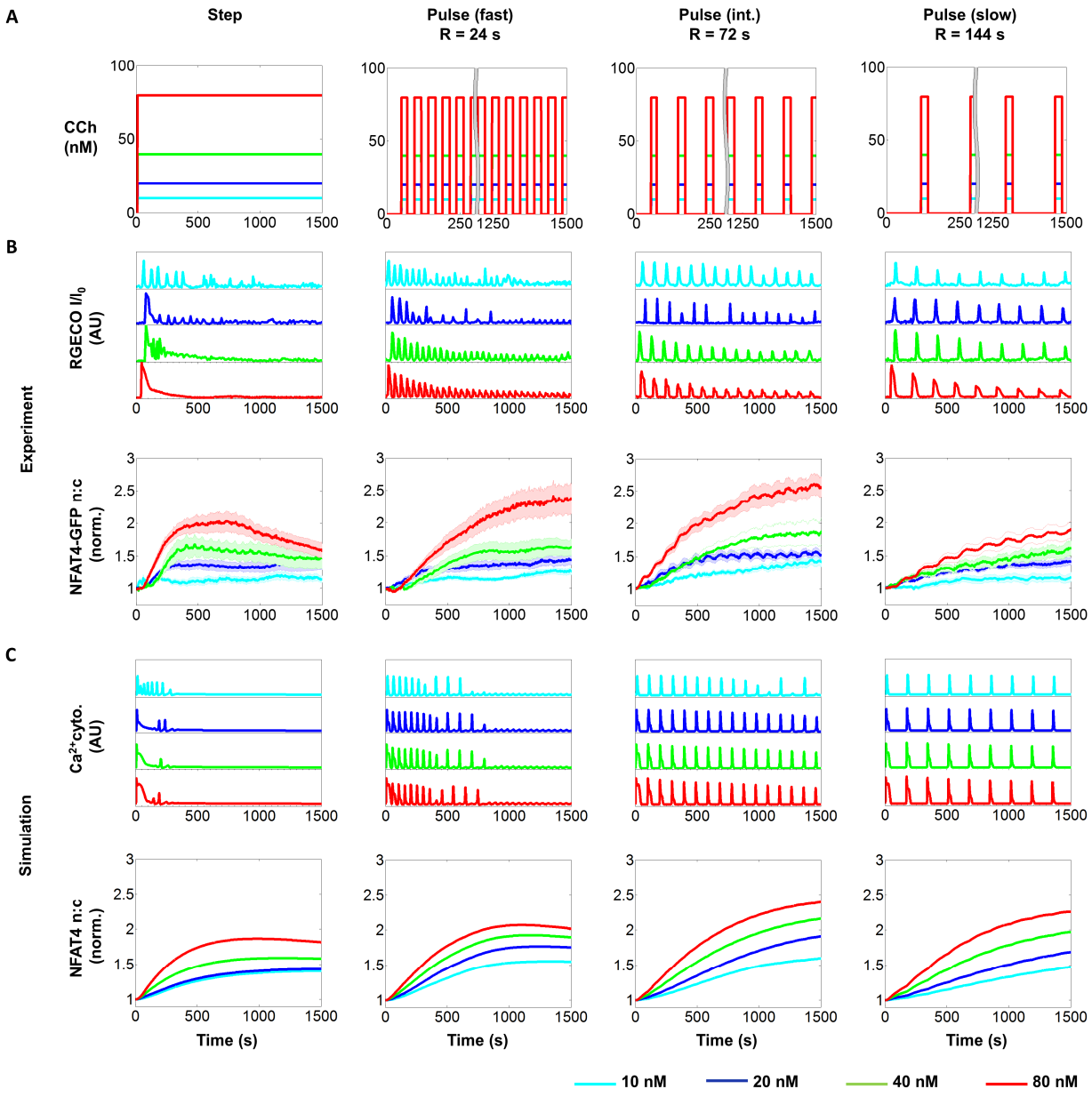

Fig. 2.2. Calcium and NFAT dynamics under step and pulsatile ligand stimulations. A. Step and pulsed stimulation with carbachol (CCh) performed in microfluidic experiments and simulations. The concentrations of CCh are as indicated in the color coded key. Pulse duration (D) was 24 s. B. CCh-induced time courses of cytosolic calcium (representative single cell traces) and NFAT4 nuclear translocation (population averages) by step (left column) and pulse (fast (R=24 s), intermediate (R=72 s) and slow (R=144 s)) stimulation in HEK293 cells stably expressing M3 receptor. Population averages are mean +/- S.E.M. for n > 20 cells from 3 sets of experiments. C. CCh-induced calcium and NFAT4 nuclear translocation in the mathematical model, which captures the characteristic features of both calcium and NFAT4 translocation response.

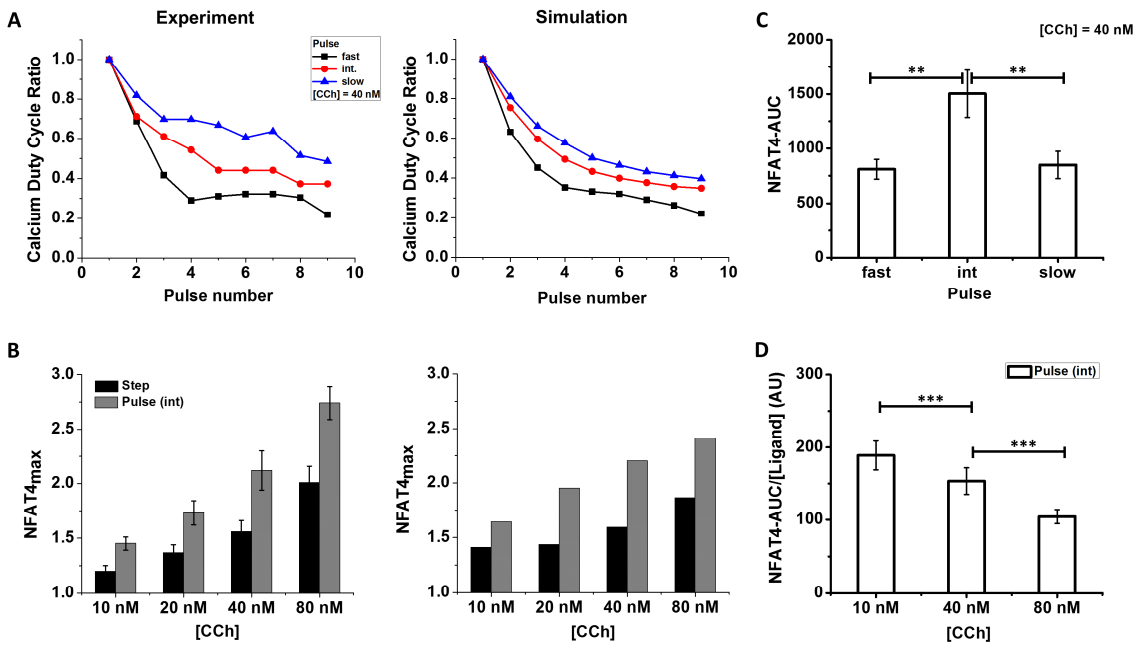

Fig. 2.3. Ligand pulse frequency affects calcium duty cycle and NFAT4 response. A. The calcium duty cycle ratio (ratio of the calcium-AUC of the nth pulse to that of the first one) decreases with consecutive stimulations. The decay is greater for faster ligand pulses than for slower pulses. Duty cycle in experiments (left) was calculated from population-averaged data for each pulse condition, and the mathematical model shows similar trends (right). [CCh] = 40 nM. B. Greater NFAT4 translocation under pulsatile stimulation (R = 72 s) for all ligand concentrations in the experimental regime (left), with a similar trend predicted by the mathematical model (right). C. NFAT4-AUC was calculated from experimental data for three pulse frequencies at [CCh] = 40 nM (mean +/- S.E.M., n > 20 single cells for three different sets of experiments), and shows that maximum NFAT4 nuclear translocation occurs at an intermediate frequency. D. NFAT4-AUC per unit ligand was calculated from experimental data for intermediate frequency pulse. Ligand efficiency is greater at low ligand concentrations. Results for other pulse frequencies and the model are shown in Appendix 2 Fig. 2B.4. (**: $P < 0.01$ based on t-test for statistical data).

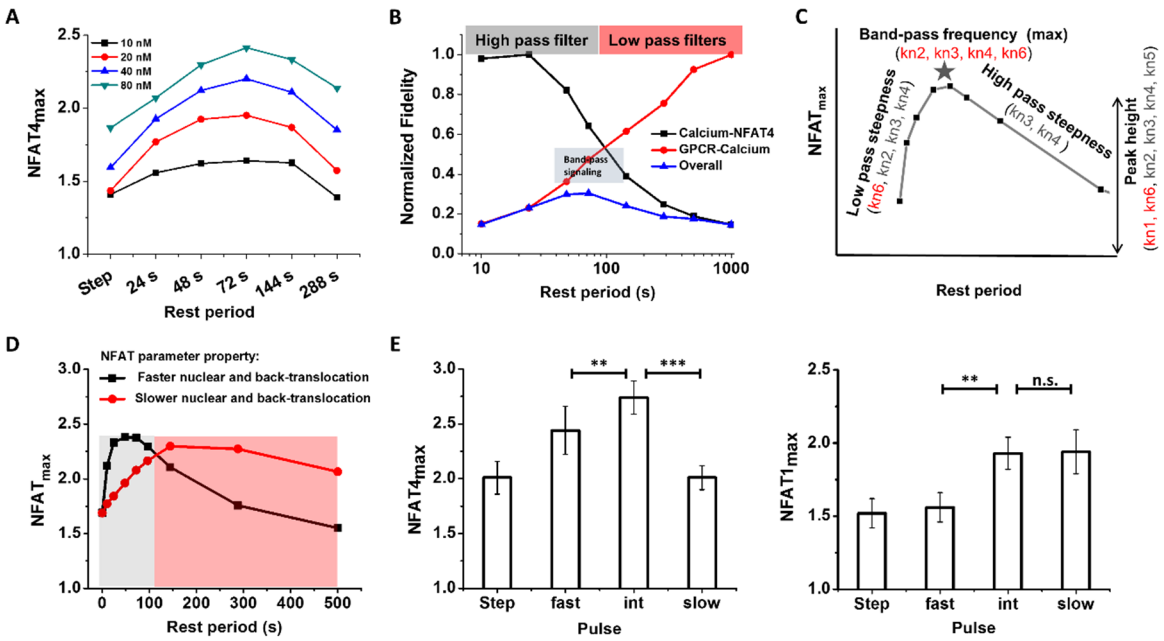

Fig. 4. Receptor and NFAT kinetics regulate band-pass behavior in GPCR-calcium-NFAT signalling. A. NFAT4max for various rest periods and ligand concentrations calculated from the mathematical model shows band-pass behavior. B. Turning off receptor desensitization in the model leads to a high-pass calcium-NFAT4 curve (black), while turning it on adds features of rapid calcium duty cycle decay with fast pulse stimulation due to desensitization and degradation (red). Both signalling fidelity curves are normalized with respect to their maximum value. Overall curve (blue) is an empirical multiplication of the two. C. Sensitivity analysis identifies parameters that significantly affect the band-pass characteristic features. Rate constants for: activated NFAT complex formation (kn1); dissociation of $NFAT_{cyto}$ from the complex (kn2); nuclear translocation of activated complex (kn3); dissociation of $NFAT_{nuc}$ from the activated complex (kn4); association of $NFAT_{nuc}$ and calcineurin (kn5); and back-translocation of $NFAT_{nuc}$ (kn6). D. The band-pass regime shows a shift to the left or right for two different parameter sets. Parameter set 1: kn2 = 0.002 s-1; kn4 = 0.000445 s^{-1}; kn6 = $2*10^{-4}$ s^{-1}; Parameter set 2: kn2 = 0.02 s^{-1}; kn4 = 0.0013 s^{-1}; kn6 = 0.25 s^{-1}. Other parameters kn1 = $7.7*10^{-6}$ $(nM\text{-}s)^{-1}$; kn3 = 0.001 s^{-1}; kn5 = $4.7*10^{-5}$ $(nM\text{-}s)^{-1}$; C = 20 nM, D = 24 s remain the same. E. Experiment demonstrating shift in optimum frequency regime for $NFAT1_{max}$ as compared to $NFAT4_{max}$ (n > 20 single cells for three different sets of experiments; **: P <0.01; ***: P <0.005; n.s.: not significant based on t-test for statistical data).

Chapter 3. Cellular responsiveness to weak physiological stimuli is fate not luck

3.1. Introduction

Fundamental to deciphering receptor-mediated cell signaling processes is to know if the processes are stochastic or deterministic (Tay *et al*, 2010; Zambrano *et al*, 2014a; Turner *et al*, 2010; Keenan *et al*, 2004; Losick & Desplan, 2008; Bhola & Simon, 2009). Stochastic models are often invoked to provide insights where deterministic models fail (Das *et al*, 2009; Ullah & Wolkenhauer, 2010; Tay *et al*, 2010; Turner *et al*, 2010). Nonetheless, deterministic models, when successful, have an advantage in terms of the ease with which characteristic behaviors can be described and predicted (Scott *et al*, 2007). Physiologically relevant stimulations that are transitory and weak often result in responses that appear stochastic. These common observations have been difficult to explain with existing deterministic models and have been attributed to stochasticity (Tay *et al*, 2010; Turner *et al*, 2010). In this chapter, we show that such cases may be well described by deterministic processes in which there is a high Hill coefficient step and cell-to-cell variability. Additionally, we describe a tractable, rest period-based, two-pulse experimental test (hereafter referred to as the "rest period test") that can confirm that an apparently stochastic response may have a deterministic basis.

Our analysis employs a combined experimental and computational approach. Single HEK-293 cells stably expressing muscarinic M3 receptors, a G-protein couple receptor (GPCR), were stimulated by two consecutive low-concentration pulses of an M3-agonist within a microfluidic device. Calcium responses were quantified using live cell imaging as described in Chapter 2 (Sumit *et al*, 2015). Building upon our previous deterministic model (Jovic *et al*, 2010, 2011; Sumit *et al*, 2015), we additionally incorporated cell population heterogeneity (sometimes referred to as extrinsic noise). To illustrate broad applicability of our findings beyond the M3 signaling pathway, we also analyzed published data on the TNFα-NFkB pathway (Zambrano *et al*, 2016, 2014a; Tay *et al*, 2010), which operates at an entirely different timescale (several

minutes to hours), and reveal that its apparently stochastic response can also be explained with a deterministic process when cell population heterogeneity is considered.

3.2. Results

3.2.1. Microfluidic two-pulse experiments show population heterogeneity in calcium response upon stimulation in a physiologically relevant concentration regime

We designed a microfluidic experiment entailing cell stimulation with two pulses of carbachol (CCh), which binds and activates the M3 muscarinic receptor, with concentration (C) and pulse duration (D), separated by a rest period (R). The concentration regime chosen (~ 5 - 10 nM CCh) was low enough to be insignificant for receptor desensitization and sufficient to generate cell populations with wide ranges of activation probability (Jovic *et al*, 2010, 2011, 2013). We measured cytoplasmic calcium as our read-out by transiently transfecting the HEK-293 cells with RGECO-1 calcium sensor (Sumit *et al*, 2015). These cells were stimulated within a microfluidic device that can deliver temporal rectangular pulses of ligand as described previously (Gu *et al*, 2004; Jovic *et al*, 2010, 2011; Sumit *et al*, 2015). For each pulse of ligand, a cell may or may not respond with a calcium peak. A full or near-full peak response is designated as output '1' in the scheme, while no response or a sub-threshold peak is designated as output '0' (Fig. 3.1. A). Thus, for a two-pulse scheme, the four combinatorial responses possible for any cell are: no response to both pulses (0,0), a calcium peak response only to the second stimulation pulse (0,1), a calcium peak response only to the first stimulation pulse (1,0) or calcium peak responses to both stimulation pulses (1,1). Choosing an intermediate concentration in the test regime (C = 7.5 nM) and pulse duration that produces non-saturating calcium responses (D = 16 s), we observed population heterogeneity in the calcium responses (Fig. 3.1. B), and the responses could be separated into the four possible outcomes (Fig. 3.1. C). The existence of (1,1) and (0,0) responses is relatively easy to explain within a deterministic framework. However, the explanation for the simultaneous existence of (0,1) and (1,0) responses using a deterministic mathematical model has not been shown and often leads to the conclusion that the response outcomes have stochastic origins. Here, we will refer to the simultaneous presence of such (0,1) and (1,0) responses within the cell population as "apparently stochastic" behavior of cells.

3.2.2. A mathematical model with deterministic reaction kinetics and cell-to-cell variability exhibits apparently stochastic responses

We previously reported a deterministic mathematical model that captures most of the population scale calcium response characteristics under step and pulsatile stimulation (Sumit *et al*, 2015; Jovic *et al*, 2011, 2010). To account for heterogeneity in responses at the single cell level, we additionally incorporated cell-to-cell variability into our mathematical model. Population heterogeneity was introduced in the model by incorporating a uniform distribution in the concentration of the three key signaling components of the model (Fig. 3.2. A). The extent of extrinsic noise in the signaling pathway was determined experimentally following a method described previously (Selimkhanov *et al*, 2014). Briefly, several hundred single cell calcium time traces were recorded for a step change in ligand concentration from C = 0 nM to C = 10, 20, 40 and 80 nM respectively in order to calculate the signal-to-noise ratio (SNR) and intrinsic-to-extrinsic noise ratio (IER) for the CCh-induced calcium response, as described in Methods. Subsequently, the distribution of the concentration of key signaling components was set such that it matches the experimentally observed SNR. Using the updated model, we generated hundreds of *in silico* single cell calcium traces under the two-pulse stimulation scheme (Fig. 3.2. B). These calcium traces show features similar to those observed in our microfluidic pulsatile stimulation experiments, and we were able to obtain all four possible combinatorial outcomes (Fig. 3.2. C). We determined how individual components in the signaling pathway determine the fate of cells in terms of one of the four possibilities. While the biochemical variability in each of the signaling components affected the responses, an overall cumulative parameter Q (calculated by multiplying together the concentrations of the three major components in the pathway that vary from cell-to-cell) clearly distinguishes the four outcomes indicating that the biochemical noise cumulatively may affect the downstream cell fates (Appendix 3 Fig. 3A.1.). Taken together, our deterministic mathematical model with added cell-to-cell variability captures the population heterogeneity and all four possible outcomes under the two-pulse scheme, including (0,1) and (1,0) responses, as observed experimentally.

3.2.3. Rest period reveals deterministic basis for 'apparent stochasticity' responses

The existence of all four possible outcomes for the two-pulse test (both in model and in experiment) raises an interesting question: is the subpopulation composition, i.e. the fraction of cells responding in each way, related to the rest period R between the pulses? In the case of deterministic origins, increasing R should allow better uncoupling of the two responses. In particular, for longer rest periods, the second response should look more like the first response,

i.e., majority of cells should behave either in (0,0) or in (1,1) fashion. Thus, the subpopulation composition should change with R. This is unlike the stochastic case, where one would not expect any relationship between R and the cellular responses. We tested this hypothesis with two widely separated rest periods (R = 24 sec and R = 120 sec, C = 7.5 nM), both *in silico* and with microfluidic experiments (Fig. 3.3.). For three different durations of pulsed stimulation (D = 8, 16 and 24 sec) the 'apparently stochastic response', denoted by the summation of (0,1) and (1,0) responses, decreases with increasing R (Fig. 3.3. A) while the repeated response denoted by the summation of (0,0) and (1,1) responses, increases with increasing R (Fig. 3.3. B). Our deterministic model and microfluidic experiments also predict that the effect of R on each subpopulation in GPCR-calcium signaling is monotonic and predictable for various pulse concentrations and durations in the tested regime (Appendix 3 Fig. 3A.2 and 3A.3.). When the 'rest period test' was extended to three pulses in the model, we observed a similar effect of rest period, i.e., with increasing R, the system tends to either respond completely (1,1,1) or not at all (0,0,0), thus showing better uncoupling as R is increased (Fig 3A.4.). Taken together, we find that the rest period determines the extent of apparent stochasticity in the response.

3.2.4. Rest period test reveals deterministic basis for apparent stochasticity in another signaling system (TNF-α -NFkB signaling)

Our model and experiments support a deterministic origin for the apparently stochastic behavior we observed in the GPCR-calcium signaling pathway. Next, we asked whether the same might be true for another oscillatory system with different components that signals at a different time scale. NFκB (Nuclear Factor κB) oscillations are observed upon TNF-α (Tumor Necrosis Factor-α) stimulation in majority of immune cells. The time scale of TNF-α induced NFkB signaling is from several minutes to hours, unlike the GPCR-calcium system where signaling is in the order of seconds to minutes. Briefly, nuclear localization and transcriptional activity of NFκB upon stimulation of TNF-receptor is regulated through negative feedbacks by A20 and IκBα at different levels of signaling. The activation of IKK-α is modeled as a high Hill coefficient pathway (Fig. 3.4. A). Model equations and parameters can be found in (Tay *et al*, 2010). Using microfluidic two-pulse stimulation of TNF-α in 3T3 mouse fibroblasts and measuring nuclear localization of NFkB, Tay *et al* (Tay *et al*, 2010) showed the existence all four possible signaling outcomes in the cell population, i.e., (0,0), (0,1), (1,0) and (1,1) responses. They suggested that the single peak responses (i.e., (0,1) and (1,0)) were stochastic in origin and developed a stochastic

model based on a previously existing deterministic model (Ashall *et al*, 2009). We hypothesized that their deterministic model alone may be able to generate all four possible outcomes upon incorporation of cell-to-cell variability and performed a sensitivity analysis of the entire parameter set of their model to identify parameters that significantly influence peak height (Marino *et al*, 2008). We limited exploration of the parameter space such that the parameters were of the same order of magnitude as reported in Tay *et al*. Table 3B.1. lists parameters significantly correlated with first and second peak responses (Appendix 3). We generated cell-to-cell variability by sampling from a uniform distribution of the sensitive parameters. Under the same stimulation conditions used by Tay *et al*, we found that a modification of their deterministic model that incorporates cell-to-cell variability in the sensitive parameters exhibits all four outcomes of the two-pulse experiment with sub-population compositions similar to the reported experimental values (Fig. 3.4. B, C). Moreover, the effect of increasing concentration and pulse duration in the NFkB model are similar to our GPCR model (Appendix 3 Fig. 3A.5.). With increasing R, the subpopulation (1,1) increases while (0,1) decreases, similar to the trends observed in the GPCR model (Appendix 3 Fig. 3A.6.). The (0,0) response increases while (1,0) decreases with increasing R, similar to the trend we observe in GPCR signaling, although these are somewhat non-monotonic around R ~ 200 min. We also applied the "rest period test" to recently reported experimental data for pulsatile stimulation with low concentration TNF-α (0.1 ng/ml) (Zambrano *et al*, 2016). We found that the 'apparently stochastic response' denoted by the summation of (0,1) and (1,0) responses is reduced at a longer rest period (R = 150 min) as compared to a shorter rest period (R = 22.5 min) while the repeated response (summation of (0,0) and (1,1) fractions) increases at longer R, similar to what we observe for the GPCR-calcium experiments (Fig 3.4. D). These computational and experimental findings suggest that the apparently stochastic NFκB signaling is more consistent with a deterministic process rather than the previously proposed stochastic mechanism.

3.2.5. A high Hill-coefficient process and pathway recovery properties govern the apparent stochastic responses

The results above raise interesting questions about the internal mechanism of the signaling pathway that leads to such apparently stochastic responses. We analyzed our GPCR-calcium model for each node in the signaling pathway for the two subpopulations (0,0) and (1,1). While the two subpopulations differed slightly in the concentrations of activated receptor complex, total

G-protein and activated PLC, a much greater difference was seen downstream of PLC, i.e., at IP_3, leading to a seemingly bifurcated downstream response (Appendix 3 Fig. 3A.7.). This is due to the high Hill coefficient step (H~3) at this point in the signaling pathway. We also tested the deterministic NFkB model. Similar to our GPCR model, we found that the bifurcation is a result of a high Hill coefficient step (H~2) in the signaling pathway, in this case in the generation of active IKK, a major component in TNFα-NFkB signaling (Appendix 3 Fig. 3A.8.). Interestingly, in both the models, a (1,0) response gradually changes to a (1,1) response and a (0,1) response to a (0,0) response with increasing R so that the sum of (1,0) and (1,1) subpopulations, as well as the sum of (0,0) and (0,1) subpopulations, remains constant (Appendix 3 Fig. 3A.9.). While the former change is generally observed in signaling pathways where increasing R increases the response fidelity (Jovic *et al*, 2011), the latter is less intuitive. We investigated this by performing a component-wise analysis of the GPCR model for three different R values (R = 120 s, 200 s and 300 s) (Appendix 3 Fig. 3A.10.). We find that although a '0' or sub-threshold calcium response occurs for a sub-population of cells for the first stimulation, it does create a short-term memory of the stimulation in the ER because calcium is pumped into the ER upon stimulation. This calcium gradually leaks out of the ER reservoir. An early second stimulation helps the ER reach its threshold to release the calcium and hence the cell responds; a delayed second stimulation does not have this advantage (Appendix 3 Fig. 3A.10.) (Jovic *et al*, 2013). Similarly, we find that, in the TNF-α-NFκB model, receptor activation creates a short memory of the stimulation through IKK kinase signaling. For shorter R, the active IKK kinase level increases more upon a second stimulation despite a '0' NFkB response against the first stimulation. This increase in IKK kinase gets amplified via a high Hill coefficient pathway downstream (Appendix 3 Fig. 3A.11.), thus making the 'apparently stochastic response' sensitive to R. Taken together, the apparently stochastic response varies with the duration of the rest period (R) due to slower recovery of intermediate signaling processes.

3.3. Discussion

Physiologically relevant weak stimulations, often low concentration pulsatile bursts, can lead to downstream responses that appear stochastic. A better understanding of how stimulation parameters govern response patterns and overall response fidelity in a signaling system is fundamental to biology, and will be useful to pharmacological, *in vitro* culture and synthetic biology applications. A simple illustration is a two pulse stimulation for which there are four

possible outcomes i.e., (0,0), (0,1), (1,0) and (1,1). The simultaneous observation of (0,1) and (1,0) responses is often interpreted to indicate stochastic origins. Here, we show instead that such responses can have a deterministic origin. To summarize our understanding from the computational and experimental results in the previous sections, we assign single peak responses (i.e., (0,1) and (1,0)) as 'apparently' stochastic events, and define 'apparent stochasticity' as follows:

$$Apparent\ stochasticity = \{f_{(0,1)} + f_{(1,0)}\}$$

where, $f_{(0,1)}$ and $f_{(1,0)}$ are the fractions of (0,1) and (1,0) subpopulations respectively. Analysis of our GPCR-calcium model showed that the apparent stochasticity decreases with C*D and R (Fig 3.5. A). While it is known that the fractions of cells responding to a pair of ligand pulses are governed by concentration C and stimulation duration D, we newly show that the role of rest period R is equally important in determining the distribution of possible outcomes. We found similar trends for an NFkB deterministic model, wherein a low C*D and R regime resulted in maximum apparent stochastic response (Fig 3.5. B). Importantly, the stochastic model reported in Tay *et al* (Tay *et al*, 2010) did not exhibit any significant changes in the fraction of (0,1) and (1,0) subpopulations and consequently the apparent stochasticity $\{f_{(0,1)} + f_{(1,0)}\}$, with changes in R (Fig. 3.5. C). This difference in subpopulation shifts between the stochastic and deterministic mechanisms allow a tractable, two-pulse, rest period test to distinguish between the two mechanisms. We find that increasing R results in a reduction of apparent stochasticity under conditions when 'true stochastic responses' should remain unchanged (Fig. 3.5.). Because our system is consistent with a deterministic framework of 'apparent stochastic responses', cell responsiveness can be tuned with stimulation parameters C, D and R. This has relevance to *in vitro* cell culture protocols in lab-on-a-chip devices with dynamic input to enhance downstream signaling (Yum *et al*, 2014) as well as in the design of pharmacological interventions that consider both responsive and non-responsive cells within a population.

An important consideration in this study is to distinguish 'apparent' stochastic events from 'true' stochastic responses. At very low concentrations of components (such as low number of ligand molecules ~ 10^0 – 10^2 per cell), true stochastic behavior is expected. However, for the microfluidic devices commonly used in pulsatile stimulation experiments, the response is

integrated over the pulse duration and the ligand is periodically or continuously replenished. Thus, the total number of ligand molecules exposed to the cells is in the order of ~10^6 (for carbachol) and ~10^4 (for TNF-α) (Appendix 3 Text 3C.1.). These relatively high levels of exposure to ligands are consistent with an apparent stochastic response rather than a true stochastic response. Similarly, the likelihood of intracellular stochasticity is quite low as the number of molecules at each step is estimated to be greater than 10^3 per cell for NFκB models (Zambrano *et al*, 2014b; Tay *et al*, 2010).

Most cell studies focus on high concentration stimulation to determine the minimum 'reset' time a signaling system might require to recover between stimulation events. Observables like peak amplitude are often used to assess this reset time, by monitoring the amount of time needed between stimulation events that results in signaling responses of equal peak amplitudes. It is often assumed that reset times that are assessed at high stimulation concentrations are sufficient for resetting the signaling system upon exposure to low concentrations (Tay *et al*, 2010). However, our work provides new insights into how this assumption could be problematic and suggests that low concentration regimes, in which receptor desensitization does not dominate in determining recovery time, should be treated differently. Rather, the positive and negative feedback mechanisms and high Hill coefficient processes in the downstream signal play crucial roles, along with cell-to-cell variability, in determining the downstream response.

Most analyses of single cell responses discard data from non-responding cells and use data only from responsive cells (Thurley *et al*, 2014; Dhumpa *et al*, 2014; Jovic *et al*, 2011). Others stimulate cells at a very high concentration of ligand to avoid this non-responsive regime (Ashall *et al*, 2009). Such analyses could miss the overall picture of signaling architecture and the role of cell-to-cell variability in governing the population response. Our results suggest that non-responding cells represent a legitimate response under a deterministic framework. More broadly, our results suggest that physiological, low concentration pulsing of signals is a deterministic strategy for the body to guide distinct subsets of cells to their appropriate fate rather than a stochastic process that leaves outcomes to chance.

3.4. Conclusion

Physiological stimulations that are transitory and weak, such as low concentrations of acetylcholine present for just tens of seconds or TNFα for just tens of minutes, lead to irregular

downstream responses that are often interpreted as stochastic. Here, we provide a deterministic explanation for this behavior that is based on cell-to-cell variability, a short-term memory of stimulation, and high Hill coefficient processes, providing data on muscarinic M3 receptor-induced calcium signaling as an example. Furthermore, we provide a tractable, two-pulse experimental test that utilizes different rest periods between the stimulation pulses to determine if an apparently stochastic response in a dynamic signaling process has a deterministic basis. These analyses reveal that the seemingly random responses of cells to weak stimuli are determined by the signaling capacity of cells and the stimulation timing. The results suggest that physiological, low concentration pulsing of signals is a deterministic strategy for the body to guide distinct subsets of cells to their appropriate fate rather than a stochastic process that leaves outcomes to chance.

3.5. Materials and Methods

Materials

Materials used for experiments in this Chapter are detailed in Appendix 1.

Methods

Methods description about cell culture, seeding cells in microfluidic device and time lapse image and analysis are detailed in Appendix 1.

Calculating signal-to-noise ratio (SNR) and intrinsic-to-extrinsic noise ratio (IER). We adapted the method for experimental noise analysis provided in the supplementary section of a recent article (Selimkhanov *et al*, 2014). We first calculate the signal magnitude σ^2_r (variance of average responses over all m input concentrations) as:

$$\sigma_r^2 = \frac{1}{m}\sum_{i=1}^{m}((\frac{1}{m}\sum_{w=1}^{m}\frac{1}{n_w}\sum_{j=1}^{n_w} r_{wj}) - \frac{1}{n_i}\sum_{j=1}^{n_i} r_{ij}))^2$$

Noise magnitude σ^2_n is calculated as the average of the variances of n_i responses to a single input level as:

$$\sigma_n^2 = \frac{1}{m}\sum_{i=1}^{m}(\frac{1}{n_i}\sum_{j=1}^{n_i}\frac{1}{n_i}\sum_{w=1}^{n_i} r_{iw} - r_{ij})^2$$

The signal-to-noise ratio (SNR) is then defined as the ratio, σ_r^2/σ_n^2.

To calculate intrinsic-to-extrinsic noise ratio (IER), we used the portion of calcium traces from step changes where the intensity did not change significantly. Intrinsic noise (σ_ξ^2) was estimated as the variance of the differences in RGECO intensities between successive time points. Total noise (σ_t^2) was calculate similar to the noise magnitude, σ_n^2, but taking only the static region of the calcium traces. Extrinsic noise is then calculated as $\sigma_e^2 = \sigma_t^2 - \sigma_\xi^2$. The ratio σ_i^2/σ_e^2 is IER. Based on the noise analysis, we incorporated cell-to-cell variability in the form of a uniform distribution of +/- 20% in the model parameters viz. the receptor, total G-protein and the PLC concentration. The intrinsic noise (+/- 5%, normally distributed throughout the dynamic data was minimal and did not affect the calculation for '0' (non-responding) and '1' (responding) cells.

Mathematical model and computational analysis

GPCR-calcium model with extrinsic noise. Previously, we developed a mathematical model that links step/pulsatile ligand stimulation, receptor/ligand binding, calcium signaling and captures the characteristic features of the microfluidic pulsatile experiments (Jovic *et al*, 2010, 2011; Sumit *et al*, 2015). The model description, reactions and parameter values are as detailed in our previous work (Sumit *et al*, 2015) as well as in Appendix 2 Text 2A.1-2. To incorporate extrinsic noise, the values for three major nodes in the pathway, the receptor, G-protein and PLC concentrations, were chosen from a uniform distribution around the mean value so that the SNR matches with the experimentally calculated value.

Computational analysis. A system of ordinary differential equations (ODEs) was generated for the model and solved in MATLAB (MathWorks Inc., Natick, MA) with the ode15s stiff solver. Experimental data for more than 1000 cells under pulsatile stimulation conditions for various concentrations (C = 10 nM, 20 nM, 40 nM, and 80 nM) were analyzed to determine Signal-to-Noise Ratio (SNR) and Intrinsic-to-Extrinsic Noise Ratio (IER) following a method described in Selimkhanov et al (Selimkhanov *et al*, 2014). These quantities provided an estimate of plausible range of extrinsic noise in our signaling system. Based on the noise analysis of experimental data, the initial values for core signaling components i.e., GPCR, G-protein and PLC were chosen from a 20% uniform distribution around the mean value using latin hypercube sampling (LHS) (Marino *et al*, 2008). Thus, *in silico* cell-to-cell variability was generated for three independent runs each consisting 250 LHS parameter sets. Analysis of the individual traces for peak finding and

determining fraction of subpopulations of (0,0), (0,1), (1, 0) and (1,1) was done by writing script files in MATLAB.

TNFα-NFkB deterministic model with extrinsic noise. We used the deterministic as well as the stochastic version of the TNFα-NFkB model from (Tay *et al*, 2010). We performed sensitivity analysis of all the parameters used in the model to determine the parameters sensitive to both first and second peak in the *in silico* two pulse experiment (Appendix Table S1). Subsequently, cell-to-cell variability was incorporated in the deterministic model using similar method as described in the previous section by generating a distribution in sensitive parameters limited within the same log scale. The rest of the analyses were done similar to that for the GPCR model.

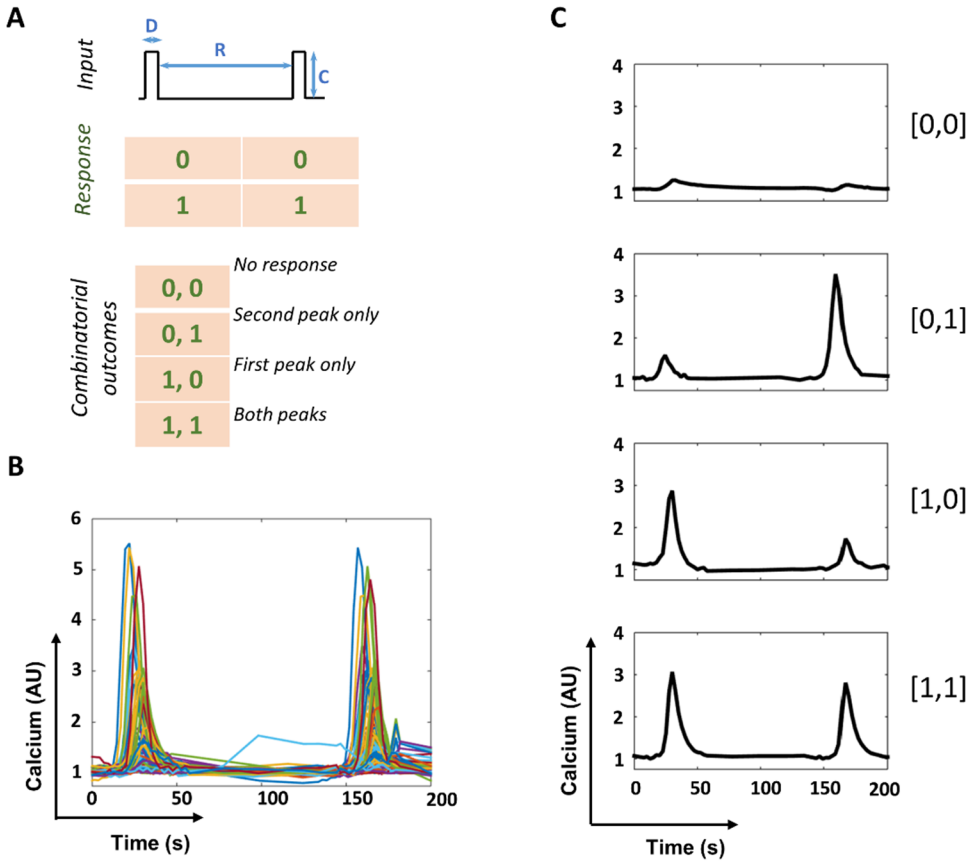

Fig. 3.1. Two pulse experiments: experimental design and data. A. Design of pulsatile stimulation experiments, in which two outcomes are possible for each stimulation (0 and 1), leading to four possibilities for two-pulse experiments. B. Cells are stimulated twice with carbachol, a muscarinic-M3 agonist, for short pulse durations D (sec) at concentration C (nM) with in-between rest period R (sec) as shown in (A) to yield digital yes/no responses against each pulse. C. Responses vary from cell to cell and can be (i) no response, (ii) only second peak response, (iii) only first peak response, or (iv) both peak responses. Sub-threshold peaks (peaks < 0.3 times the maximum) are not counted as responses. C = 7.5 nM, D = 16 s, R = 200 s, for a total of 90 cells from 3 different experiments.

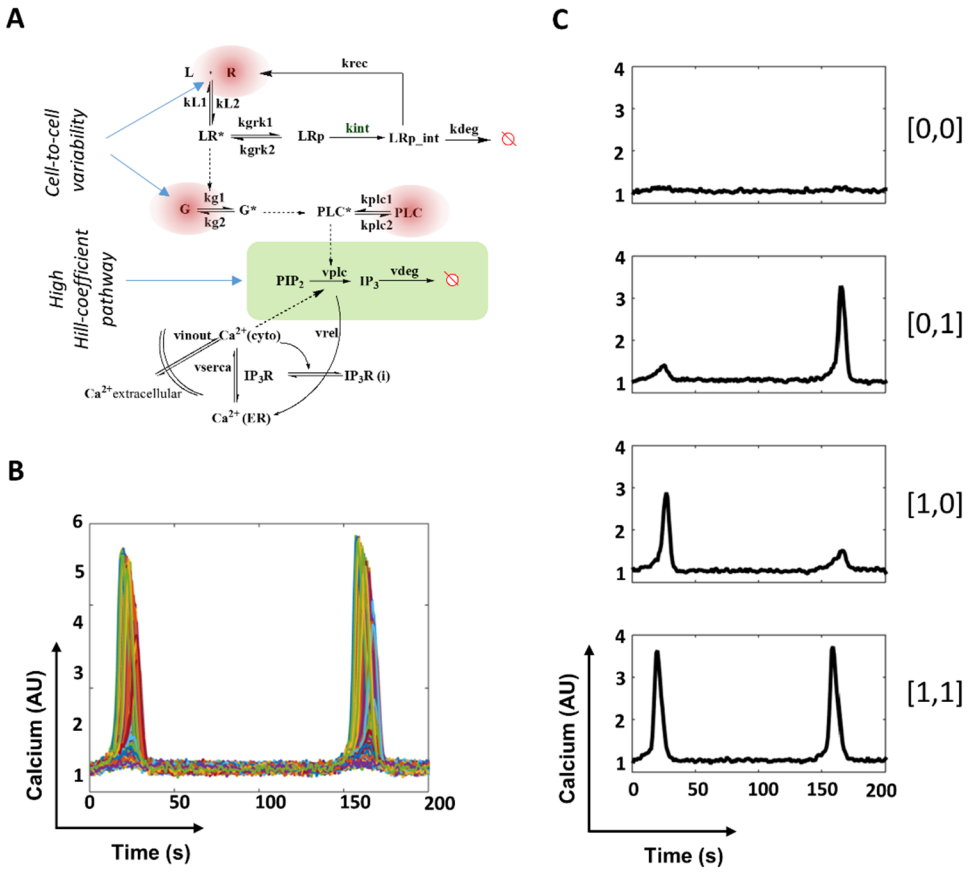

Fig. 3.2. Deterministic mathematical model with cell-to-cell variability exhibits all four possible outcomes. A. Model Schematic. Ligand (L) binds to receptor (R) to form LR complex which initiates G-protein mediated PLC activation and IP3 generation, ultimately leading to the observed calcium responses. The nodes shaded in red indicate where cell to cell variability is introduced in the model. PIP2 to IP3 pathway activated by PLC (shaded in light green) denotes a high Hill coefficient pathway. Model equations can be found in Appendix to Chapter 2 as well as in (Sumit *et al*, 2015). B. *In silico* ligand stimulation, generated with the model with cell-to-cell variability (extrinsic noise) of +/- 20 % in [GPCR], $[G]_{tot}$ and $[PLC]_{tot}$. C. Model calcium traces showing the four possible outcomes similar to the experimental data, i.e., (i) no response, (ii) only second peak response, (iii) only first peak response, or (iv) both peaks. Sub-threshold peaks (defined here as peaks < 0.3 times the maximum) are not counted as responses. C = 7.5 nM, D = 16 s, R = 120 s.

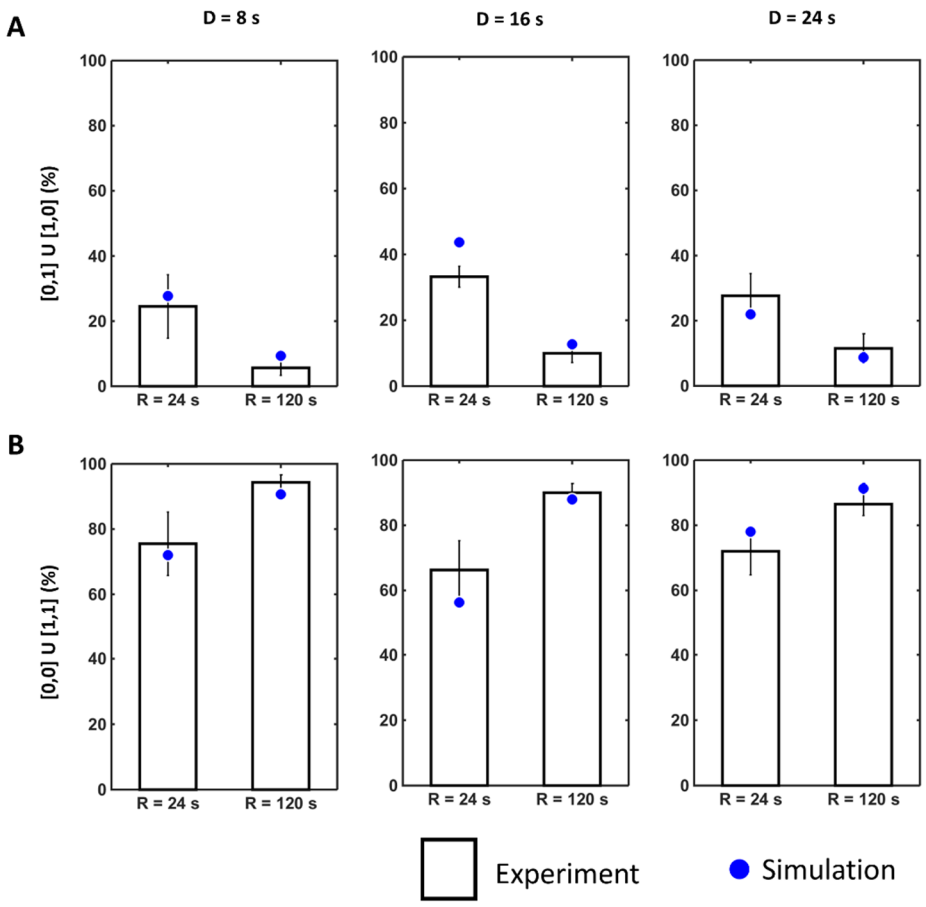

Fig. 3.3. Rest period determines subpopulation composition and apparent stochasticity. Microfluidic two-pulse test with widely separated rest periods (R = 24 s and R = 120 s) shows that subpopulation composition changes with R in a predictable fashion for different pulse durations tested (D = 8 s, 16 s and 24 s; C = 7.5 nM). A. The 'apparently stochastic' response denoted by the summation of (0,1) and (1,0) subpopulations (i.e., [0,1] U [1,0]) decreases with increasing R for all the pulse duration tested. B. The response denoted by the summation of (0,0) and (1,1) subpopulations (i.e., [0,0] U [1,1]) increases with increasing R, indicating greater uncoupling of responses at longer rest periods. Experimental results are shown as bars, and simulation results are shown as blue scatter points. Data information: In (A-B), experimental data (bars) are presented as mean +/- standard deviation (s.d.) for three sets of experiments, with ~ 50 cells in each set.

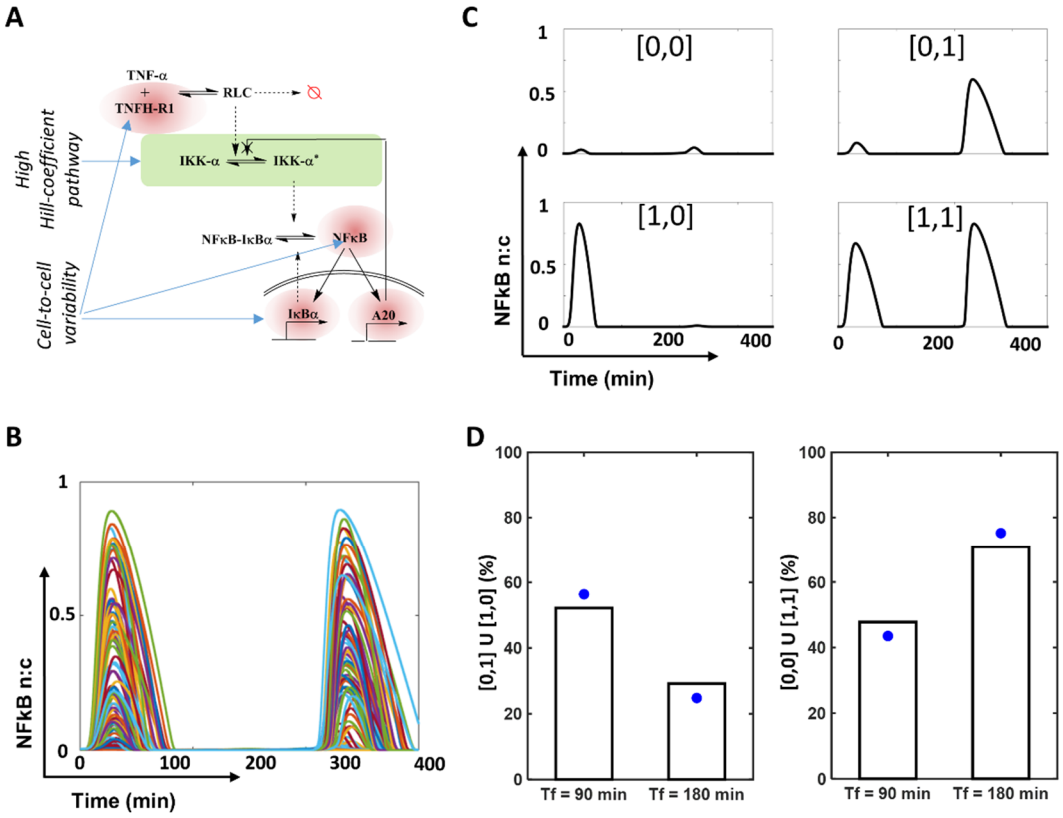

Fig. 3.4. TNF-α-NFkB signaling model also shows apparent stochastic behavior under low concentration pulsatile stimulation, similar to the GPCR-calcium signaling. A. Brief schematic of TNF-α-NFκB signaling. Nuclear localization and transcriptional activity of NFκB upon stimulation of TNF-receptor is regulated through negative feedbacks by A20 and IκBα at different levels of signaling. The activation of IKK-α is modeled as a high Hill coefficient pathway. Model equations and parameters can be found in (Tay *et al*, 2010). B. Using sensitivity analysis to determine parameters affecting the first and second peaks differentially and then imposing a small cell-to-cell variability in the parameters, the deterministic NFkB model can produce the four subpopulation outcomes, including apparently stochastic responses. C. Representative *in silico* single cell traces of nuclear NFkB, showing all the four possible outcomes in a two pulse test using a deterministic model with cell to cell variability. D. Rest period test of NFκB signaling. Experimental data from (Zambrano *et al*, 2016) was examined by calculating the fraction of apparently stochastic response (0,1) and (1,0) and the rest of the sub-population (0,0) and (1,1) at low TNF-α stimulation (0.1 ng/ml). A shorter rest period (Tf = 90 min, D = 45 min, and R = 45 min) and a longer rest period (Tf = 180 min, D = 30 min, R = 150 min) were compared to find that the apparent stochastic response decreases with longer rest periods, similar to our experimental data for calcium response. The modified deterministic NFkB model also predicted similar results.

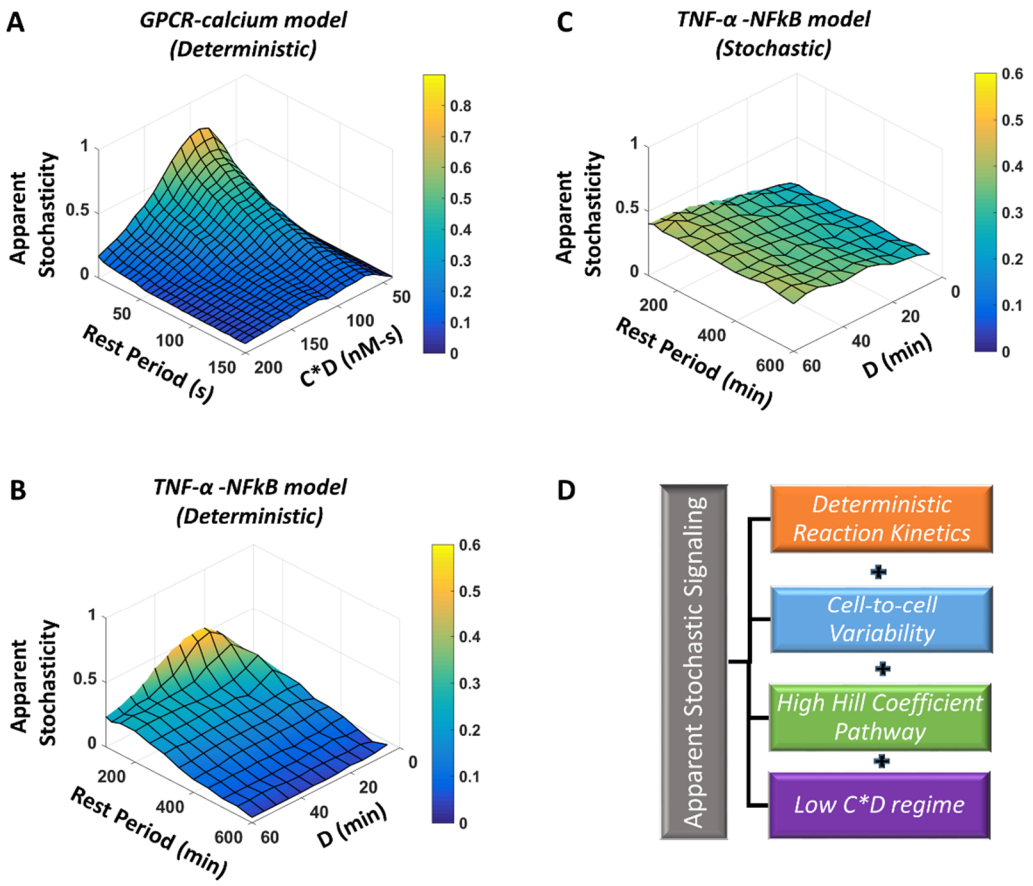

Fig. 3.5. Components that constitute an apparent stochastic cell signaling response. A. Analysis of our GPCR-calcium deterministic model reveals that the apparent stochasticity forms a hill-top in the low C-D-R regime and decreases with increasing R. B. Analysis of the TNF-α-NFκB deterministic model shows similar trend, with apparent stochasticity forming a hill-top in the low C-D-R regime and decreases with increasing R. C. TNF-α-NFκB stochastic model with no cell-to-cell variability shows an almost flat surface for apparent stochasticity, indicating that the rest period test would show no significant trend in the 'apparently stochastic response' in such models and experimental systems. D. Apparently stochastic signaling is a result of deterministic reaction kinetics with a high Hill coefficient pathway in a population with cell-to-cell variability, and is prominent in the low C-D-R regime, tractable by the rest period test.

Chapter 4. Pulsatile input enhances information transfer and downstream NFAT isoform sensitivity in a noisy GPCR-mediated pathway

4.1. Introduction

A primary role of biochemical signaling pathways is to communicate or access information from the extracellular micro-environment. This allows cells to respond to a variety of external cues and to bring about physiological or phenotypic changes. However, variability in the molecular abundance of signaling components (extrinsic noise) and inherent stochasticity in molecular interactions (intrinsic noise) often contribute to noisy transmission of signal information (Cheong *et al*, 2011). How cells process these noisy signals to facilitate reliable transmission of information is a fundamental question.

Of course, cells can respond to both step changes in signal as well as time-varying signals. In this chapter, we ask whether pulsed inputs facilitate information transfer in such noisy biochemical pathways. Taking muscarinic M3 receptor mediated signaling as an example, we employ information theoretic analysis to show that the pulsed input not only enhances information transfer to the downstream effectors, but also increases informational sensitivity towards topologically similar transcription factor isoforms.

Although a century old field of study (Nyquist, 1924; Hartley, 1928; Shannon, 1948, 1998), information theory has recently been applied to explore several biochemical pathways and motifs, as it provides a quantitative tool to estimate the maximum possible information transfer (Levchenko & Nemenman, 2014; Rhee *et al*, 2012; Cheong *et al*, 2011; Selimkhanov *et al*, 2014). These studies suggest that cells may not be capable of discerning very many ligand concentrations under noisy transmission and that the signaling dynamics may be playing a key role in partially mitigating the loss of information in a noisy pathway (Selimkhanov *et al*, 2014). Often, input to these biochemical pathways are not constant concentrations of ligands. They are rather pulsatile bursts of chemical release from neighboring tissue sources (and sometimes even paracrine), and are therefore time-varying (or dynamic) inputs (De Pittà *et al*, 2009; Chappell *et al*, 2003; Dyachok *et al*, 2006; Dunant *et al*, 1974; Bergendahl *et al*, 1998). To our knowledge, information

theoretic analyses of noisy signaling pathways have been limited to step changes in the input and do not account for the dynamic changes in the micro-environment, which seems more physiologically relevant in certain signaling networks, and should be able to provide better insights into temporally modulated signaling circuits.

To test the hypothesis that dynamic changes in the ligand input may contribute towards enhanced information transfer as compared to step stimulations, we performed information analysis of a mathematical model and single-cell measurements of M3-mediated calcium and NFAT (Nuclear Factor of Activated T-Lymphocytes) response under pulsatile ligand stimulation. The term 'information transfer capacity' or simply 'information' that we use in this chapter is the Shannon information which is concerned with statistical properties of a given system and correlation between the states of the two systems. A mathematical description of information transfer capacity is provided in Methods section. We define mutual information (MI) as the information transfer capacity for a given set of inputs (or even outputs). First, we utilize a computational model for GPCR-calcium-NFAT signaling to validate that our information theoretic analysis is able to discriminate the dynamic response from scalar responses (Selimkhanov *et al*, 2014). Second, we utilize a microfluidic platform to deliver rapid pulsed stimulations (Gu *et al*, 2004) and record thousands of single cell calcium and NFAT traces. These data were analyzed to show that dynamic input enhances information transfer of the signaling responses. Additionally, we show that pulsed input increases the information transfer of two widely occurring isoforms of the NFAT transcription factor, viz. NFAT1 and NFAT4, as compared to their information transfer capacity alone.

4.2. Results

4.2.1. A deterministic approach to modeling a noisy GPCR signaling pathway

For any noisy biochemical pathway, it is important to know how many input ligand concentrations can be distinguished by the pathway and how noise affects this sensitivity. To analyze this with our information theoretic approach, we first took our deterministic model for GPCR-calcium-NFAT signaling that we developed in Chapter 2. Briefly, ligand-receptor binding (here muscarinic M3 receptor) leads to calcium response via G-protein activation. Cytoplasmic calcium dephosphorylates cytoplasmic NFAT that leads to its nuclear localization and subsequent transcriptional activation (Fig. 4.1. A). In Chapter 3, we have shown that noisy downstream

responses observed at the single cell level may be attributed to a deterministic framework with high cell-to-cell variability (extrinsic noise) coupled with stimulation and pathway properties such as a high Hill coefficient pathway and low concentration-duration stimulations. Here, we introduced various levels of extrinsic and intrinsic noise in our deterministic model in the form of cell-to-cell variability in the signaling components and white Gaussian noise in the output response, respectively. The deterministic model yields solutions (calcium responses) to each step change input (Fig. 4.1. B). However, it is well established that cells have biochemical variability in the concentrations of their signaling components (Bowsher & Swain, 2012; Cohen-Saidon *et al*, 2009; Voliotis *et al*, 2014). We added this variability by choosing the initial values for the concentrations of three major signaling components, GPCR, total G-protein and PLC, from a uniform or a normal distribution. The values were sampled using Latin Hypercube sampling (LHS) to minimize any correlation among them. Sampling from such a distribution (for example +/-15%, uniform) leads to highly variable signaling response wherein it is difficult to relate the response to the input concentrations (Fig. 4.1. C). In addition to extrinsic noise, the signaling system may also be prone to intrinsic noise such as stochastic errors in signal measurement and errors from the limited resolution of the measurement setup. We further added empirically 2% Gaussian noise normalized to the signal value and additional 2% white Gaussian noise to account for such intrinsic variability (Fig. 4.1. D). The signaling responses generated by including noise are less distinguishable in terms of the concentration input than purely deterministic solutions, and thus carry less information. We also used an intentiometric calcium fluorescence sensor RGECO1 transiently transfected in the M3 receptor expressing HEK293 cells. Cells were stimulated with carbachol (CCh), a chemical analog of acetylcholine (natural ligand for M3 receptors). Experimental data for carbachol stimulation for the same concentration regime for a population of cells also shows similar non-distinguishability (Fig. 4.1. E). Taken together, we find that adding extrinsic and intrinsic noise within a deterministic framework decreases distinguishability of calcium response and its informational content but mimic experimental data. Next, we determine how information transfer to the downstream NFAT response is affected by increasing levels of noise.

4.2.2. Noise limits the information transfer downstream to NFAT dynamics

Adding noise in model and finding that both model and experiments exhibit noisy calcium responses, it is interesting to understand how noise affects the downstream response such as

calcium-mediated NFAT activation. We investigated the effects of extrinsic noise (cell-to-cell variability) on the extent of information transfer at NFAT level in our model (Fig. 4.2. A). For two different levels of extrinsic noise (2% and 15%), we predict that the NFAT signaling responses vary widely and it becomes increasingly less discernible as to which response came from which ligand input (Fig. 4.2. B). We used a recently developed approach to calculate information transfer capacity of a dynamic response using k-nearest neighbor (knn) search algorithm (Kraskov *et al*, 2004; Selimkhanov *et al*, 2014) (see Methods and Materials) to quantify entropy and mutual information transfer capacity (MI) for each level of noise in the model. There are two approaches available for MI calculation. The scalar measurement simply considers a single time-point value of response such as the response after a fixed time, or the response at mid-point, or maximum of the response curve. In contrast, the dynamic or vector measurement considers '*d*' equi-spaced time-points in the dynamic part of the response. As expected, we find that for our model, the dynamic response (red curve, $d = 5$) always contains more information than the scalar response (black curve) (Fig. 4.2. C, D). With increasing number of input concentrations, the mutual information transfer increases until a plateau. As expected, we also find that with increasing levels of extrinsic noise, the mutual information capacity decreases (Fig. 4.2. C). This is true regardless of the type of distribution we choose to sample the initial values (concentrations of GPCR, total G-protein and PLC) from. However, a uniform distribution exhibits less informational loss as compared to a normal distribution (Fig. 4.2. D). We also calculated the signal-to-noise ratio (SNR) of the response using a method provided in (Selimkhanov *et al*, 2014), and found that it follows similar logarithmic relationship as their theoretical prediction (Fig. 4.2. E). Taken together, these results suggest that our approach of quantifying information is able to delineate the essential features predicted theoretically for such noisy biochemical pathways. In the following sections, we transition to real experimental data, and apply our approach to quantify MI for step and pulsatile ligand stimulation.

4.2.3. Dynamic calcium response partially mitigates informational loss

Single cell calcium traces were recorded for several step and pulsed input concentrations in multiple sets of experiments to collect > 200 single cell calcium traces for each stimulation condition. Under step stimulation, cells tend to respond in a wide range of calcium dynamics that includes oscillations, peak-and-plateau and single spikes (Fig. 4.3. A). Overall, the response traces appear asynchronous and highly noisy. Responses at each concentration are compared to a

no stimulation condition (control, 0nM CCh) to determine the information capacity of stimulation (Fig. 4.3. B). Since the input information is of 1 bit (0 nM or X nM), the maximum output information under ideal conditions would be 1 bit. We find that the information transferred under scalar read-out ranges from ~ 0.7-0.8 bit, which suggests partial loss of information during signal transduction. For all the concentrations tested, the dynamic or vector response were found to transfer more information as compared to the scalar response (~ 0.9 - 0.96 bit). We also calculated the mutual information (MI) transferred when all the input concentrations are considered together. Since our model predicted that the maximum information transfer plateaus out at ~ 4 concentrations, we chose 4 input concentrations (equivalent to 2 bits of input information) to calculate the maximum mutual information the system can transfer downstream to calcium. MI for calcium response increased with increasing dimension of the vector response. While the scalar response yields the least mutual information (~ 0.97 bit), the vector measurements yield more MI (~ 1.15 bits for d = 3, and ~ 1.3 bits for d = 5) (Fig. 4.3. C). The vector dimension, d (or the number of time-points) up to which we can calculate the MI depends on the sample size (Cheong *et al*, 2011; Selimkhanov *et al*, 2014) and therefore we restricted our analysis to d = 5 which gives a good estimate of information for the sample size we have in our experiments (~200). It is also worth noticing that this method may overestimate the information content, and the estimation can be corrected by plotting information (in bits) against 1/sample-size ('n') (by randomly dividing the samples in halves and three parts) and extrapolating the curve for an infinitely large sample size for which 1/n ~ 0 (Appendix 4 Fig. 4A.1.). The trends for information transfer, however, remains the same. Our analysis of determining the maximum information capacity also optimizes the probability distribution (or contribution) of each of the concentrations to the maximum mutual information possible. We find that with increasing the dimension of response dynamics, the distribution becomes more uniform (Fig. 4.3. D). This suggests that the information content in scalar response (d = 0) is primarily contributed by the low (0 nM) and the high (80 nM) concentration stimulations and cells may not be able to sense intermediate concentrations (such as 10 nM and 40 nM) as well, despite being able to yield a response upon stimulation. In contrast, the uniformity in the distribution increases with increasing vector dimension of the read-outs, which suggests that the dynamic part of the response is crucial in discerning more number of input ligand concentrations.

4.2.4. Pulsed (or dynamic) ligand input together with dynamic response enhances information transfer

To test the hypothesis that pulsed input may enhance information transfer, hundreds of single cell calcium traces were recorded for various pulsatile stimulation conditions. Concentration and duration of the stimulation were fixed at 80 nM and 24 s, respectively. The rest period was set at R = 24 s, 72 s or 144 s (Fig. 4.4. A). These calcium responses were compared with the control 'no stimulation' (0 nM) traces. In the event that cells were not sensitive to the frequency of input, the upper limit of information transfer under dynamic response would be 1 bit (for two concentrations 0 and 80 nM). In contrast, if the cells were highly sensitive to input frequency, four distinct inputs would have a maximum information transfer of 2 bits. In our case, we find that the maximum information output ranges between ~ 0.9 bits – 1.5 bits (Fig. 4.4. B), suggesting that the cells are not only sensitive to the input concentration but are also sensitive to the input frequency. The mutual information for pulsatile input (~ 1.5 bits) is thus not only greater than for step changes, but also exceeds the maximum information transfer possible under non-pulsatile conditions (1 bit). Similar to the previous section where we varied input concentrations (Section 4.2.3.), the informational content increases with increasing dimension of the dynamic response. We also find that the probability distribution of information for varying rest period becomes more uniform as the vector dimension increases (Fig. 4.4. C). This suggests that the dynamics of the response is essential for frequency sensitivity. Taken together, we show that dynamic input (e.g. pulsatile ligand stimulation) combined with vector measurements (i.e., multiple time-point measurements) maximizes the amount of information that can be transferred downstream amidst a highly noisy biochemical network.

4.2.5. NFAT isoforms exhibit enhanced mutual information transfer with pulsed input than alone

Enhanced information transfer under pulsed ligand input raises an interesting question: how do cells utilize this additional information that may be coming from the dynamic microenvironment, for example via pulsatile release of stimulants? To address this question, we seek insights from Chapter 2, where we showed that the two NFAT transcription factor isoforms have slightly different band-pass windows. We hypothesize that the excess information in the form of pulsed ligand dynamics may be sensed by the two NFAT isoforms somewhat distinctively. We recorded single cell traces for NFAT1 and NFAT4 nuclear translocation for two stimulation conditions: step change (black bar) and pulsed stimulation with R = 72 s (red bar)

with concentration (80 nM) and pulse duration (24 s) remaining the same (Fig. 4.5. A). We then calculated the information capacity of each of the isoforms alone as well as the mutual information between the two isoforms (Fig. 4.5. B-D). Multi-dimensional responses (d = 5) yielded more information as compared to scalar (d = 0) for each of the conditions. Interestingly, the mutual information between NFAT1 and NFAT4 is greater than the individual transcription factors alone. This suggests that the two isoforms sense the extracellular dynamics information differently and together process more information than alone. Taken together, these results show that existence of two different isoforms may complicate the signaling network, but it also utilizes the additional temporal information present in the cellular micro-environment.

4.3. Discussions

In this chapter, using information theory, we investigated the hypothesis that cells can sense the dynamics in the external micro-environment and transfer the information downstream up to transcription factor activation. Based on Chapter 3, we used a deterministic framework to introduce cell-to-cell variability for generating noisy downstream response, and showed that the levels of extrinsic noise directly affects the information transfer at transcription factor activation (Fig. 4.2.). These conclusions about the relationship between signal-to-noise ratio and information capacity drawn from our model are consistent with the theoretical predictions of (Selimkhanov *et al*, 2014), validating that the approach works for non-linear systems such as GPCR-calcium signaling. In non-linear signaling pathways, extrinsic noise may give rise to a wide range of behavior such as oscillations, peak-and-plateau and single spikes, thus making the system appear highly noisy at population level. However, such systems have also been shown to phase-lock based on external frequencies (Jovic *et al*, 2010, 2011; Sumit *et al*, 2015; Jovic *et al*, 2013). Phase-locked systems respond with high synchrony, and although the exact peak amplitudes may differ from cell to cell, it partially eliminates the noise generated by the cell-to-cell variability. Here we show that pulsed stimulations that result in phase locked responses increase the information transfer capacity of such noisy signaling pathways (Fig. 4.4.). We also notice that the information transfer capacity decreases from the calcium to the NFAT response. The reason for this is cumulative addition of noise for the downstream signals. While we used a minimal model in Chapter 2 to explain frequency modulation, the exact mechanism of calcium-induced NFAT activation is still debated and several kinases and phosphatases maybe involved in the pathway (Fisher *et al*, 2006). Their variability would add more extrinsic noise to the NFAT response,

further decreasing the overall information capacity. It also suggests that with increasing network complexity, cells tend to have decreased information capacity as they accrue more extrinsic noise. However, with pulsed/dynamic input as well as with dynamic output, cells may be able to mitigate the effects of extrinsic noise and may be able to optimize information transfer (Fig. 4.6.). It may be inferred that with increasing complexity in the signaling network, although the cumulative noise levels may increase, the system may be able to mitigate the noise by processing more information by utilizing the dynamics of the inputs and the output. We also found that the mutual information between NFAT1 and NFAT4 is greater than that of the individual transcription factors alone, suggesting that the two isoforms sense the extracellular dynamics information differently and together process more information than alone. This enables cells to utilize the same ligand input in two different temporal regimes to elicit different downstream responses (Sumit *et al*, 2015). We speculate that, in future, several other network motifs such as linear and oscillatory motifs with multiple feedback and feedforward loops will be investigated in order to thoroughly understand the effects of noise and advantages of using pulsed stimulation in mitigating the noise in that particular signaling network.

4.4. Conclusions

We used pulsed and step ligand inputs and measured single cell responses to quantify information transfer via M3 receptor to calcium and NFAT responses. We show that the mutual information for pulsatile input is not only greater than for step changes, but also exceeds the maximum information transfer possible under non-pulsatile conditions. Focusing on the deterministic model, we show that the extent of cell-to-cell variability critically determines the amount of information that can be transferred downstream. We also show that the two isoforms of NFAT with different band-pass windows also exhibit different levels of information transfer and their mutual information transfer is greater than their information transfer capacities alone. Additionally, we show that the dynamic output (vector measurement) enhances the information transfer in all the cases. Taken together, we conclude that the pulsed dynamic input from the micro-environment combined with vector measurements (i.e., multiple time-point measurements) enable cells to maximize the information transfer downstream, despite the inevitable cell-to-cell variability present in the system.

4.5. Materials and Methods

Materials

Materials used for experiments in this Chapter are detailed in Appendix 1.

Methods

Methods description about cell culture, seeding cells in microfluidic device and time lapse image and analysis are detailed in Appendix 1.

GPCR-calcium-NFAT model. We used our previously developed mathematical model that links step/pulsatile ligand stimulation, receptor/ligand binding, calcium and NFAT signaling and captures the characteristic features of the microfluidic pulsatile experiments described in Chapter 2 (Jovic *et al*, 2010, 2011; Sumit *et al*, 2015). The model description, reactions and parameter values are as detailed in our previous work (Sumit *et al*, 2015) and Appendix 2 Text 2A.1-2., except for the initial values of the total GPCR, G-protein and PLC concentrations. The initial values for these components were selected from either a uniform or a normal distribution with varying width. The parameter selected was done using Latin hypercube sampling (LHS) to minimize any correlation between the initial value selections (Marino *et al*, 2008). A system of ordinary differential equations (ODEs) was generated for the model and solved in MATLAB (MathWorks Inc., Natick, MA) with the ode15s stiff solver.

Calculation of information capacity (info), mutual information (MI) and signal-to-noise ratio (SNR). We adapted the method for information and noise analysis provided in (Selimkhanov *et al*, 2014). Briefly, for input signal S with 'm' discrete levels of ligand concentrations ($S = [s_1, s_2, s_3, \ldots, s_m]$), we have output response trajectories ($Ri = [r_{i1}, r_{i2}, \ldots r1_{ni}]$ corresponding to each input s_i. Each trajectory occupies a single point in continuous Euclidean space of dimension 'd', where 'd' is the number of time-points in the output trajectory. The information transfer (I) is estimated by:

$$I(R;S) = H(R) - H(R|S)$$

Here, H(R) and H(R|S) are the Shannon entropies. This method uses k-nearest neighbor estimator to determine the probability of existence of a point x_j in X as:

$$f(x_j|X) = \frac{k}{N_x V_d z(x_j|X)_k^d}$$

Here, V_d is the volume of a unit sphere of dimension d, N_x is the number of x_j in X, and $z(x_j|X)_k^d$ is the Euclidean distance to the kth nearest neighbor in X from xj (Kraskov *et al*, 2004). Applying this estimation, the Shannon entropies can be given by:

$$H(R|S) = -\sum_{i=1}^{m} \frac{q_i}{n_i} \sum_{j=1}^{n_i} log_2 \left(\frac{k}{N_x V_d z(x_j|X)_k^d}\right)$$

$$H(R) = -\sum_{i=1}^{m} \frac{q_i}{n_i} \sum_{j=1}^{n_i} log_2 \left(\sum_{w=1}^{m} \frac{k}{N_x V_d z(x_j|X)_k^d}\right)$$

Without prior knowledge of the probability distribution coefficient, q_i, the information transfer *I* cannot be estimated. However, the maximum information capacity can be estimated as

$$C(R;S) = max_Q\{I(R;S)\}$$

Calculation of signal-to-noise ratio (SNR):

The method for estimation of SNR is adapted from (Selimkhanov *et al*, 2014). We calculate the signal magnitude σ^2_r (variance of average responses over all m input concentrations) as:

$$\sigma_r^2 = \frac{1}{m}\sum_{i=1}^{m}\left(\left(\frac{1}{m}\sum_{w=1}^{m}\frac{1}{n_w}\sum_{j=1}^{n_w} r_{wj}\right) - \frac{1}{n_i}\sum_{j=1}^{n_i} r_{ij}\right)^2$$

Noise magnitude σ^2_n is calculated as the average of the variances of n_i responses to a single input level as:

$$\sigma_n^2 = \frac{1}{m}\sum_{i=1}^{m}\left(\frac{1}{n_i}\sum_{j=1}^{n_i}\frac{1}{n_i}\sum_{w=1}^{n_i} r_{iw} - r_{ij}\right)^2$$

The signal-to-noise ratio (SNR) is then defined as the ratio, σ_r^2/σ_n^2.

To calculate intrinsic-to-extrinsic noise ratio (IER), we used the portion of calcium traces following step changes in ligand concentration where the intensity did not change significantly. Intrinsic noise (σ_ξ^2) was estimated as the variance of the differences in RGECO intensities

between successive time points. Total noise (σ_t^2) was calculated similarly to the noise magnitude, σ_n^2, but taking only the static region of the calcium traces. Extrinsic noise is then calculated as $\sigma_e^2 = \sigma_t^2 - \sigma_\xi^2$. The ratio σ_i^2/σ_e^2 is IER. Codes for these analyses were written and executed in MATLAB (MathWorks Inc., Natick, MA).

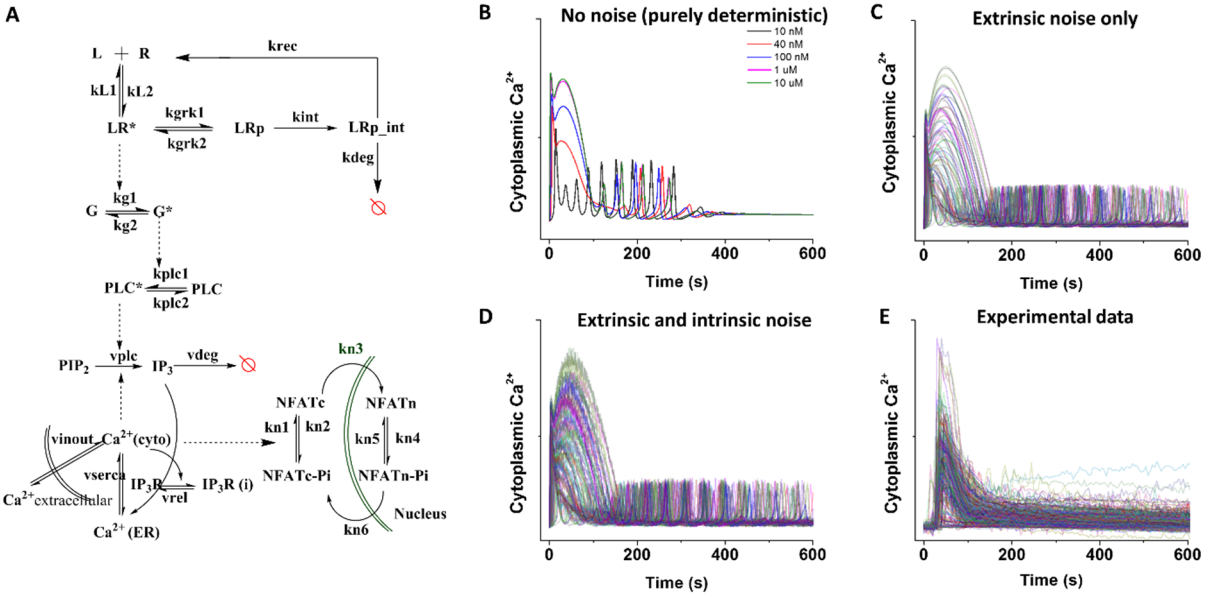

Fig. 4.1. A deterministic approach to modeling a noisy GPCR signaling pathway. A. Deterministic GPCR-calcium-NFAT model schematic. All the equations and parameters are as described in Chapter 2. B. Without any additional noise in the system, the calcium time traces from the deterministic model are easily distinguishable from each other. C. Deterministic model with added extrinsic noise (i.e., cell-to cell variability) introduced as initial values for major signaling nodes) yields a range of solutions. D. Adding intrinsic noise (white Gaussian) to account for measurement errors and stochasticity in the molecular activity, in addition to extrinsic noise, leads to an even noisier output. E. Experimental measurement of cytoplasmic calcium using RGECO intentiometric sensor (C = 10 nM, 40 nM, 100 nM all plotted together) is quite similar to a deterministic model with extrinsic and intrinsic noise.

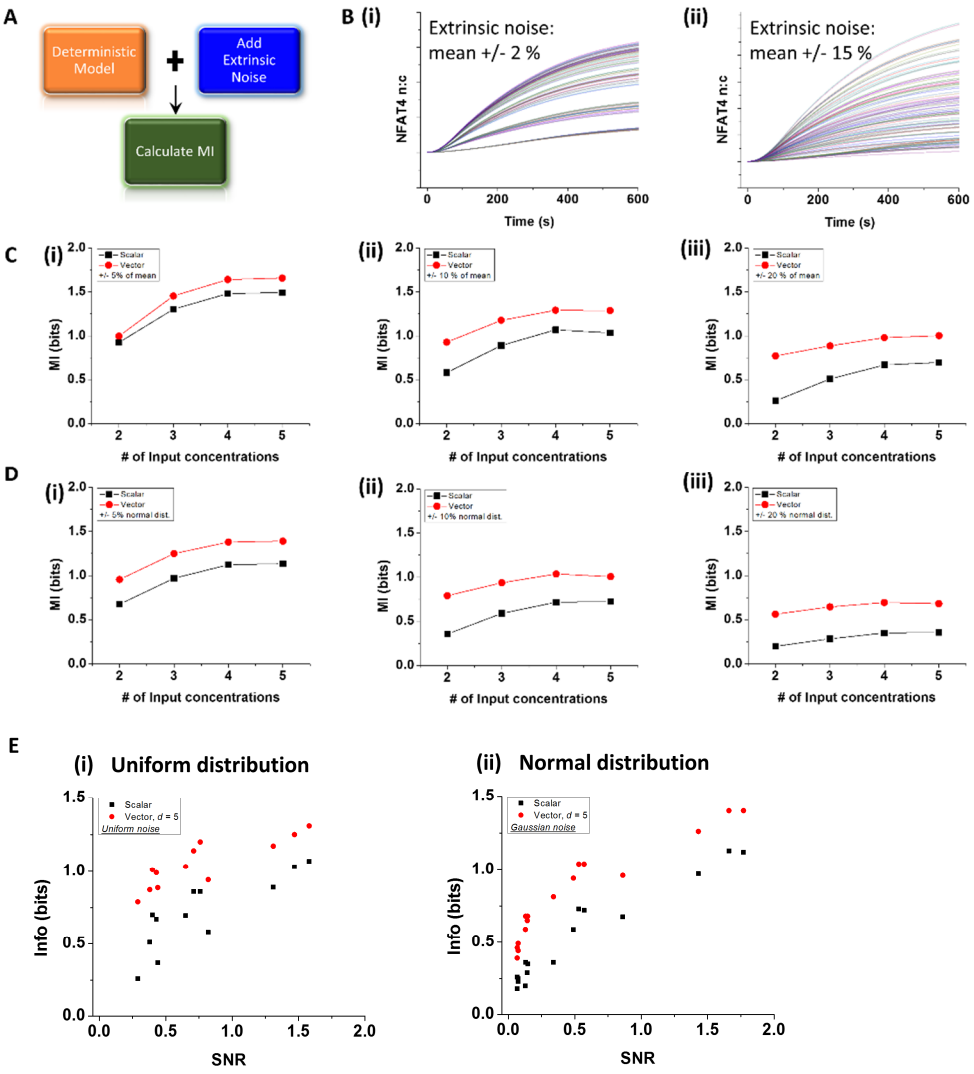

Fig. 4.2. Biochemical noise limits the information transfer to downstream NFAT dynamics. A. Model approach to calculate mutual information. Time traces for cytoplasmic calcium and NFAT are obtained for the deterministic model (Fig. 4.1. A), with added extrinsic noise to calculate the mutual information. B. Representative *in silico* single cell NFAT traces for two different levels of noise (i) low noise: mean+/- 2% and (ii) high noise: mean +/- 15%. C-D. Mutual information (MI) transferred to NFAT is calculated for the deterministic model with intrinsic and extrinsic noise. The number of input concentrations as well as the extent of extrinsic noise is varied. Extrinsic noise is sampled either from uniform distribution (C) or normal distribution (D). In all cases, multiple time-point or vector measurements yield more information. MI decreases with increasing noise in the system. Uniform distribution yields greater information transfer as compared to normal distribution, with all other characteristic features remaining the same. E. Plots of information transfer vs signal-to-noise ratio (SNR) shows that information transfer increases with increasing SNR, and seems to follows a logarithmic relationship as predicted theoretically. N = 400 *in silico* time traces for each input obtained from the deterministic model with extrinsic noise sampled using Latin hypercube sampling method.

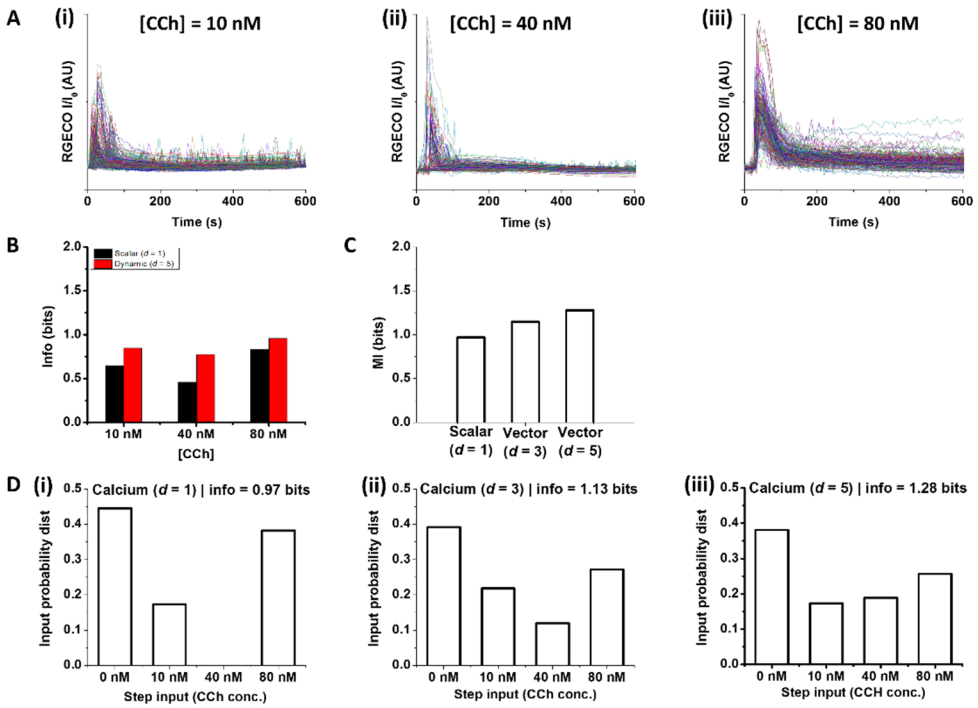

Fig. 4.3. Dynamics of calcium response partially mitigates informational loss. A. Cytoplasmic calcium time traces for a population of cells up on CCh step stimulation with various concentrations: (i) 10 nM, (ii) 40 nM, and (iii) 80 nM. B. Information transfer for each concentration when compared to no (0 nM) stimulation for scalar (single-point) and dynamic (multi-point) measurements. Dynamics of calcium response increases the information transfer in each case. C. Mutual information transferred from input through all the concentrations tested shows that with increasing number of time-point measurement, MI also increases. D. Contribution of each input in the maximum mutual information transfer (Fig. 4.3. C) as depicted by the input probability distribution. More and more intermediate concentrations contribute when *d* (number of time-points in the measurement) increases. N > 200 cells for each input obtained from several sets of microfluidic experiments.

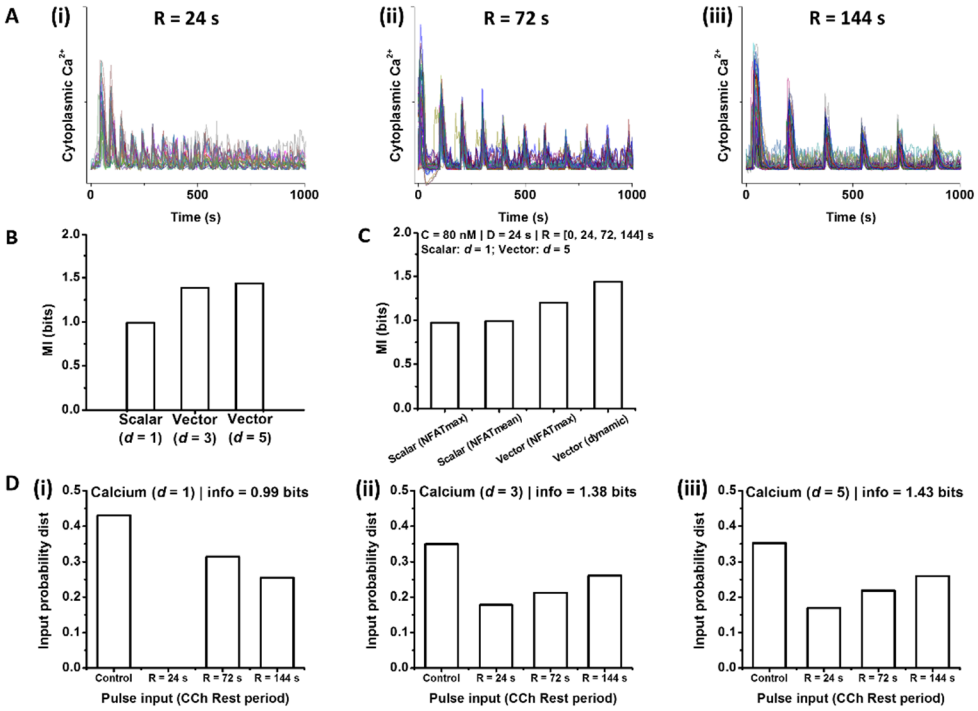

Fig. 4.4. Pulsed ligand input together with dynamics of the response enhances information transfer. A. Cytoplasmic calcium time traces for a population of cells up on CCh pulsed stimulation (C = 80 nM) with various rest periods: (i) 24 s, (ii) 72 s, and (iii) 144 s. B. Mutual information transferred from input through all the rest periods tested shows that with increasing number of time-point measurement, MI also increases. C. Comparison of MI calculated using various scalar and vector methods such as $NFAT_{max}$ measurement, $NFAT_{mean}$ measurement and dynamic (equispaced multiple time-point) measurement, shows that dynamic vector yields maximum information transfer in case of pulsed stimulation. D. Contribution of each rest period input in the maximum mutual information transfer (Fig. 4.4. B) as depicted by the input probability distribution. More and more intermediate rest periods contribute when *d* (number of time-points in the measurement) increases. N > 200 cells for each input obtained from several sets of microfluidic experiments.

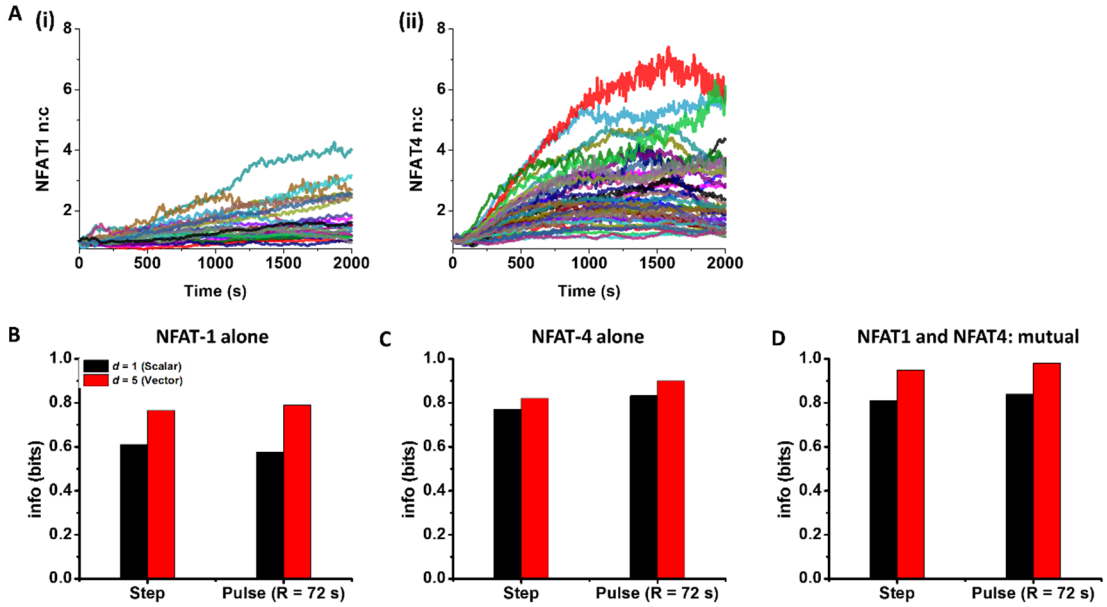

Fig. 4.5. NFAT isoforms exhibit enhanced mutual information transfer than alone for both step and pulsed stimulation under vector measurements. A. NFAT nuclear translocation time traces for a population of cells up on CCh pulsed stimulation (C = 80 nM, D = 24 s, and R = 72 s) for (i) NFAT1 and (ii) NFAT4. B-D. Comparison of information transfer under step and pulsed ligand input for scalar (d = 1) and vector (d = 5) measurements. In all cases, pulsed stimulation with vector measurement results in maximum information transfer. Also, mutual information transfer when NFAT1 and NFAT4 are taken together is more than their individual capacity. For step stimulation, C= 80 nM. For pulsed stimulation, C = 80 nM, D = 24 s, and R = 72 s. N > 200 cells for each input obtained from several sets of microfluidic experiments.

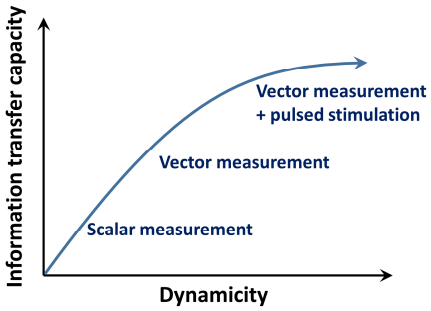

Fig. 4.6. Information transfer capacity increases with dynamicity for noisy signaling networks. Scalar measurement with step stimulation yields the least information while dynamic or vector measurement with pulsed stimulation provides maximum information transfer.

Chapter 5. Biochemical noise affects the rescuing capacity of drug action at single cell level in a GPCR-mediated signaling pathway

5.1. Introduction

G-protein coupled receptors (GPCRs) are the major pharmaceutical drug targets accounting for more than a third of the available pharmaceutical drugs (David, 2004). Drug responses for cell signaling pathways such as GPCR-mediated signaling pathways are generally studied by measuring population-averaged responses of genetically identical cells against step changes in ligand concentration. However, averaging over a population of cells occludes the behavior of individual cells which may vary distinctively in response to drugs or ligand inputs (Altschuler & Wu, 2010; Spencer *et al*, 2009, 2013). Yet, as described in Chapter 4, single cell measurements with step changes in ligand stimulation have limitations as they generate widely varying sets of response, owing to both intrinsic as well as extrinsic noise (Elowitz *et al*, 2002; Raser, 2004; Newman *et al*, 2006). Experimental measurements are often limited by the sample size, and information theoretic analysis may not be applied in such cases. To address this, other methods of noise or variability estimation have been developed over past decade (Rhee *et al*, 2014; Elowitz *et al*, 2002; Raser, 2004). Although noise at gene expression level has been well characterized (Elowitz *et al*, 2002; Raser, 2004; Newman *et al*, 2006), it remains challenging to quantify the biochemical noise, which is essential for understanding cellular heterogeneity and its implications for drug action (Rhee *et al*, 2014; Cheong *et al*, 2011).

Prior studies of biochemical noise in signaling networks have been focused on development of two-reporter techniques (Rhee *et al*, 2014; Elowitz *et al*, 2002; Raser, 2004). This involves intensity measurement of two downstream fluorescent reporter proteins that are activated by the same upstream signaling node. The upstream node thus becomes the source of extrinsic noise, whereas the two parallel downstream pathways become the source of intrinsic noise in the system. However, this technique is limited to linear signaling motifs as well as by the availability of multiple fluorescent reporters, and may also be difficult to measure noise for signaling pathways

that respond at shorter timescales. Here, we develop a simple microfluidic pulsing technique with single fluorescence read-out under two different pulsatile stimulation regimes to estimate biochemical noise and to understand its implications in drug action. Quantification of biochemical variability and how it changes under perturbations such as overexpression of a signaling node or after applying a drug inhibitor. Combining the microfluidic technique with computational approaches developed in Chapters 3 and 4, we show that the biochemical noise in a GPCR-mediated calcium signaling does affect drug action at the single cell level. Population-averaged responses may not be able to provide us these insights for use in pharmacology and synthetic biology applications.

Major modulators of downstream of GPCR signaling are the RGS (Regulators of G-protein Signaling) proteins, which catalyze deactivation of $G_{\alpha i}$ and $G_{\alpha q}$ family G-proteins (Neubig & Siderovski, 2002). The cell line HEK 293 M3R4 used in our experiments stably expresses muscarinic M3 receptors (a GPCR) and also expresses one of the RGS proteins (RGS4) upon 12-24 h induction with doxycycline (DOX) (Bodenstein *et al*, 2007). RGS4 increases the hydrolysis of activated G-protein and thus reduces calcium signaling. Thus, in our experiments, DOX-induction is equivalent to a perturbation that reduces G-protein activity due to the presence of RGS4. We also use a recently discovered drug molecule (CCG-203769) that is shown to have Anti-Parkinson's potential. It reversibly inhibits RGS4 activity and enhances the G-protein activity and, thus rescues the cells from the lowered response (Storaska *et al*, 2013; Blazer *et al*, 2015).

Study of a drug response behavior often involves comparing the output response upon stimulation in the presence or absence of drugs. A more detailed method to study targeted response is to overexpress (or sometimes knockdown) a protein that is known to be targeted by the drug, thus altering its normal output response. Thus, overexpression of the target protein such as DOX-induced RSG4 expression acts as a 'perturbation' in the system (denoted by 'perturbation experiment' in this chapter), and the application of target-specific drug such as RGS4 inhibitor CCG-203769, should be able to 'rescue' the cells from such perturbations (denoted by 'rescue experiment'). A downstream read-out is used to quantify how the perturbed and drug-treated cells respond to that particular read-out as compared to control cells (Fig. 5.1. A). Although this approach is frequently used for pharmacological studies, the single cell response may vary quite widely and may even overlap for the three conditions (Fig. 5.1. A (ii)). Thus, the probability

distributions of output responses at the single cell level may overlap and may not be able to provide insights into several cell-specific response characteristics such as non-linear and bifurcated responses (Fig. 5.1. B). In this chapter, we investigate single cell characteristics of drug response in the GPCR-mediated signaling under normal, perturbation, and rescue conditions.

5.2. Results

5.2.1. Population scale measurements obscures drug response behavior at single cell level

We measured cytoplasmic calcium response downstream of G-proteins, in single HEK293 M3R4 cells transiently transfected with RGECO plasmid (an intentiometric calcium sensor) upon carbachol (CCh) ligand stimulation under control, perturbation, and rescue conditions (Fig. 5.1. C). Calcium response upon carbachol stimulation is significantly lowered in case of DOX-treated cells that express RGS4, as compared to the control set. Stimulation of cellular population that was induced by DOX but was also treated with the RGS4 inhibitor resulted in slight recovery of the calcium response. Although, maximum of RGECO intensity of the calcium response for the three conditions showed that drug treated cells responded better than those treated with DOX alone, a similar overlap of response is observed for the three conditions as schematized earlier (Fig. 5.1. D). Population scale measurements may not be sufficient to gain mechanistic insights into drug action when there is significant amount of noise or variability in the signaling pathway as suggested by the overlap in responses. To address this, we exploited an interesting observation made with microfluidic pulsatile stimulation.

Cells under step stimulation with CCh exhibit distinct calcium responses in low and high concentration regimes. Low concentration stimulations result in oscillatory response, whereas high concentration stimulations result in peak-and-plateau response (Appendix 5 Fig. 5A.1. A-B). On the other hand, pulsatile stimulation of cells results in phase locking of the calcium response (Jovic *et al*, 2010). Interestingly, these phase locked responses have characteristic features in the two concentration regimes. Low concentration pulses (~10 nM CCh) result in complete amplitude recovery but partial frequency recovery (beat skipping) (Appendix 5 Fig. 5A.1. C). High concentration pulses (~100 nM CCh) result in complete frequency recovery but partial amplitude recovery (Appendix 5 Fig. 5A.1. D). We define two microfluidic observables, viz. frequency recovery index (FRI) and amplitude recovery index (ARI) such that FRI varies in the low concentration regime while ARI varies in the high concentration regime (Materials and Methods,

section 5.5.). Additionally, FRI and ARI increase with increasing rest period in the respective regimes (Appendix 5 Fig. 5A.1. E-F). Because the two observables are measured for same stimulation conditions, we hypothesized that these observables can be used as "two-reporter system" to explore biochemical noise and how it affects drug action at single cell level.

5.2.2. Two regime pulsed stimulation (TRePS) shows correlation between the microfluidic observables that can be attributed to biochemical variability in a deterministic model

To delineate the relationship of biochemical variability with output response, we designed an experimental scheme in which cells are stimulated with low concentration (C_1) ligand pulses followed by stimulation with high concentration (C_2) ligand pulses, with a sufficiently long recovery period (R_0) in between (Fig. 5.2 A, Appendix 5 Fig. 5A.2. A). Rest periods were determined for the two concentrations such that the average FRI and ARI values in C_1 and C_2 are greater than 0.95. R_0 was chosen to be much greater than those rest periods (~ 8 min). Under such conditions, the stimulation scheme would provide two readouts for the same cell at same node (calcium). This experimental system is analogous to the two reporter system mentioned earlier, and these two microfluidic observables (viz. FRI and ARI) are read-outs that depend on biochemical state of the cell. The idea of this scheme is to use these two-readouts in perturbation and rescue experiments to quantify how biochemical noise behaves under the three conditions at single cell level, and use the computational model developed in Chapter 3 and 4 to determine how changing biochemical noise levels would affect drug action (Fig. 5.2. A). Since this scheme involves testing in two concentration regimes, we term it as 'Two Regime Pulsed Stimulation' or TRePS, wherein we measure FRI in C_1 regime and ARI in C_2 regime in single cells.

We measured calcium responses for cells stimulated under the TRePS scheme, and calculated FRI and ARI for each cell. Thus, each cell could be represent by a single dot in the FRI-ARI plot (Fig. 5.2. B). Similar to the 'two-fluorophore' method, we find an interesting correlation between the two microfluidic observables. Cells exhibiting high amplitude recovery index in C_2 also exhibit high frequency index in C_1 (Fig. 5.2. B). To visualize how cell are distributed along this correlation, the results were also plotted as a contour histogram (Fig. 5.2. C). The histogram indicates that the cells that have not been treated with any drug or vehicle are mostly evenly distributed along the correlation.

Assuming that the genetic composition remains unperturbed during the experimental timescale (a few minutes), we hypothesize that cells only vary in terms of the biochemical composition such as receptor density, total G-protein and PLC concentration, and is reflected in the FRI-ARI correlation. Cellular responses may also vary because of intrinsic noise. However, based on our analysis in Chapters 3 and 4, we ignore the contribution of intrinsic noise in this study. We used our existing mathematical model for GPCR-mediated calcium signaling (Chapter 2 and Fig. 5.2. D). We varied the initial values for the major biochemical nodes in our deterministic model to see the effects on FRI and ARI (Fig. 5.2. E). Our model analysis suggests that varying each of the node, viz. GPCR concentration, RGS4 activity (indicated by a parameter k4) and total G-protein concentration, results in FRI-ARI correlation. Thus, our hypothesis can at least be validated mathematically that the correlation is an indication of biochemical noise, and is contributing to the scatter along the correlation. The scatter across the correlation may be attributed to intrinsic factors as well as errors in the quantification technique. Since we are interested in the correlated biochemical noise, we may ignore the scatter across the correlation in this study. Taken together, we find an interesting correlation between the two microfluidic observables in the TRePS experiments that can be attributed to biochemical variability in a deterministic model, similar to a two reporter system for the estimation of noise/variability in a signaling pathway. Next, we exploit this correlation, both in experiments as well as in simulation, to determine the effects of biochemical noise in perturbation experiments and understand its implications in drug action.

5.2.3. Perturbation and rescue experiments shift the distribution of cells along the amplitude-frequency correlation in a noise dependent fashion

We performed TRePS experiments on single cells under with various conditions and determined how cells are distributed along the frequency-amplitude correlation (Fig. 5.3. A-D). The distribution for control cells that are treated overnight with DMSO (vehicle) was found similar to the non-treated cells (Fig. 5.3. A). Cells treated with a high concentration of trypsin (0.25% Trypsin in EDTA) exhibit reduction in their surface receptor density (Zhang *et al*, 2012). TRePS analysis of trypsin-treated cells (negative control) shows that almost all the cells shift to the low FRI-ARI regime (Fig. 5.3. B). Next, we performed TRePS experiments on doxycycline-induced HEK293 M3R4 cells that express RGS4 proteins. These cells showed a similar (and a rather mild) reversal in the calcium response, i.e., majority of the cell exhibited a low values for FRI and ARI (Fig. 5.3. C). When doxycycline induced cells were stimulated in the presence of RGS4 inhibitor

CCG-203769, we observe a partial shift of low responding cells to high responding regime (Fig. 5.3. D). There are two possibilities of rescue by drug action. First is that all the cells might have moved a little up. Because a sub-population of cells with low values of FRI and ARI (< 0.5) still exist after the treatment, it rules out the possibility that every cell moved along the correlation. This leaves us with the second possibility that the drug treatment rescues a sub-population from low response to high response. Thus, these results suggest that the perturbation of key components in the signaling pathway may lead to a shift of a sub-population of cells from high responding to low responding and vice versa.

To gain quantitative insights, we next used our mathematical model to introduce biochemical noise, and performed *in silico* TRePS experiments to simulate the microfluidic experimental observations (Appendix 5 Fig. 5A.3.). Population scale comparison of amplitude and frequency recovery indices in experiments and simulation indicates that apart from generating varied responses from cell-to-cell, our model also qualitatively captures the overall population scale features (Appendix 5 Fig. 5A.4.). For different levels of biochemical noise (depicted by the width of uniform distribution from which initial values of the signaling nodes are selected), frequency and amplitude recovery indices were measured for a sample size of 400 *in silico* cells in each case (Fig. 5.3. E-P). While the trends for low receptor density, RGS4 expression and drug inhibition for all the noise levels remain similar to the experimental data, the distribution of cells along the correlation varies significantly with noise. For low levels of biochemical noise (μ +/- σ, $\sigma = 0.05\mu$, μ= mean value), most of the cells in the non-perturbed set remain localized to high FRI-ARI regime (Fig. 5.3. E), that appears less physiological when compared to experimental data (Fig. 5.3. A). When the experimental data is compared to the model data for the three noise levels tested, we find that high noise levels better mimic the experimental data (Fig. 5.3. I-P). In summary, the results suggest that perturbation and rescue experiments lead to a shift in the distribution of cells along the amplitude-frequency correlation in a noise dependent fashion.

5.2.4. Biochemical noise affects the rescuing capacity of drug action at single cell level in a GPCR-mediated signaling pathway

Next, we calculate the fraction of high fidelity responses for the cell population in each case depicted in Fig. 5.3. We define cells to have high signaling fidelity if ARI and FRI are both greater than 0.5 and low fidelity if either is less than 0.5. As expected, for all the noise conditions

tested, as well as for the experimental data, the control cells (non-perturbed) exhibit greater fraction of high fidelity responses (Fig. 5.4. A). However, the fraction decreases with increasing noise levels. Thus, biochemical noise limits the fraction of cells that can respond with high fidelity. Interestingly, for the same rescue conditions (RGS4 expression and drug inhibition), the fraction of cells that could be rescued from low fidelity response to high fidelity response increases with increasing noise levels. We define 'drug rescue coefficient' as the fraction of cells that could be rescued from low fidelity response after drug treatment divided by the fraction of cells high fidelity response without any treatment, to estimate how drug action can be affected by noise levels. Interestingly, the rescue coefficient increases with increasing noise levels (Fig. 5.4. B). This suggests that biochemical noise enhances the chances of a cell to be rescued upon drug action from a low fidelity response. Taken together, we find that increasing biochemical noise indeed helps more number of cells rescue back to high-fidelity response.

5.3. Discussions

Understanding how individual cells process temporal signals and respond to external perturbations such as overexpression of a signaling protein or drug inhibition, amid population heterogeneity is a major challenge in biology. The aim of the work presented in this chapter is to develop a simple method that can assess cellular heterogeneity in drug response and to understand how biochemical noise affects that response. Taking advantage of the fact that phase locked signals generated through pulsatile microfluidics can provide two observables for the same cell, we eliminated the tedious task of developing a 'two fluorescence reporter' (Rhee *et al*, 2014; Raser, 2004; Elowitz *et al*, 2002) and still be able to estimate biochemical noise for drug study purposes. Since our technique is based on pulsatile phase locked stimulations, the time scale of measurement matches well with the time scale of signaling and is independent of the gene expression of a particular fluorophore. Our technique (TRePS method) is, however, an indirect method of measuring biochemical correlations, and is therefore prone to additional intrinsic (stochastic) noise and may not be used to estimate exact amount of noise in the system. The other limitation is that the method can only be used for signaling systems that are inherently oscillatory and exhibit phase locked responses. Regardless of these limitations, when this method is used along with computational modeling of noise, it may provide valuable insights into mechanisms of how noise affects certain physiological or pharmacological responses in that particular signaling system. We also speculate that with the advent of better spatio-temporal resolution and imaging techniques

coupled with microfluidics, better observables can be defined and tested to estimate biochemical noise in the system.

Our results from the TRePS analysis raise a few essential questions regarding pharmacological studies done with cell population alone, such as: (1) Are overexpression and knockdown methods to study drug action sufficient? (2) Does the quantification of drug action on cell population really mirror what happens at single cell level? Overexpression or knockdown of signaling components may shift the response regime where a potential drug is sensitive enough to bring (on an average) the response back to normal from perturbed or pathological conditions. However, under physiological conditions, the sensitivity may be lost. Similarly, with biochemical noise existing in the system, the drug may be able to partially rescue the perturbed condition at population-averaged level, and still not be able to rescue a subpopulation of cells if the signaling exhibits bifurcation in the cellular response as we observed in Chapter 3. Thus, a drug may appear to be having an effect in laboratory conditions (under population scale measurements), and may still fail during clinical trials, which happens to a majority of potential drugs. Our results in section 5.2.4 suggest that biochemical noise plays a role of a dual-sword in signaling pathways. On one hand, it limits the fraction of high-fidelity cells. On the other hand, it also facilitates a sub-population of cells to be rescued back by potential drug action. Thus, based on our results, we speculate that, although noise costs efficiency (or fidelity) in the signal transduction, it also makes the system more robust to be brought back from perturbed conditions. A better understanding of noise and how we can exploit it for our advantage will bring a great stride in the drug discovery protocols.

5.4. Conclusions

In this chapter, we asked how biochemical noise may affect the drug action at single cell level. We showed that population averaged response with step stimulation of ligand may occlude the single cell response behavior, and there may be overlap between the response of population of perturbed cells and the cells rescued by the drug action. We explored the reason for this overlap and how it may impact drug action. To address this, we developed a microfluidic experiment to measure two observables in the same cell, similar to a 'two-reporter' system to estimate biochemical noise in the system. Our analysis with microfluidic experiments and mathematical

modeling suggests that the drug action on rescuing perturbed cells increases with increasing noise. Appropriate exploration of biochemical noise may be used to our advantage in drug discovery.

5.5. Materials and Methods

Materials

Materials used for experiments in this Chapter are detailed in Appendix 1.

Methods

Cell culture. HEK293 M3R4 cells stably expressing human muscarinic acetylcholine receptor M3 and doxycycline inducible RGS4 were cultured in DMEM with 10% FBS, geneticin G418 (400 µg/ml), hygromycin (200 µg/ml) and blasticidin (15 µg/ml) in T-25 flasks (Bodenstein *et al*, 2007). Transient transfection with R-GECO1 plasmid was carried out using Lipofectamine 3000 following the protocol prescribed.

Methods description about seeding cells in microfluidic device and time lapse image and analysis are detailed in Appendix 1.

Calculation of frequency and amplitude recovery indices. In the low concentration regime (C_1), Frequency Recovery Index is defined as the number of phase-locked calcium peaks above a threshold value divided by the total number of pulsed stimulations:

$$Frequency\ Recovery\ Index\ (FRI) = \frac{\#\ of\ calcium\ peaks\ above\ a\ threshold\ value}{Total\ \#\ of\ input\ pulsed\ stimulations}$$

Similarly, in the high concentration regime (C_2), Amplitude Recovery Index is defined as the ratio of calcium amplitude of the 'mth' pulse to the first pulsed stimulation:

$$Amplitude\ Recovery\ Index\ (ARI) = \frac{Amplitude\ of\ mth\ calcium\ peak}{Amplitude\ of\ first\ calcium\ peak}$$

Note: The threshold in calculating FRI is empirically taken as one-sixth of the maximum amplitude. Similarly m is taken as 8 in case of calculating ARI.

Mathematical model and computational analysis

GPCR-calcium model with extrinsic noise. The mathematical model for GPCR-calcium signaling used in this work is taken from our previously published articles (Jovic *et al*, 2010, 2011; Sumit *et al*, 2015). The model description, reactions and parameter values are as detailed in our previous work in Chapter 2 (Sumit *et al*, 2015).

Computational analysis. A system of ordinary differential equations (ODEs) was generated for the model and solved in MATLAB (MathWorks Inc., Natick, MA) with the ode15s stiff solver. The initial concentrations of three critical signaling components, GPCR, G-protein and PLC, were chosen from uniform distributions around the mean value using Latin hypercube sampling (LHS) (Marino *et al*, 2008). Thus, *in silico* cell-to-cell variability was generated for 400 LHS parameter sets. Analysis of the individual traces to identify peaks and determine frequency and amplitude recovery indices were done using script files written in MATLAB.

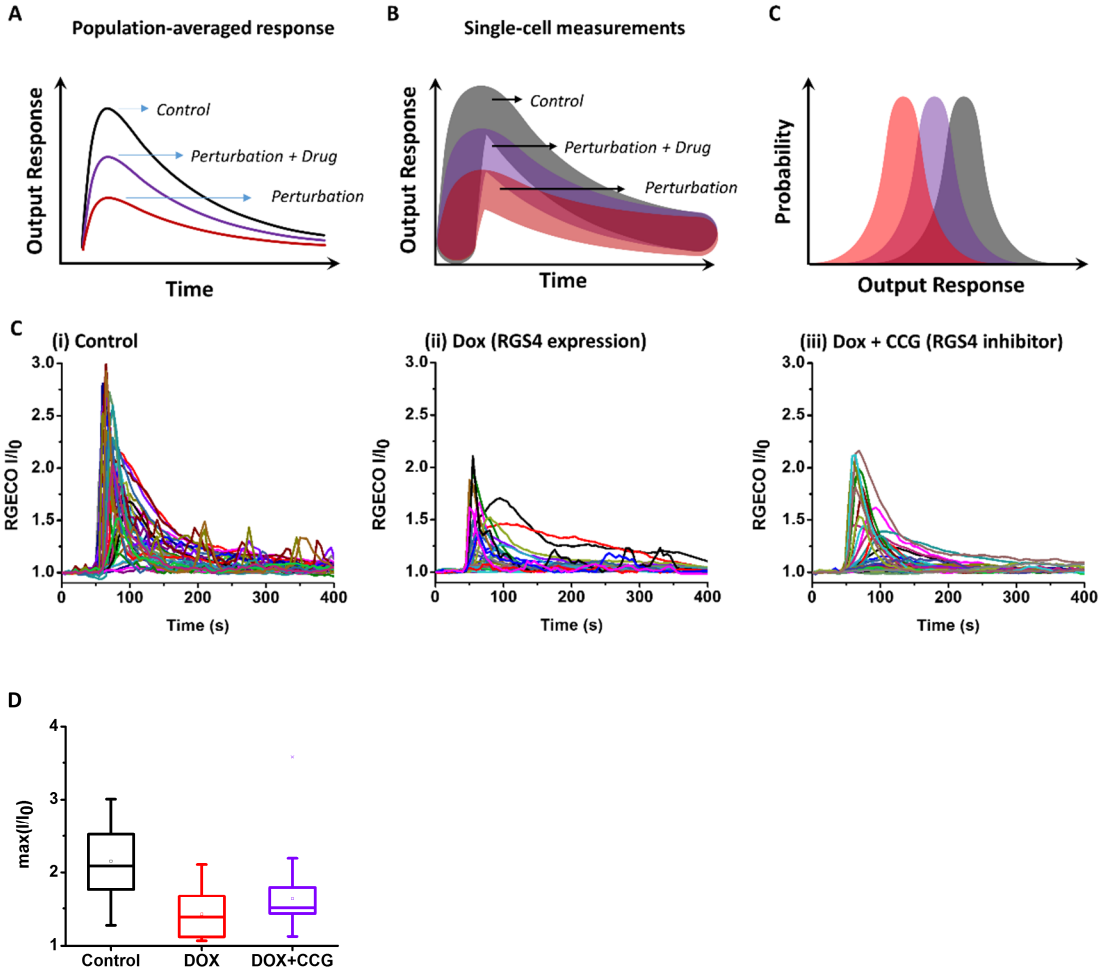

Fig. 5.1. Population scale measurements obscure drug response behavior at single cell level. While population-averaged behavior may show a change in the response upon perturbation and drug treatment (A), single cell measurements may be highly noisy and partially overlapping (B). The overlap in single cell measurements can be shown as a probability distribution of the maximum response (C). C. Single cell traces for RGECO-calcium response up on step stimulation for three different conditions: (i) control: M3R4 HEK 293 cells treated with DMSO (vehicle) and stimulated with 10 nM carbachol; (ii) perturbed cells: cells treated with 1 µg/mL doxycycline overnight to induce RGS4 expression, and stimulated with 10 nM carbachol; (iii) perturbed cells with drug treatment: cells treated with 1 µg/mL doxycycline overnight to induce RGS4 expression, and stimulated with 10 nM carbachol along with treatment with 3 µM of RGS4 inhibitor CCG-203769. D. Maximum RGECO response for the three conditions shown as box-plot, indicating overlap of response between perturbed cells and cells treated with the drug.

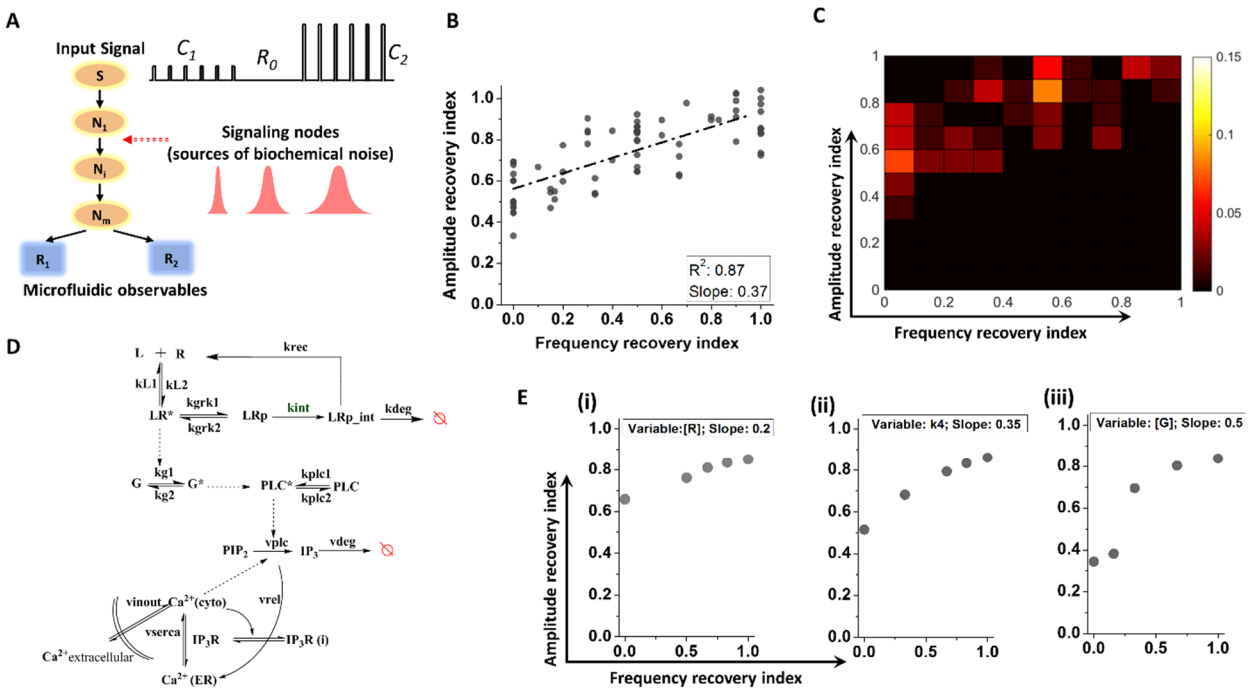

Fig. 5.2. Two regime pulsed stimulation (TRePS) shows correlation between two microfluidic observables that can be attributed to biochemical variability. A. Schematic outlining single cell TRePS method. The same cell is stimulated with pulses of ligands in two different regimes C_1 and C_2, to yield the values R_1 and R_2, corresponding to the two microfluidic observables. Similar to the "two reporter system", correlation between R_1 and R_2 can be related to the biochemical noise exhibited by the signaling nodes. The method is applied to microfluidic experiments as well as in silico testing of deterministic model with varying amount of biochemical noise to understand the effects of perturbations and drug response at single cell scale. B. The observables, frequency and amplitude recovery indices, show a positive correlation for the TRePS experiment. C_1 = 10 nM, C_2 = 100 nM, D = 24 s, R_0 = 8 min, and R varied from 90 s – 200 s to explore the correlation space. C. Contour histogram of the amplitude and frequency indices correlation space showing cells with better frequency recovery also exhibit a better amplitude recovery. D. A deterministic model for GPCR-calcium signaling, developed in Chapter 2 that captures several characteristic features of pulsed stimulation. The signaling nodes are with possible biochemical variations are GPCR, G-protein and PLC. The remaining nodes, IP_3, calcium and calcium-ER equilibrate based on the initial conditions of previously mentioned nodes. E. Variation in the initial value of nodes in the deterministic model gives similar positive correlation between amplitude and frequency indices.

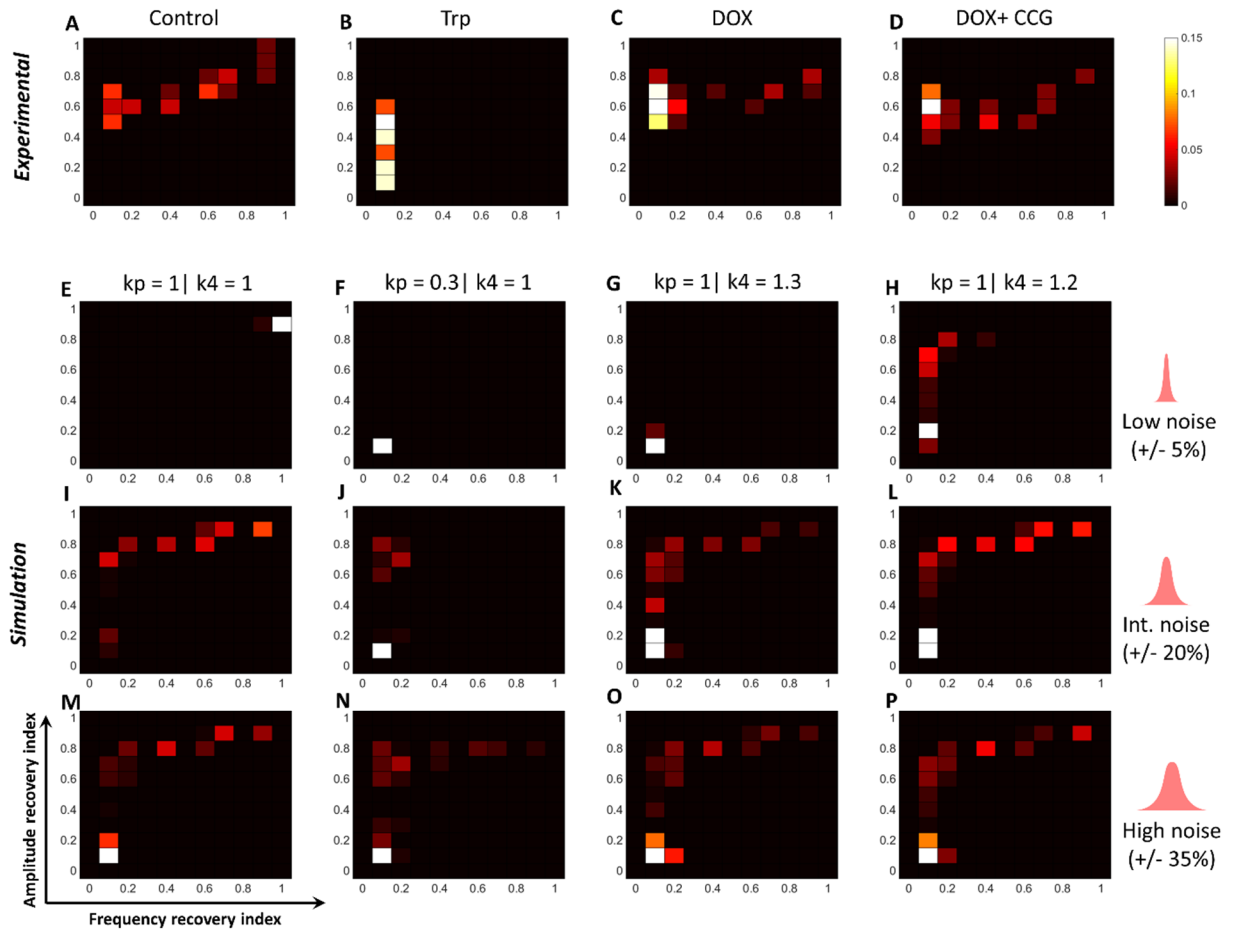

Fig. 5.3. Perturbation and rescue experiments shift the distribution along the amplitude-frequency correlation in a noise dependent fashion. A-D. Contour histograms of amplitude and frequency indices for microfluidic TRePS experiments with various perturbations: (A) control: M3R4 HEK 293 cells treated with DMSO (vehicle) and stimulated with 10 nM carbachol; (B) 0.25% Trypsin treated cells stimulated with 10 nM carbachol; (C) perturbed cells: cells treated with 1 µg/mL doxycycline overnight to induce RGS4 expression, and stimulated with 10 nM carbachol; (D) perturbed cells with drug treatment: cells treated with 1 µg/mL doxycycline overnight to induce RGS4 expression, and stimulated with 10 nM carbachol along with treatment with 3 µM of RGS4 inhibitor CCG-203769. E-P. Contour histograms of amplitude and frequency indices for *in silico* TRePS experiments with various perturbations: relative fraction of receptor density (kp; 1 or 0.3) and relative fraction of G-protein deactivation based on RGS4 activity and drug inhibition (k4; 1, 1.3 and 1.2 respectively). Experimental data (A-D) from > 60 cells from three sets of experiments. Simulation data from 400 *in silico* traces in each case, generated from uniform distribution of initial values of the signaling nodes with Latin hypercube sampling method.

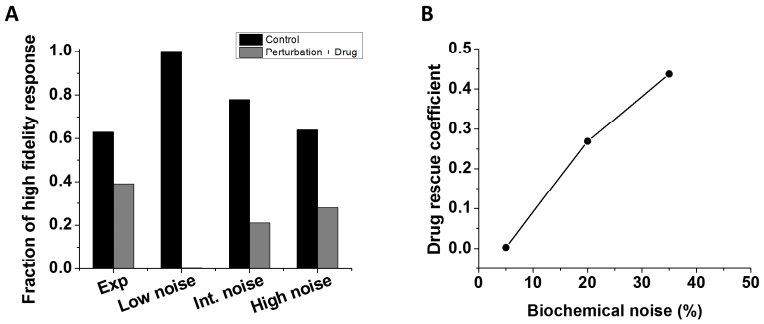

Fig. 5.4. Biochemical noise affects the rescuing capacity of drug action at single cell level in a GPCR-mediated signaling pathway. A. Fraction of high fidelity response (frequency and amplitude recovery indices > 0.5) for control (black bars) and DOX+CCG treated (gray bars) cells as a measure of the drug efficacy. B. Drug rescue coefficient (defined as the fraction of high fidelity cells after perturbation divided by the fraction of high fidelity cells in the control sets of experiments) increases with increases the biochemical noise.

Chapter 6. Conclusions and future directions

6.1. Conclusions

In this thesis, I use both experimental and computational approaches to explore how information is processed in a GPCR signaling pathway under physiological pulsatile stimulations. Various techniques including pulsatile stimulation using microfluidics, single cell analysis, mathematical modeling, and information and noise analysis have been implemented to understand information processing in such signaling pathways. The main hypothesis driving this work is that cells must be able to discern time-varying inputs and must have evolved evolutionarily to exploit temporal information available in their microenvironment to their advantage. Although this thesis focuses on one particular receptor (viz. muscarinic M3 receptor), it endeavors to develop a general understanding about temporal information processing that may be applicable to many signaling pathways. Understanding the signaling circuit architectures that drive temporal information processing through noisy transduction pathways will provide mechanistic insights into several biological processes that are poorly understood, such as achieving selective downstream responses, epigenetic selectivity and robustness in signaling response. It will also provide tools to synthetic biologists interested in manipulating cellular responses for *in vitro* applications including lab-on-chip development. Moreover, understanding how biochemical noise may affect drug action will facilitate development of drugs that are more potent, despite the presence of biochemical variability in the cells they are meant to target.

Band-pass processing selects for downstream transcription factor activation

Temporal signal processing in receptor-mediated pathways is increasingly appreciated as a tool that cells utilize to achieve enhanced activity and selectivity, and to distinguish signal from noise. To understand how temporal modulation of an input signal influences downstream responses, we employed microfluidic pulsatile stimulation of a G-Protein coupled receptor, the muscarinic M3 receptor, in single cells with simultaneous real-time imaging of both intracellular calcium and NFAT nuclear localization. Interestingly, we find that reduced stimulation with pulses of ligand

can give more efficient transcription factor activation, if stimuli are timed appropriately. Our experiments and computational analyses show that M3 receptor-induced calcium oscillations form a low pass filter while calcium-induced NFAT translocation forms a high pass filter. The combination acts as a band-pass filter optimized for intermediate frequencies of stimulation. We demonstrate that receptor desensitization and NFAT translocation rates determine critical features of the band-pass filter and that the band-pass may be shifted for different receptors or NFAT dynamics. As an example, we show that the two NFAT isoforms (NFAT4 and NFAT1) have shifted band-pass windows for the same receptor. While we focus specifically on the M3 muscarinic receptor and NFAT translocation, band-pass processing is expected to be a general theme that applies to multiple signaling pathways.

Cellular responsiveness to weak physiological stimuli is fate not luck

Physiological stimulations that are transitory and weak, such as low concentrations of acetylcholine present for just tens of seconds or TNFα for just tens of minutes, lead to irregular downstream responses that are often interpreted as stochastic. In Chapter 3, we provide a deterministic explanation for this behavior that is based on cell-to-cell variability, a short-term memory of stimulation, and high Hill coefficient processes, providing data on muscarinic M3 receptor-induced calcium signaling as an example. Furthermore, we provide a tractable, two-pulse experimental test that utilizes different rest periods between the stimulation pulses to determine if an apparently stochastic response in a dynamic signaling process has a deterministic basis. These analyses reveal that the seemingly random responses of cells to weak stimuli are determined by the signaling capacity of cells and the stimulation timing. The results suggest that physiological, low concentration pulsing of signals is a deterministic strategy for the body to guide distinct subsets of cells to their appropriate fate rather than a stochastic process that leaves outcomes to chance.

Pulsatile input enhances information transfer in a noisy biochemical pathway

In Chapter 4, we measured single cell response to quantify information transfer via M3 receptor to calcium and NFAT response under step and pulsed conditions. We showed that the mutual information transfer for pulsed stimulation is not only greater than that for the step changes alone, but also exceeds the maximum information transfer possible under non-pulsatile conditions.

Focusing on the deterministic model, we show that the extent of cell-to-cell variability critically determines the amount of information that can be transferred downstream. We also show that the two isoforms of NFAT with different band-pass windows exhibit different levels of information transfer and their mutual information transfer is greater than their information transfer capacities alone. Additionally, we show that the dynamic output (vector measurement) enhances the information transfer in all the cases. Taken together, Chapter 4 concludes that pulsed input from the micro-environment along with the dynamics of the output enable cells to maximize the information transfer downstream, despite the presence of cell-to-cell variability in the system.

Biochemical noise affects the rescuing capacity of drug action at single cell level

In this chapter, we asked how biochemical noise may affect the drug action at single cell level. We showed that population averaged response with step stimulation of ligand may obscure the single cell response behavior, and there may be overlap between the response of population of perturbed cells and the cells rescued by drug action. We explored the reason for this overlap and how it may impact drug action. To address this, we developed a microfluidic experiment to measure two observables in the same cell, similar to a 'two-reporter' system to estimate biochemical noise in the system. Our analysis with microfluidic experiments and mathematical modeling suggests that the drug action on rescuing perturbed cells increases with increasing noise. Appropriate exploration of biochemical noise may be used to our advantage in drug discovery.

6.2. Insights and perspectives

Investigation of cellular signaling dynamics using microfluidics and mathematical/computational modeling possesses unique advantages in dissecting signaling circuitry by utilizing a wide observability space while reducing response heterogeneity through phase locking and/or entrainment. Several insights are possible from this study, including:

Multi-tasking through temporal compartmentalization

Components of signal transduction pathways are often involved in multi-tasking. One of the best examples is calcium, which is involved as a second messenger in several signaling pathways. For such multi-tasking components, it is essential to decide which downstream signal to elicit and which not to. One way these signaling components evolved for multi-tasking is through the

compartmentalization of space. It is now known that life evolved towards spatial compartmentalization to facilitate more complex tasks that a non-compartmentalized living system may be unable to perform. However, compartmentalization within the temporal regime is much less understood. In Chapter 2, we found that cells prefer timings that are "just right" – not too fast, not too slow. Analogous to the concept of space, we may conceptualize 'time' to be compartmentalized as well. In different 'temporal compartments' the same signaling molecule may be involved in a different task. The findings in Chapter 2 that the same spatially confined calcium may be able to activate two distinct isoforms of a transcription factor in two different 'temporal compartments' is a working proof of the same.

Band-pass analysis to dissect hidden/unknown temporal signaling motifs

We speculate that the band-pass concept should be applicable to several other signaling pathways and it can help understand the circuit architecture and hidden/unknown motifs. Recent findings of Ryu *et al* (Ryu *et al*, 2015) about ERK activation (Section 1.5) suggests that the two growth factors (EGF and NGF) generate different band-pass windows for ERK signaling and subsequent differentiation of neurite cells, consistent with our findings in GPCR-calcium-NFAT signaling. While the EGF acts in a narrow intermediate regime window (R = 10 min – 20 min), NGF acts in a much wider window, almost as a high pass filter. Thus, EGF signaling must comprise of additional low pass filter along with the downstream high pass amplification. This conclusion based on the band-pass concept is consistent with the predictions of Ryu *et al* that EGF may be inducing a fast negative feedback through the channels yet unknown. Additionally, the high pass filtering properties of NGF that works only with high dosage can be attributed to a positive feedback speculated to be present in the NGF signaling network, but not in the EGF signaling network. Similarly, in TGFβ signaling (Sorre *et al*, 2014), the existence of negative feedback and lowering of Smad4 amplitude upon rapid stimulation also suggests that the system works in a band-pass manner similar to GPCR-mediated NFAT translocation and EGF mediated differentiation (Ryu *et al*, 2015). This negative feedback under spatial constraints gives rise to an "adaptive mechanism" for embryonic development that is predicted to be more robust pattern as compared to the linear model without any negative feedback. Even in non-mammalian systems such as yeast, researchers have showed that the oscillatory stress stimulation results in an intermediate frequency regime for which the growth is slowed down significantly (Mitchell *et al*,

2015). While they attribute this regime to be non-natural and interpret this as a hidden sensitivity of cellular regulatory networks, it may be possible that the regime ~ 8 min period for which the MAPK activation is maximized may have some physiological relevance that is yet unknown. These observations strengthen our argument that band-pass processing of temporal information may exist in a variety of signaling pathways. Thus, band-pass processing appears to a general theme of how temporal information is processed and can be utilized to discover hidden/unknown motifs in similar signaling pathways.

Temporal selectivity through biochemical noise

A fundamental problem in biology is to understand how selectivity is achieved in a cell population. In case of spatial selectivity (such as cellular differentiation during embryonic development), several experimental and mathematical insights are available (Kholodenko, 2006). However, mechanisms for temporal selectivity, wherein timing alone may be able to segregate responsive and non-responsive cells, remains largely unknown. In Chapter 3, we showed that cellular responsiveness may significantly depend on biochemical content and non-linearity in the system. The biochemical variability along with pulsed stimulation may lead to selective activation and deactivation of a cellular sub-population. Thus, one way to achieve temporal selectivity may be through the pulsatile stimulation of cellular population with inherent biochemical variability and non-linearity in the signaling pathway. Apart from selectivity, another arena where insights from biochemical noise analysis can be of great importance is in the field of drug development, particularly in developing personalized medicines. In Chapter 5, we showed that the drug action can be altered based on biochemical variability. Under pathological conditions, protein expressions may vary for person-to-person. A drug may be effective in overcoming the pathology for one patient, while it may not be able to do so for another. Slight variability may result in drastic alterations in the effectiveness of a drug. Development of drugs that are not only potent towards pathology, but also robust against variability is essential, and will help avoid clinical trial failures to some extent.

6.3. Future directions

As an emerging field of investigation that incorporates quantitative experiments and modeling, microfluidic pulsatile stimulation approach possesses immense opportunities to seek

answers to scientific problems that may not be possible to get using conventional methods. As the microfabrication technology becomes more accessible and affordable, we speculate that investigating the band-pass regime for additional signaling pathways will uncover hidden or unknown motifs. Immense opportunities lie in investigating signaling pathways where external fluctuations and dynamics in the micro-environment may be playing a critical role. Advancements in biochemistry and genetics in the past century have provided us with plethora of information and understanding of complex signaling pathways in bits and pieces. Approaches that involve spatio-temporal interrogation will prove to be a great tool for integrating that information and understanding the signaling behavior at systems scale. From theoretical aspects, it will be interesting to investigate whether a signaling pathway can be predicted for its range of temporal modulation and also to determine if the existence of such patterns make systems more robust.

There are several future directions possible based on the study in thesis, including:

Distinct downstream responses for metabotropic glutamate receptors

In Chapter 2, we predicted that band-pass regimes will differ for different receptors and calcium-regulated transcription factors. Two of the metabotropic glutamate receptors, mGlu1 and mGlu5 have been shown to have distinct functional roles (Kotlinska & Bochenski, 2007; Bradley & Challiss, 2012; Mannaioni *et al*, 2001; Sun & Neugebauer, 2011; Pietraszek *et al*, 2005; Gubellini *et al*, 2003). It remains largely unknown how same signaling circuitry functionally diverges into two distinct downstream responses for these two receptor subtypes. While the known mechanism through which they signal remains the same, they do possess distinct receptor regulation kinetics (Bradley & Challiss, 2012). Upon stimulation, mGlu1 receptor desensitizes rapidly and recovers slowly, leading to single peak-and-plateau type calcium response. In contrast, mGlu5 receptor gets phosphorylated and dephosphorylated rapidly (also known as "dynamic uncoupling") (Dupont *et al*, 2011b). This results in robust calcium oscillations. It can be inferred that mGlu5 receptor can elicit downstream response for fast pulsed stimulations and even step stimulations by producing rapid calcium oscillations. In contrast, mGlu1 receptor would require intermittent, slow stimulations that would provide the receptor sufficient time to recover from desensitization. Thus, mGlu1 and mGlu5 receptors are expected to have different band-pass regimes. It would be interesting to explore how the same receptor-mediated calcium response may lead to two different outcomes downstream simply on the basis of receptor desensitization.

Exploring frequency modulated signaling mediated by Luteinizing hormone (LH)

LH is produced by gonadotropic cells and is involved in triggering ovulation in females, and in stimulating cells that produce testosterone in males. Additionally, studies on LH dependent oocyte maturation suggest its link to protein kinase C and calcium oscillation (Woods & Johnson, 2007; Fan, 2003; Robinson *et al*, 2012; Hsieh *et al*, 2011). It is known that LH is secreted in pulsatile bursts with time period ~2 h (Santen & Bardin, 1973; Bergendahl *et al*, 1998). Interestingly, the time period of secretion increases during the menstrual cycle. The shift in LH pulse frequency is expected to be the key to transition from ovulation to menstruation. It would be interesting as well as medically important to explore how different LH frequencies may alter the downstream response. Understanding such mechanisms will help develop drugs targeted to regulate the LH oscillation frequency in females with abnormal menstrual cycles or issues with oocyte maturation.

Understanding mechanobiology of receptor signaling

Recent evidence suggests that surface stiffness and other mechanical properties (such as geometry and shear) activate receptor regulatory kinases (Lembong *et al*, 2015; Kim *et al*, 2009). Preliminary data on phase locking experiments on soft PDMS devices indicates decreased calcium response across cell population. This relates well with the current understanding of increased G-protein regulatory kinase (GRK) activity on soft surfaces (Gurevich *et al*, 2012; Freeman *et al*, 1998; Luo *et al*, 2008; Goldberg *et al*, 2010). Pulsatile stimulation provides a quantitative platform to explore how mechanical properties of the cellular microenvironment affect downstream response at single cell level, and also to compare mathematical models to develop deeper insights into mechanobiology of receptor signaling, in particular, GPCR-mediated downstream responses.

Neuronal stimulation for eliciting immunological responses

Recent studies in neuroscience and immunology suggest links between neural reflexes and immune responses (Abboud *et al*, 2012; Sternberg, 2006). Even our study suggests that neurotransmitters such as acetylcholine can induce NFAT activation. Our band-pass analysis also predicts that at a longer (and rather more sustained) rest periods, calcium oscillations may elicit NFκB response (Xu *et al*, 2014). Both NFAT and NFκB play crucial roles in immune response. It would be interesting to explore how different rest periods (and also different ligand) may elicit

immune response upon pulsatile stimulation of cells. This study will not only provide scientific insights into mechanisms of immune response, but also aid development of relevant and more potent therapeutics.

Information analysis of signaling motifs to build 'cellular lasers'

Results in Chapter 2 demonstrate that phase-locked responses under a particular stimulation frequency window lead to maximum downstream response. Moreover, we also found that incoherent behavior in signaling pathways may be due to cell-to-cell variability or biochemical noise (Chapter 3-5). Taking these two results together, we hypothesize that by minimizing cell-to-cell variability using genetic tools and stimulating cells in pulsatile fashion using automated microfluidic oscillators, we should be able to get coherent downstream response in a cell population, analogous to the concept of lasers in optics. 'Cellular lasers' would greatly enhance desired output in biotechnology-related applications.

Novel methods for investigating noisy and complex circuit architectures

There are multiple new methods and techniques that have been developed recently or are being developed that can be used for investigating noisy and complex circuit architectures. In the future, they can be used together to address some of the important questions in the field. Advancements in microfluidic technology to enhance temporal and spatial resolution with high throughput analysis of signaling dynamics in live single cells with multiple read-outs (multiple probes) will further expand the observability space (Kilinc *et al*, 2015; Siltanen *et al*, 2016; Hansen *et al*, 2015; Frank & Tay, 2015; He *et al*, 2015). Simultaneously, the large amount of single cell data from noisy biochemical pathways requires advanced data analysis tools (Tseng *et al*, 2014). Utilizing information theory to analyze the signal and noise in the data is an example of how we can address important questions (Selimkhanov *et al*, 2014). Advancements in the field of mathematical and computational modeling such as multi-scale modeling and agent-based modeling for systems pharmacology will further push the investigation at systems scale (Cilfone *et al*, 2015; Behar *et al*, 2013). With the advent of tools like optogenetics (Toettcher *et al*, 2013) and high resolution imaging, we speculate that the investigation will expand from temporal modulation to spatiotemporal modulation and mathematical modeling to further elucidate how spatiotemporal constraints (Warmflash *et al*, 2014; Kar & Parekh, 2015) modulate the signaling dynamics. Thus, a deeper understanding of signal transduction pathways using these tools will provide us

opportunity to utilize this approach for synthetic biology applications, designing novel pharmaceutical interventions, as well as understanding fundamentals of spatio-temporal coordination.

Appendices

Appendix 1. Materials and Methods common to Chapter 2-5

Materials

High glucose Dulbecco's Modified Eagle's Medium (DMEM) with phenol red, 0.05% Trypsin, 10X HBSS (with Ca^{2+} and Mg^{2+}), HEPES buffer (1 M), Geneticin and OPTIMEM were obtained from Gibco (life technologies, Grand Island, NY), Fetal Bovine Serum (FBS) was obtained from Gemini Bioproduct (West Sacramento, CA), Lipofectamine 3000 was obtained from Invitrogen (life technologies, Carlsbad, CA), D-Glucose 10% (w/v) from Sigma (St. Louis, MO), Carbachol from Calbiochem (EMD Biosciences, La Jolla, CA), PDMS and curing agent from Dow Corning (Midland, MI). Imaging media (1X HHBSS, pH 7.4) was prepared as described in (Palmer & Tsien, 2006). CMV-R-GECO1 was a gift from Robert Campbell (Addgene plasmid # 32444) (Zhang *et al*, 2015). HA-NFAT4-GFP and HA-NFAT1-GFP were a gift from Anjana Rao (Addgene plasmid # 21664) (Aramburu *et al*, 1999).

Methods

Cell culture. HEK293 cells stably transfected with human muscarinic acetylcholine M3 receptor described previously (Bodenstein *et al*, 2007) were cultured in DMEM with 10% FBS and Geneticin (400 μg ml-1) in T-25 flasks (Jovic *et al*, 2011). Transient transfection with R-GECO1 and NFAT4-GFP or NFAT1-GFP was carried out using Lipofectamine 3000 following prescribed protocol.

Microfluidic device. The devices were fabricated based on the computerized microfluidic cell culture system using Braille display as described in (Gu *et al*, 2004). The chips were filled with laminin (100 μg/ml) and incubated overnight. Subsequently, the chips were washed and incubated with DMEM/10% FBS under sterilized conditions. Cells were seeded in the outlet channel of the device as described in (Jovic *et al*, 2010, 2011). The microfluidic setup was used to deliver periodic and step stimulation of carbachol controlled by a custom written software as described in (Gu *et al*, 2004).

Time lapse imaging and analysis. Cells were imaged with a TE-2000 U Nikon microscope using a 20X Flour objective illuminated by a 100W Hg lamp. Sequential acquisition of R-GECO1 and NFAT-GFP fluorescence was carried out every 5 s using ET572/35 (ex), ET630/50 (em), ET490/20 (ex) and ET535/50 (em) filters respectively (Chroma Technology Corp, Rockingham, VT). The excitation and emission filters were equipped in filter wheels controlled by a Lambda 10-3 Shutter Controller (Sutter Instruments, Novato, CA). MetaFluor Software (Molecular Devices, Downington, PA) was used to select regions of interest (ROIs) in single cells and to determine the area-averaged intensity I(t) both in cytoplasmic region (I(t)cyto) and in the nuclear region (I(t)nuc). Calcium response was measured by the ratio I(t)cyto/I0 where I0 corresponds to the basal RGECO1 intensity in the cytoplasmic ROI (Appendix 2 Fig. 2B.1). NFAT translocation was quantified by determining I(t)nuc/I(t)cyto ratio from the GFP fluorescence data (Appendix 2 Fig. 2B.2).

Appendix 2. Supplementary to Chapter 2

Text 2A.1. *Brief description of the model development*

The mathematical model for GPCR-calcium-NFAT signaling can be described in two modules: A. GPCR-calcium signaling and B. Calcium-NFAT signaling. The model has been described in Section 1.6. In Chapter 2, based on the calcium data obtained for various step and pulsatile stimulation, we modified the receptor regulatory mechanism in the existing model (Jovic *et al*, 2013; Politi *et al*, 2006), to explain the calcium duty cycle ratio decay (Fig. 2.3. A). In the earlier version, the ligand-receptor complex (L-R) reversibly phosphorylates to form inactive L-R-P state. To this, we added receptor internalization, partial degradation and recycling via endosomal sorting i.e., the inactive complex can be dephosphorylated to reform the free receptor or can be internalized and either degraded or recycled back to the surface (French & Lauffenburger, 1996). The calcium-NFAT module remains the same, except the parameters values were adjusted to fit experimental data for NFAT4 and NFAT1.

Text 2A.2. *Variables, Parameters and Equations for GPCR-Calcium-NFAT4 model*

Variable	**Initial Value**	**Units^**	**Description**
R	0.114	μM	Free M3 receptors
L	Input	μM	Extracellular carbachol (ligand)
C	0	μM	Ligand/receptor complex
C_p	0	μM	Phosphorylated C
R_{int}	0	μM	Internalized Receptor
G	0.2	μM	Inactive G-protein
G_{GTP}	0	μM	GTP-bound alpha-subunit
G_{GDP}	0	μM	GDP-bound alpha-subunit
$\beta\gamma$	0	μM	Beta-gamma dimer subunit
$\beta\gamma_{int}$	0	μM	Beta-gamma subunit internalized
PLC	0.25	μM	Inactive PLC
$PLC*$	0	μM	Activated PLC (bound to G_{GTP})
IP_3	0.03	μM	Inositol trisphosphate

$f_{IP_3R_a}$	0.9	*Fraction*	Fraction of active IP_3R vs total
Ca_{ER}	2.9	μM	Calcium in endoplasmic reticulum
$Ca_{cytosol}$	0.03	μM	Calcium in cytosol
$NFATpi_{cyto}$	1.22	*nM*	Cytoplasmic phosphorylated NFAT
$NFAT_{cyto}$	0.01	*nM*	Cytoplasmic dephosphorylated NFAT
$NFAT_{nuc}$	0.25	*nM*	Nuclear dephosphorylated NFAT
$NFATpi_{nuc}$	0.0035	*nM*	Nuclear phosphorylated NFAT

Ligand-binding and G-protein kinetics

Parameter	**Model Value**	**Units**	**Description**	**Literature Value***	**Ref.**
$k_{f,L}$	2.27	$\mu M^{-1}s^{-1}$	Rate constant for binding of L to R	0.8 – 5.1	(Schreiber *et al*, 1985; Dowling & Charlton, 2006; Sykes *et al*, 2009; Jovic *et al*, 2011)
$k_{r,L}$	0.07	s^{-1}	Rate constant for dissociation of L from C	0.01 – 0.11	(Schreiber *et al*, 1985; Dowling & Charlton, 2006; Sykes *et al*, 2009; Jovic *et al*, 2011)
k_3	0.0077	s^{-1}	Exchange rate constant of GDP for GTP	0.005 – 0.05	(Chay & Lee, 1995; Jovic *et al*, 2011)
k_4	1.9	s^{-1}	Hydrolysis rate constant of GTP to GDP	0.100 – 2.00	(Thomsen & Neubig, 1989; Jovic *et al*, 2011)
k_5	$2.0*10^{-5}$	$(\#/cell)^{-1}s^{-1}$	Encounter rate of C and G	$2*10^{-5}$	(Thomsen & Neubig, 1989; Jovic *et al*, 2011)
k_6	$2.0*10^{-5}$	$(\#/cell)^{-1}s^{-1}$	Encounter rate of PLC and G_{GTP}	$2.0*10^{-5}$	(Jovic *et al*, 2011)
k_7	$1.0*10^{-5}$	$(\#/cell)^{-1}s^{-1}$	Encounter rate of G_{GDP} and $\beta\gamma$	$10^{-5} – 10^{-4}$	(Mahama & Linderman,

					1994a; Jovic *et al*, 2011)

Receptor desensitization kinetics adapted from (Vayttaden *et al*, 2010) modeled for a different GPCR (Beta Adrenergic Receptor) &&

Parameter	Model Value	Units	Description
$k_{grk,1,f}$	0.029	s^{-1}	Phosphorylation rate constant for C
$k_{grk,1,r}$	$3.6*10^{-3}$	s^{-1}	Dephosphorylation rate constant for C_p
k_{int}	0.0037	s^{-1}	Rate constant for internalization of C_p
k_{deg}	0.0004	s^{-1}	Rate constant for degradation of internalized receptors
k_{rec}	0.001	s^{-1}	Receptor recycle rate constant

Calcium and IP_3 kinetics adapted from (Politi *et al*, 2006) &&

Parameter	Model Value	Units	Description
V_{serca}	0.267	$\mu M^{-1}s^{-1}$	Maximal SERCA pump rate
K_{serca}	0.076	μM	Half-activation constant of SERCA pump
V_{pm}	0.0138	$\mu M^{-1}s^{-1}$	Maximal PMCA pump rate
K_{pm}	0.0756	μM	Half-activation constant of PMCA pump
v_0	10^{-4}	$\mu M^{-1}s^{-1}$	Basal calcium flux into cell
ϕ	0.0024	s^{-1}	Stimulant-dependent calcium flux into cell
ε	3	a.u.	Calcium flux strength
beta	0.185	a.u.	Ratio of effective volume of endoplasmic reticulum to cytosol
p	1.7	a.u.	Hill coefficient for PLC-Calcium binding
k_{ca}	950	s^{-1}	Activated rate constant of IP_3synthesis per molecule of PLC
k_{basal}	0.3	$\mu M^{-1}s^{-1}$	Rate constant for basal IP_3 synthesis
k_{3k}	0	s^{-1}	Phosphorylation rate of IP_3
K_{3k}	0.465	μM	Half activation constant of IP_3 -kinase
k_{5p}	0.56	s^{-1}	Dephosphorylation rate of IP_3
K_{plc}	0.213	μM	Half-activation constant of PLC
k_1	0.85	s^{-1}	Maximal rate constant of calcium release through IP_3R

k_2	0.014	s^{-1}	Rate constant for calcium leak through IP_3R
K_a	0.059	μM	Equilibrium constant of calcium binding to activating site on IP_3R
K_i	0.47	μM	Equilibrium constant of calcium binding to inhibiting site on IP_3R
K_p	0.13	μM	Equilibrium constant of IP_3 binding to IP_3R
τ_r	7	s	Characteristic time of IP_3R inactivation

Calcium-NFAT dynamics adapted from (Cooling *et al*, 2009) &&

kd1	1760	*nM*	Calcineurin-Calmodulin dissociation constant
kn1	$7.7*10^{-6}$	$(nM\text{-}s)^{-1}$	Rate constant for association of activated calcineurin and $NFATpi_{cyto}$
kn2	0.002	s^{-1}	Rate constant for dissociation of $NFATpi_{cyto}$ from Calcineurin-$NFAT_{cyto}$ complex
kn3	$1.0*10^{-3}$	s^{-1}	Rate constant for nuclear translocation of activated NFAT &
kn4	$4.45*10^{-4}$	s^{-1}	Dissociation rate of activated nuclear NFAT
kn5	$4.71*10^{-5}$	$(nM\text{-}s)^{-1}$	Rate constant for association of nuclear NFAT and Calcineurin
kn6	0.003 - 0.0003	s^{-1}	Rate constant for back-translocation of nuclear NFAT to the cytoplasm &
KmN	535	*nM*	Half-maximal activation coefficient of calcium
M	6000	*nM*	Calmodulin concentration
N_{tot}	2000	*nM*	Total Calcineurin concentration
n	2.92	*a.u.*	Calcineurin hill coefficient
C_cn	8	*a.u.*	Scaling to adjust cytoplasmic versus nuclear volume
Ca_basal	100	*nM*	Basal bound cytoplasmic calcium

& parameter values vary for different NFAT isoforms; adjusted and optimized based on determined experimental values in (Yissachar *et al*, 2013; Tomida *et al*, 2003).

&& parameter values optimized using Latin Hypercube Sampling. The values are either same or lie in the same order of magnitude as the reference.

^ $conv = 3.1725 \times 10^{-6} \frac{\mu M}{\#/cell}$, used to convert units

Model Reactions	**Description**

Ligand-Receptor kinetics	
$v_1 = k_{f,L}[L][R] - k_{r,L}[C]$	Rate of ligand binding free receptor $(\mu M/s)$
$v_2 = k_{grk1,f}[C] - k_{grk1,r}[C_P] \times conv$	Rate of phosphorylation of C $(\mu M/s)$
$v_{int} = k_{int}[C_p]$	Rate of receptor internalization
$v_{deg} = k_{deg}[R_{int}]$	Rate of degradation of internalized receptors
$v_{rec} = k_{rec}[R_{int}]$	Rate of receptor recycling
G-protein kinetics and PLC activation	
$v_5 = k_3[G]$	Exchange rate of GTP for GDP on alpha subunit of G $(\mu M/s)$
$v_6 = \frac{k_5}{conv}[G][C]$	Encounter rate of G with C to form G_{GTP} $(\mu M/s)$
$v_7 = \frac{k_6}{conv}[G_{GTP}][PLC]$	Encounter rate of G_{GTP} with PLC to form PLC^* $(\mu M/s)$
$v_8 = k_4[G_{GTP}]$	Rate of hydrolysis of G_{GTP} to G_{GDP} $(\mu M/s)$
$v_9 = k_4[PLC^*]$	Rate of inactivation of PLC^* to PLC $(\mu M/s)$
$v_{10} = \frac{k_7}{conv}[G_{GDP}][\beta\gamma]$	Encounter rate of G_{GDP} with $\beta\gamma$ $(\mu M/s)$
IP_3-calcium kinetics	
$v_{11} = (k_{ca}[PLC^*] + k_{basal})\left(\frac{[Ca_{cyt}]^p}{[Ca_{cyt}]^p + K_{plc}{}^p}\right)$	Rate of IP_3 synthesis $(\mu M/s)$
$v_{12} = \left(k_{3k}\left(\frac{[Ca_{cyt}]^2}{[Ca_{cyt}]^2 + K_{3k}{}^2}\right) + k_{5p}\right)[IP_3]$	Rate of IP_3 degradation $(\mu M/s)$
$v_{13} = \left(k_1\left(f_{IP_3R_a}\left(\frac{[Ca_{cyt}]}{[Ca_{cyt}]+K_a}\right)\left(\frac{[IP_3]}{[IP_3]+K_p}\right)\right)^3 + k_2\right)\left([Ca_{ER}] - [Ca_{cyt}]\right)$	Rate of Ca_{ER} release into cytosol $(\mu M/s)$
$v_{14} = V_{serca}\left(\frac{[Ca_{cty}]^2}{[Ca_{cty}]^2 + K_{serca}{}^2}\right)$	Rate of pumping Ca_{cty} back into ER $(\mu M/s)$
$v_{15} = \varepsilon\left(v_0 + \phi + k_{ca}[PLC^*] + k_{basal} + \frac{1}{k_{3k}+k_{5p}} - V_{pm}\left(\frac{[Ca_{cyt}]^2}{[Ca_{cyt}]^2 + K_{pm}{}^2}\right)\right)$	Flux of calcium into and out of cell across plasma membrane $(\mu M/s)$
$v_{16} = \frac{1}{\tau_R}$	Recovery of inactivated IP_3R $(1/s)$
$v_{17} = \frac{f_{IP_3R_a}}{\tau_R}\left(\frac{K_i}{[Ca_{cyt}]+K_i}\right)$	Inactivation of IP_3R $(1/s)$
Calcium-NFAT kinetics	

$Ca = Ca_{basal} + [Ca_{cyt}]$	Total cytoplasmic calcium available for NFAT activation
$actN = \frac{Ca^4}{Ca^4 + KmN^4 * (1 + Kd1/M)}$	Fraction of activated calcineurin
$J1 = kn1[NFATpi_{cyto}]N_{tot} * actN - kn2[NFAT_{cyto}](1-actN)$	Flux of Activated NFAT complex formation
$J2 = kn3 * [NFAT_{cyto}]$	Flux of nuclear import of activated NFAT
$J3 = kn4[NFAT_{nuc}](1 - actN) - kn5[NFATpi_{nuc}]N_{tot} * actN)$	Flux of Activated NFAT complex dissociation in the nucleus
$J4 = kn6[NFATpi_{nuc}]$	Flux of nuclear export of phosphorylated NFAT

Model Equations
$[G] = [G_T] - [G_{GTP}] - [PLC^*] - [G_{GDP}]$ - $[\beta\gamma_{int}]$
$[PLC] = [PLC_T] - [PLC^*]$
$[\beta\gamma] = [G_{GTP}] + [PLC^*] + [G_{GDP}]$
$\frac{d[C]}{dt} = v_1 - v_2$
$\frac{d[C_p]}{dt} = \frac{v_2}{conv} - v_{\text{int}}$
$\frac{dR_{int}}{dt} = v_{int} - v_{deg} - v_{rec}$
$\frac{dR}{dt} = -v_1 + conv * v_{rec}$
$\frac{d[G_{GTP}]}{dt} = v_5 + v_6 - v_7 - v_8$
$\frac{d[PLC^*]}{dt} = v_7 - v_9$
$\frac{d[G_{GDP}]}{dt} = v_8 + v_9 - v_{10} - v_{\beta\gamma}$
$\frac{d[\beta\gamma_{\text{int}}]}{dt} = v_{\beta\gamma}$
$\frac{d[IP_3]}{dt} = v_{11} - v_{12}$
$\frac{d[Ca_{cyt}]}{dt} = v_{13} - v_{14} + v_{15}$
$\frac{d[Ca_{ER}]}{dt} = \frac{-v_{13} + v_{14}}{\beta}$
$\frac{d[f_{IP_3R_a}]}{dt} = v_{16} - v_{17}$

$\frac{d[NFATpi_{cyto}]}{dt} = -J1 + J4/C\_cn$
$\frac{d[NFAT_{cyt}]}{dt} = J1 - J2$
$\frac{dNFAT_{nuc}]}{dt} = J2 * C\_cn - J3$
$\frac{dNFATpi_{nuc}]}{dt} = J3 - J4$

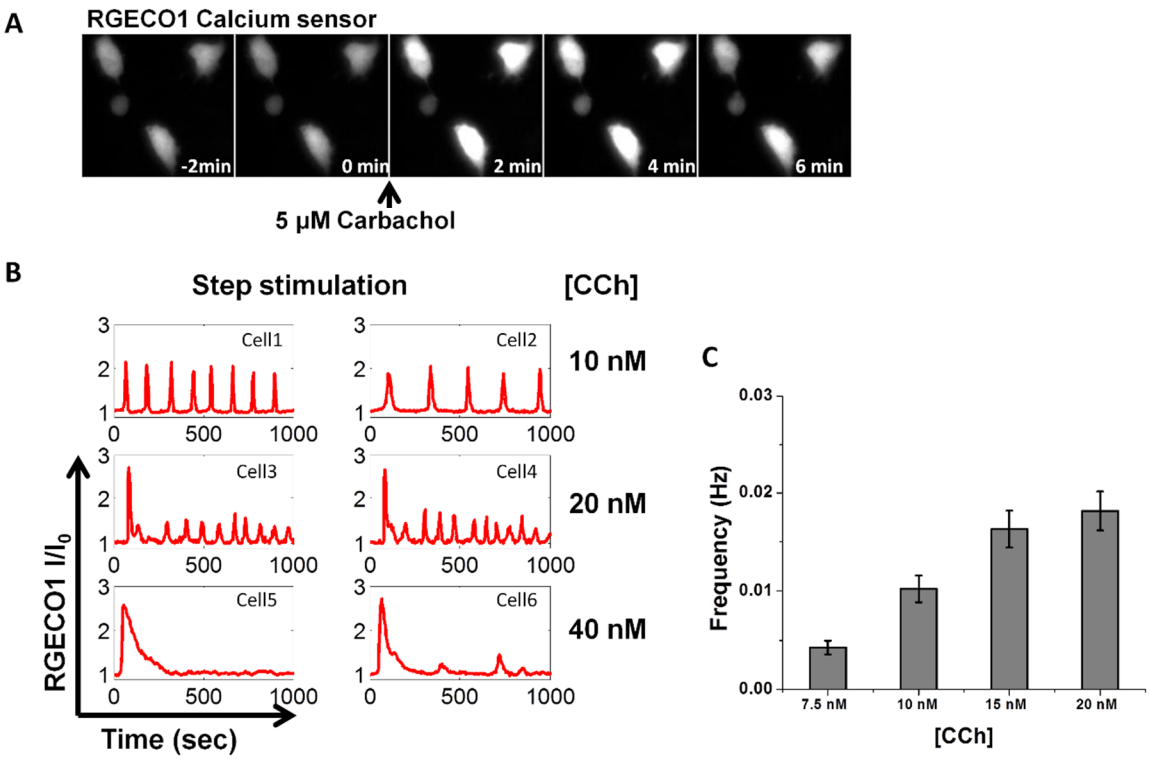

Fig. 2B.1. Quantification of oscillatory calcium responses using RGECO calcium sensor in HEK 293 cells. A. Cells stimulated 5 µM with carbachol show increase in RGECO1 intensity. B. Amidst cell-to-cell variability, ligand stimulation leads to calcium response (oscillatory and/or peak and plateau). C. The frequency of calcium oscillation in cells eliciting oscillatory response is dose dependent. Error bars are +/- S.E.M., n > 20 each case.

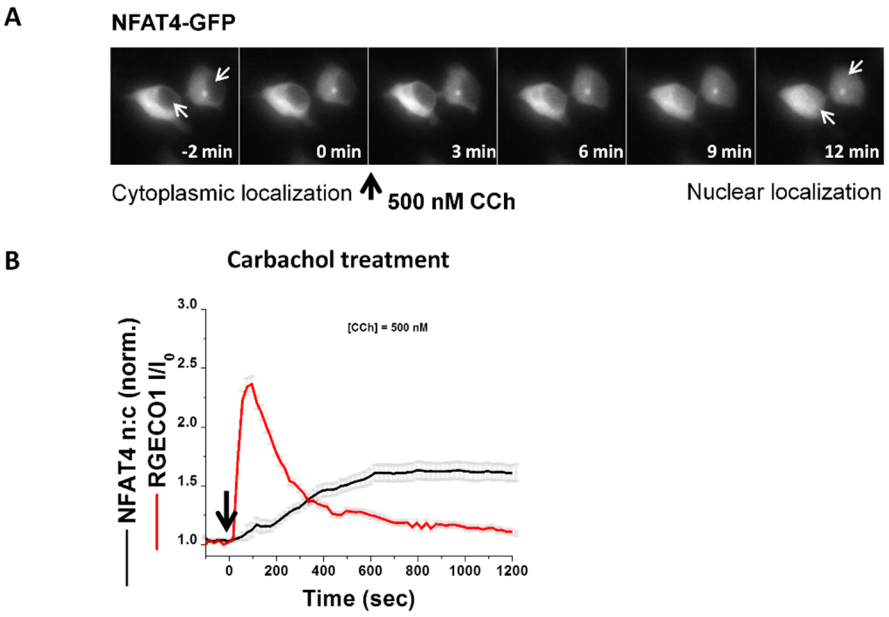

Fig. 2B.2. Carbachol-induced GPCR activation leads to increase in cytoplasmic calcium and subsequently leads to nuclear translocation of NFAT4. A. NFAT4 is primarily localized in the cytoplasm (arrows pointing to the nuclei show relatively much less NFAT4-GFP intensity before carbachol treatment). Upon treatment with 500 nM carbachol, the nuclear intensity gradually increases, indicating nuclear translocation of cytoplasmic NFAT4-GFP. B. Time-resolved dynamics of cytoplasmic calcium and NFAT translocation upon carbachol treatment. Error bars are +/- S.E.M., n>20.

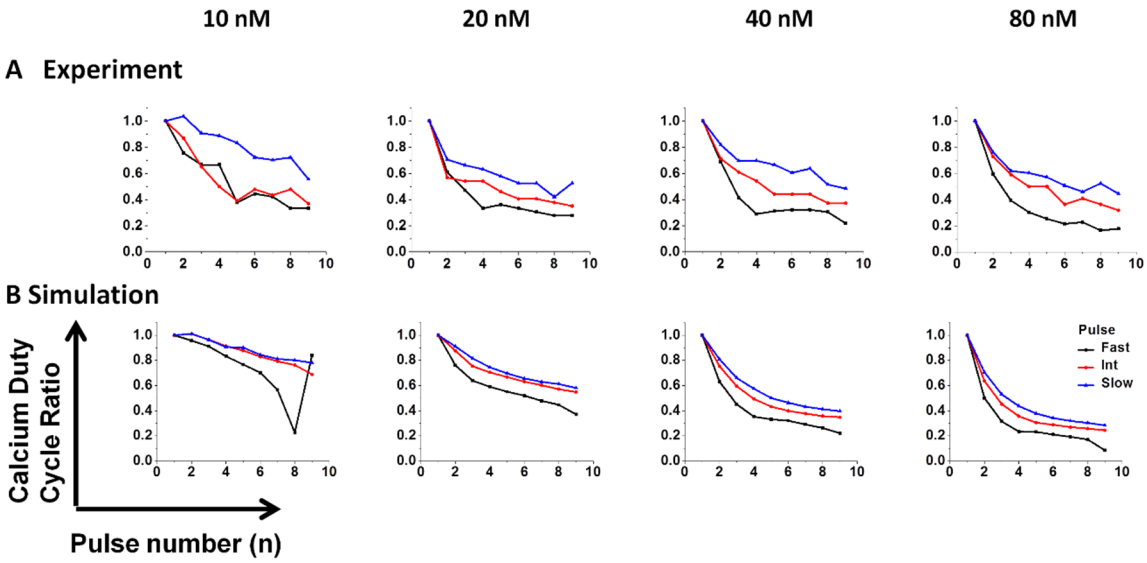

Fig. 2B.3. Calcium Duty Cycle Ratio decays over time upon pulsatile ligand stimulation. A. The calcium duty cycle ratio for the population-averaged calcium response decays faster for fast pulse and vice versa (top panel) indicating frequency modulation. Higher concentrations (left to right: 10 nM, 20 nM, 40 nM and 80 nM respectively) lead to greater extent of decay indicating amplitude modulation. B. Our mathematical model captures both the frequency and amplitude modulation features as observed experimentally.

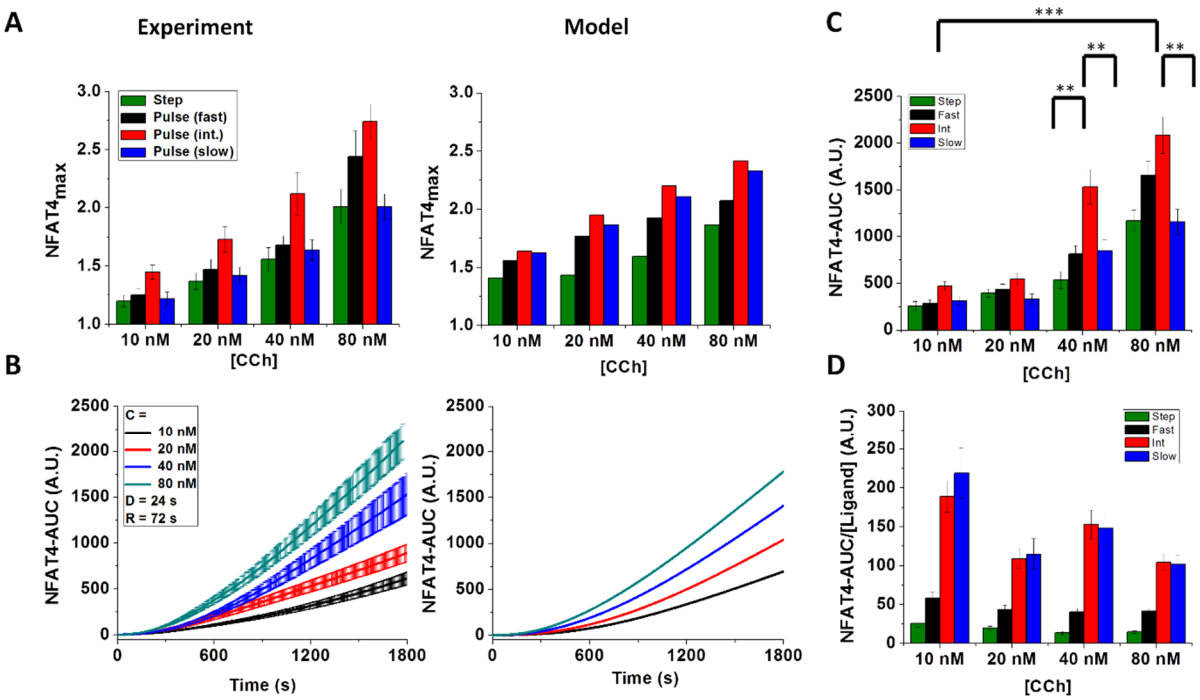

Fig. 2B.4. Nuclear translocation of NFAT4 depends upon pulse frequency as well as amplitude (concentration) of the ligand. A. $NFAT4_{max}$ response is greater for intermediate pulse when compared to slow pulse or fast pulse or step change (left). Our mathematical model captures similar trend as observed experimentally (right). B. Time-dependent NFAT4-AUC response at different concentrations shows amplitude (concentration) dependence of NFAT4 translocation (left). Mathematical model captures similar trend as observed experimentally (right). C. NFAT4-AUC response is greater for intermediate pulse when compared to either slow pulse or fast pulse, similar to $NFAT4_{max}$ response. D. Total NFAT4 response per unit ligand is greater for lower ligand concentrations with slower pulse stimulations. Error bars are +/- S.E.M., n>20.

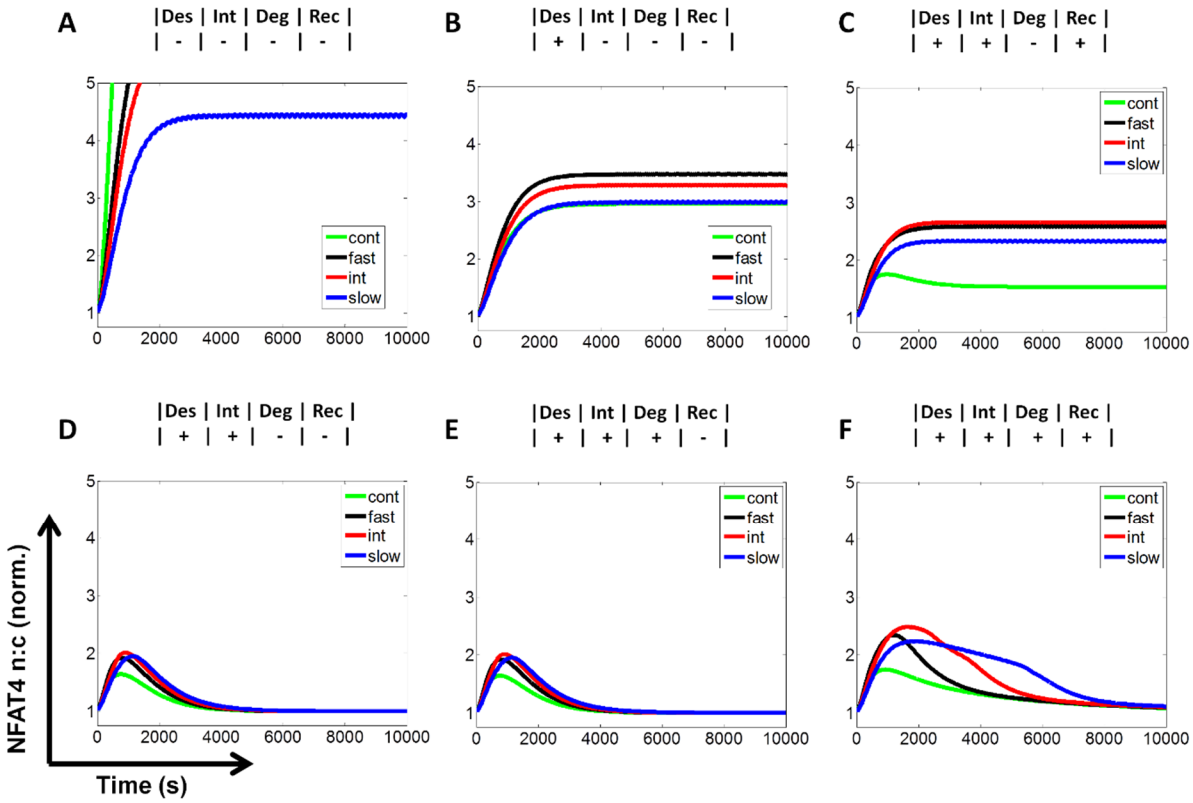

Fig. 2B.5. Analysis of the mathematical model: Turning off receptor regulation modules by setting the corresponding parameter values to zero. A. Turning off desensitization shoots off the calcium response[1] and also the corresponding NFAT response indicating the receptor desensitization is essential for controlled transcription factor activation. B. Receptor phosphorylation but no receptor internalization leads to calcium oscillations *ad infinitum*, and consequently a high pass bound NFAT4 response. C. Complete recycling of internalized receptors without ligand mediated receptor degradation shows similar calcium-NFAT response as in (B). D. – E. Complete internalization of phosphorylated receptors without any recycling doesn't produce band-pass response for different pulse frequencies. F. Ligand-mediated endosomal sorting of receptors towards partial degradation and recycling leads to the band-pass response as we observe in the microfluidic experiments. For all cases of simulations, C = 40 nM, and D = 24 s for pulsed stimulations, R = 24 s (fast), 72 s (int.) and 144s (slow).

Table 2C.1. **Sensitivity analysis of the GPCR-calcium-NFAT model.** PRCC results (positive and negative correlations) for the receptor parameters[$] (top) and NFAT parameters[$] (bottom) show strong correlations of receptor and NFAT kinetics to the band-pass characteristics (+/-: $p<10^{-3}$, ++/--: $p<10^{-6}$, +++/---: $p<10^{-9}$ with positive or negative correlation).

Band-pass feature	kgrk1f	kgrk1r	Kint	kdeg	krec
NFAT_max peak shift	---				++
NFAT_max peak height	---	+++	---	---	+++
Low pass steepness	---	+++	---	---	+++
High pass steepness	---	+++	---	---	+++

Band-pass feature	kn1	kn2	kn3	kn4	kn5	kn6
NFAT_max peak shift	-	--	---	---		--
NFAT_max peak height	---	+++	+++	+++	+++	---
Low pass steepness		+++	+++	+++	+	-
High pass steepness			+++	+++		

[$]***Abbreviations***: kgrk1f: phosphorylation rate constant of the L-R complex; kgrk1r: dephosphorylation rate constant of phosphorylated L-R complex; kint: rate constant for internalization of the phosphorylated L-R complex; kdeg: rate constant for degradation of internalized L-R-p; krec: rate constant for receptor recycling of internalized L-R-p; kn1: rate constant for association of activated calcineurin and $NFAT4_{cyto}$; kn2: rate constant for dissociation of $NFAT4_{cyto}$ from Calcineurin-$NFAT_{cyto}$ complex; kn3: rate constant for nuclear translocation of activated NFAT; kn4: rate constant for dissociation of activated nuclear NFAT; kn5: rate constant for association of nuclear NFAT and Calcineurin ; kn6: rate constant for back-translocation of nuclear NFAT.

Appendix 3. Supplementary to Chapter 3

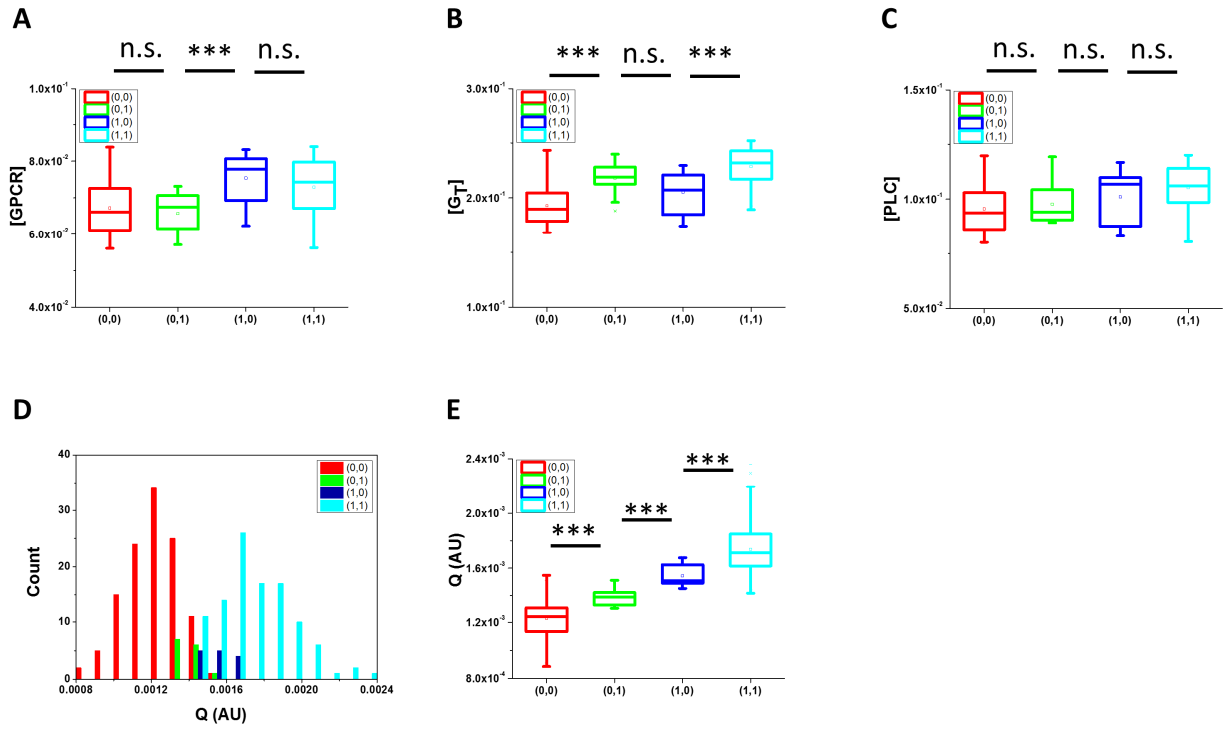

Fig. 3A.1. Distribution of the initial value of the signaling components in the deterministic model that distinguish the four responses in a two-pulse test. A - C. Box plots showing distribution of individual components in the GPCR model: total receptor [GPCR], total G-protein [G_T] and total PLC [PLC]. The individual components may not be able to discern the four outcomes. D - E. A cumulative distribution of components, defined by Q (Q = *[GPCR]*[G]*[PLC]*) is able to discern the four outcomes. Data-set and statistical test method remain the same as above. Data information: In (A-E), data are presented as box plot for n = 750 in silico single cell time traces. ***: $p < 0.001$; n.s.: not significant, $p > 0.05$ (Student's t-test).

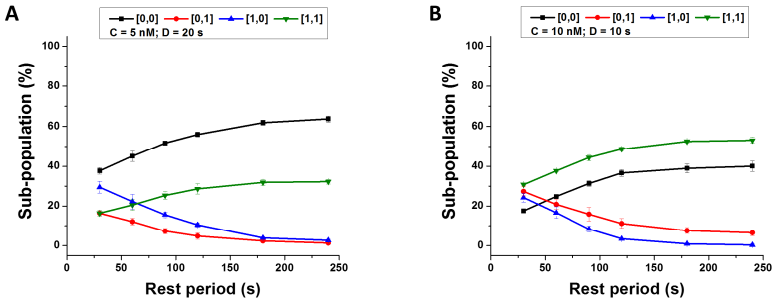

Fig. 3A.2. Effect of rest period on subpopulation composition in a 2-pulse *in silico* experiment with GPCR-calcium model. Two sets of stimulation parameters were tested *in silico*: A. C = 5 nM, D = 20 s and B. C = 10 nM, D = 10 s. The model suggests that the (0,0) and (1,1) sub-populations gradually increase with increasing R, while the (0,1) and (1,0) sub-populations decrease with increasing R.

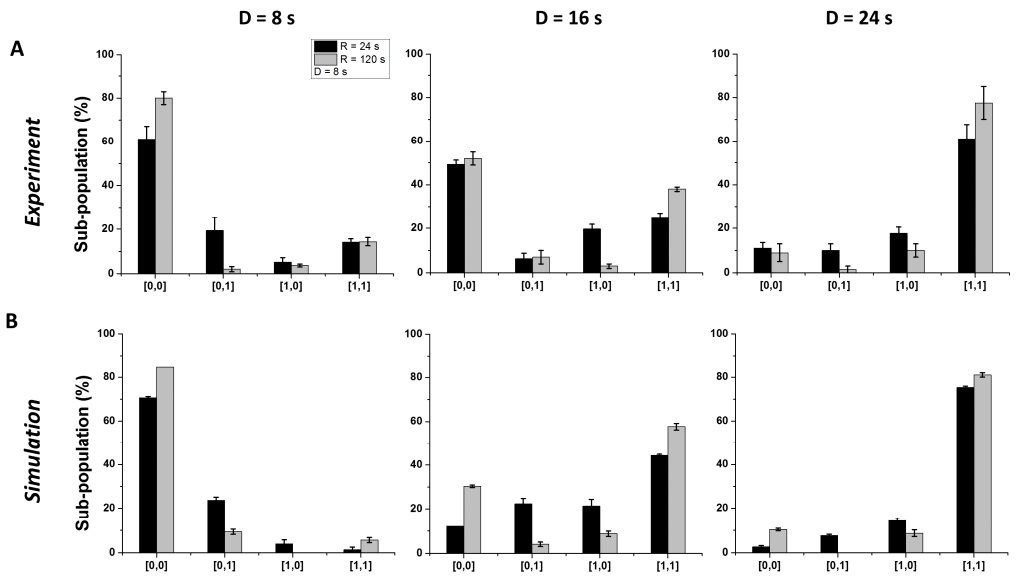

Fig. 3A.3. Rest period test suggests a deterministic framework for apparent stochastic calcium responses. A. Increasing rest period between two consecutive pulsed stimulations results in increase in (0,0) and (1,1) sub-population, while a decrease in (0,1) and (1,0) sub-populations. Three sets of two-pulse microfluidic experiments with ~ 50 cells/set were obtained to calculate the sub-populations. Error bars are standard errors of the mean. B. Simulation data of the above experimental scheme, showing an increase of responding (1,1) cells with increasing D. However, for each D, the sub-populations (0,1) and (1,0) decrease with increasing R. Three sets of two-pulse *in silico* experiments with 250 cells/set were obtained to calculate the sub-populations. Error bars are standard deviations.

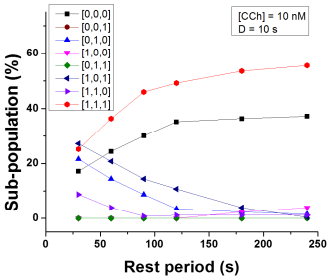

Fig. 3A.4. A three-pulse *in silico* experiment with GPCR-calcium model. For a three-pulse stimulation, there are eight possible outcomes as shown in the graph. Increasing rest period leads to either (0,0,0) response (black squares) or a (1,1,1) response (red circles).

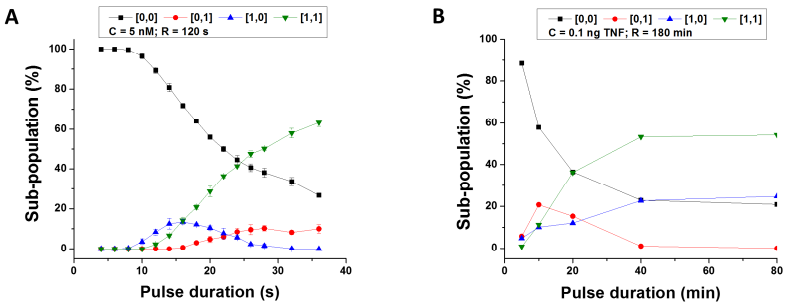

Fig. 3A.5. Effect of pulse duration on subpopulation composition under two-pulse test for GPCR-calcium model. A. In GPCR-calcium model, increasing D increases the (1,1) sub-population (green lower triangles) and decreases the (0,0) sub-population (black squares). The other two responses increase and then decrease with increasing D. C = 5 nM, R = 120 s. Three sets of two-pulse *in silico* experiments with 250 cells/set were obtained to calculate the sub-populations. Error bars are standard deviations. B. Similar trends can be observed in a TNF-α NFκB signaling pathway that acts at an entirely different timescale. TNF input = 0.1 ng, R = 180 min. Data obtained from two-pulse *in silico* experiments with 1000 cells/set to calculate the sub-populations.

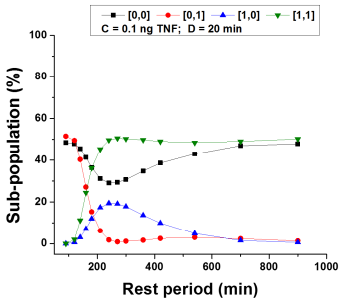

Fig. 3A.6. Effect of rest period on subpopulation composition under two-pulse test for TNFα-NFκB model. C = 0.1 ng/ml, D = 20 min. Similar to our GPCR-calcium model, this model also suggests that the sub-population composition changes with increasing R, and the apparent stochastic responses i.e., (0,1) and (1,0) vanish at sufficiently long rest period.

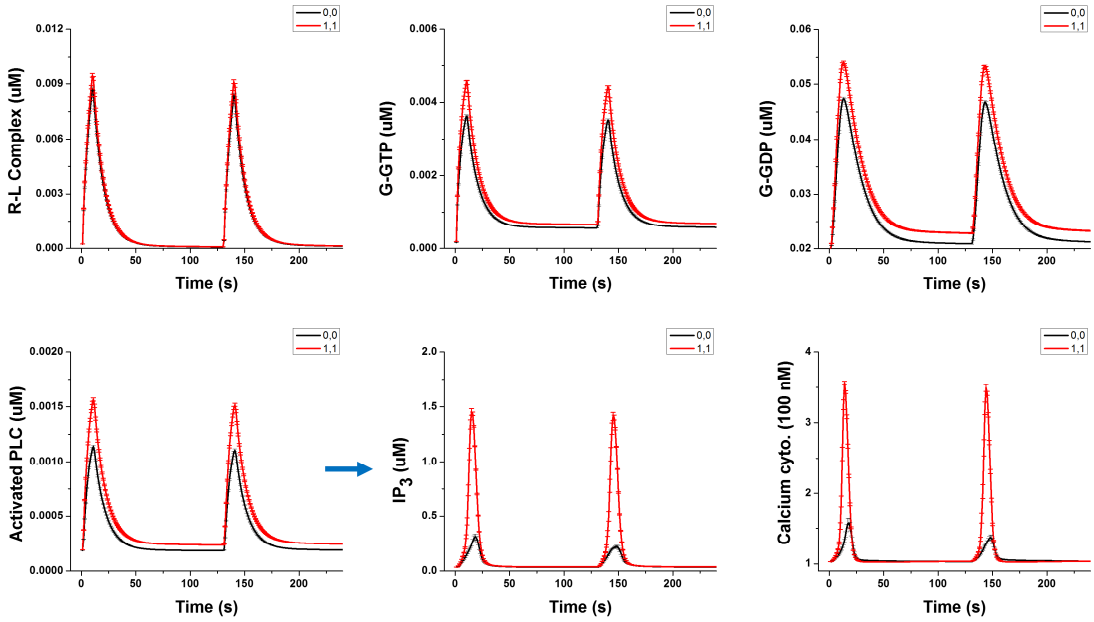

Fig. 3A.7. Component-wise model analysis of the two sub-populations (0,0) vs (1,1) reveal a high hill-coefficient reaction kinetics leads to amplification of the difference. Basal PLC activity brings about the major difference leading to either (0,0) or (1,1) response (a node of high hill coefficient (h ~ 3))

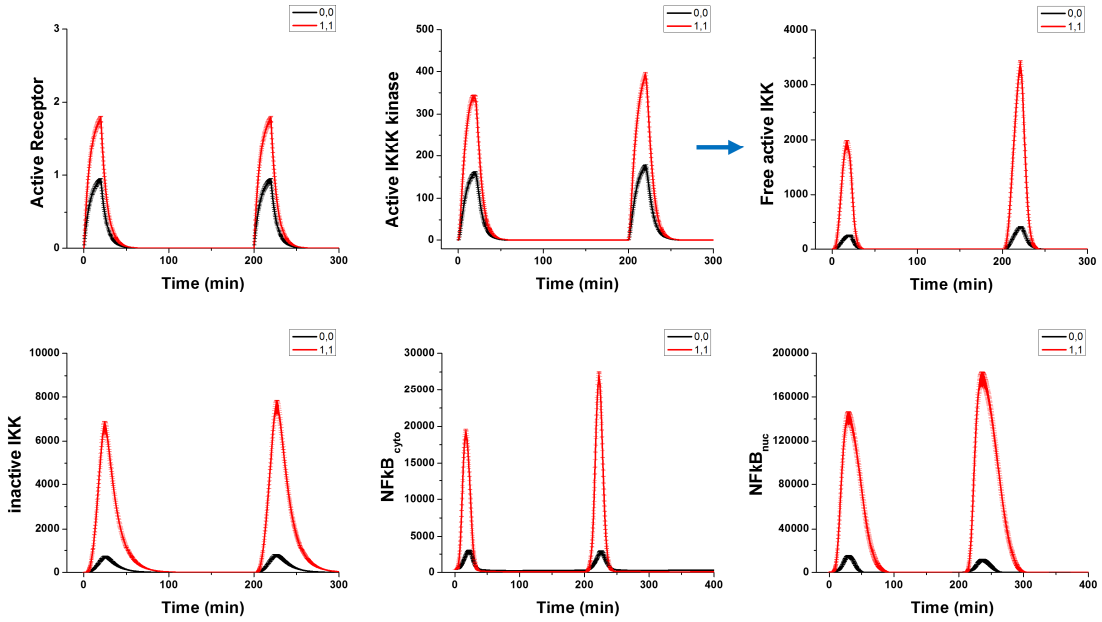

Fig. 3A.8. Component-wise analysis of (0,0) and (1,1) sub-populations in NFkB model. Basal IKK kinase activity brings about the major difference leading to either (0,0) or (1,1) response (also a node of high hill coefficient (h = 2))

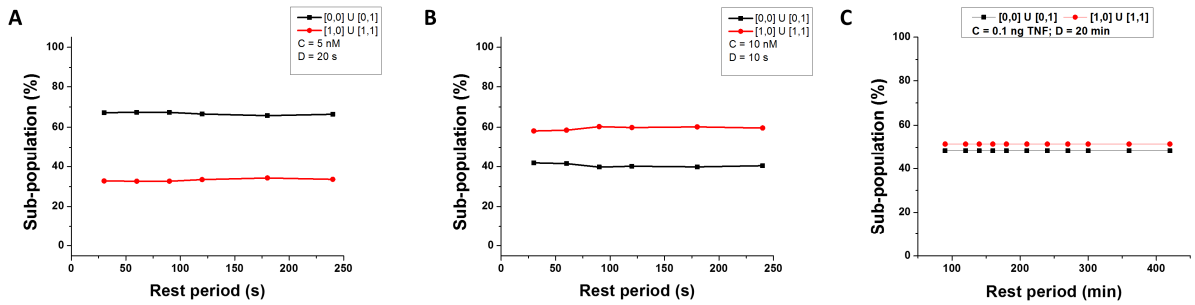

Fig. 3A.9. Deterministic models predict that subpopulation composition changes with rest periods in a two-pulse test. A. The sum of (1,0) and (1,1) subpopulations, as well as the sum of (0,0) and (0,1) subpopulations remain constant for both the models. B. Same plot with a different C,D value. C. Similar conclusions can be drawn for the deterministic NFkB model operating at an entirely different time scale.

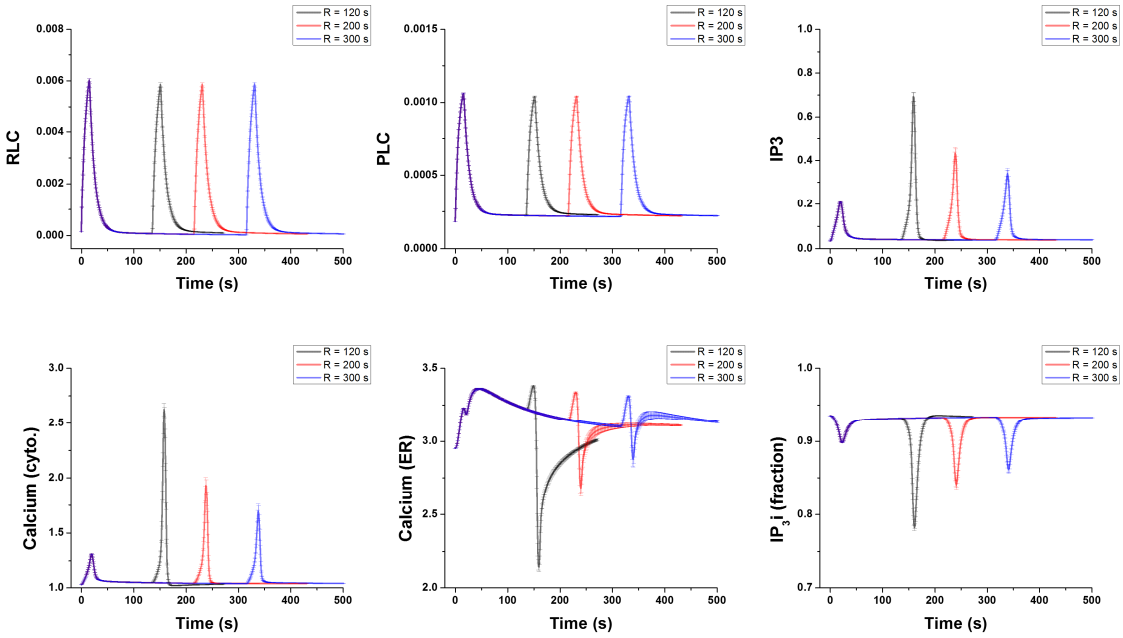

Fig. 3A.10. Component-wise analysis of why (0,1) changes to (0,0) response upon increasing rest periods in GPCR-calcium model. Although a 0 or sub-threshold calcium response occurs for some cells for the first stimulation and the cells appear to be not responding, it does create a short memory of the stimulation in ER calcium reserve which pumps in some extra calcium from extracellular matrix. This calcium gradually leaks out in the context of no response to maintain equilibrium. However, an early second stimulation helps ER reach its threshold to release the calcium and hence respond.

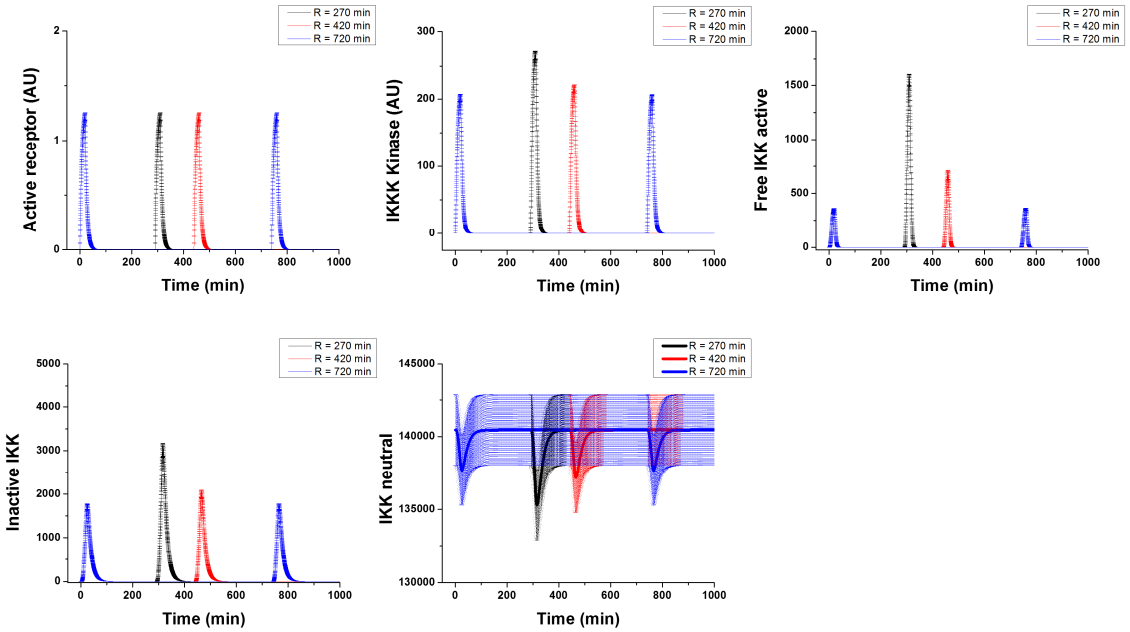

Fig. 3A.11. Component-wise analysis of why (0,1) changes to (0,0) response upon increasing rest periods in TNFα-NFkB model. Although a 0 or sub-threshold NFkB response occurs for some cells for the first stimulation and the cells appear to be not responding, the receptor activation does create a short memory of the stimulation at IKKK kinase level. For shorter R, the active IKKK Kinase level shoots up more than that for a longer R upon second stimulation, which in turn gets amplified via a high Hill coefficient pathway.

Table 3B.1. Sensitivity analysis of TNF- NFkB deterministic model. LHS-PRCC analysis of deterministic model for TNF-NFkB signaling (Tay *et al,* 2010). + and – show positive and negative correlation of the parameter with the peak amplitude. The p-value of correlation is indicated by number of signs, i.e., ++++/----- : $p < 10^{-12}$; +++/---- : $p < 10^{-9}$; ++/--- : $p < 10^{-6}$; ++/--- : $p < 10^{-3}$; n.s.: not significant. Abbreviations remain the same as in the source code provided with Tay *et al*, 2010.

LHS parameter	Sensitivity to 1st	Sensitivity to 2nd
NFkB	----	n.s.
TNFR	++++	++++
IKK	n.s.	n.s.
A20	n.s.	n.s.
k1	++++	++
k2	+++	n.s.
k3	----	----
k4	n.s.	n.s.
Ka	++++	++++
ka20	+	n.s.
KN	++++	++++
KNN	++++	++++
Ki	----	----
c1	----	--
c3	+	+++
c4	---	---
c5	++++	+++
a1	n.s.	n.s.
A20	n.s.	n.s.
a3	++++	+
c1a	++	n.s.
c5a	n.s.	n.s.
c6a	----	n.s.
Kb	++++	+++
Kf	----	---

Text 3C.1. Calculation of order of magnitude for number of ligand molecules interacting with single cells for single pulse stimulation under constant flow and diffusion limited cases

Case 1. Calculation of order of magnitude for ligand exposure during a single pulsed stimulation.
Suppose the ligand concentration is x *M*. Let the cell volume be V m^3. The, total number of molecules in volume V is given by:
# of molecules (static) $= x*N_A*V*1000$
This will be the average number of molecules the cells would be exposed to for a static stimulation.
Now, suppose we have a microfluidic flow of ligand exposure, wherein the fluid flow is v *m/s*. And the average characteristic length for cells is assume l *m*. Then, number of molecules exposed to cells per second is given by:
# of molecules/s $= x*N_A*V*1000*l/v$
If the duration of stimulation is D *s*, then total number of agonist exposed per stimulation is:
# of molecules per stimulation $= D*x*N_A*V*1000*l/v$
Parameters: Average cell-volume of HeLa cells/HEK cells is taken as 2000 um^3.
Therefore, $V = 2000*10^{-18}$. Characteristic length for cells is taken as 20 μm. Hence, $l = 20*10^{-6}$.
Concentrations: $x = 10*10^{-9}$ (for carbachol), $x = 2*10^{-12}$ (for TNF-α). D = 10 s (for carbachol), D = 20 min = 20*60 s. N_A: Avogadro number: ~ 10^{24}. Using the above parameters,
# of molecules per stimulation ~ 10^6 *(for carbachol)*
# of molecules per stimulation ~ 10^5 *(for TNF-α)*
We assume that during a continuous flow stimulation, the role of diffusion may be neglected.

Case 2. Calculation for TNF-α when replenishment is hourly (not continuous), i.e., under diffusion limited condition (Stimulation method in Tay et al, 2010)
Volume of the chamber = 35 nl;
Concentration of TNF- α = 2 pM;
Total # of molecules present in the chamber = $35*2*\ 10^{-21}\ *\ 10^{24} = \sim 10^4$
Diffusion constant for TNF- $\alpha \sim 0.5 – 1.0\ *10^{-6}$ cm^2/s;
Length scale to traverse = 0.3 mm (35nl chamber);
Time scale to traverse diffusively ~ 450 s = 8 min ($t \sim x^2/2D$)
Therefore, a stimulation of ~ 20 min should be sufficient to allow TNF-α molecules in the same order of magnitude to be able to bind to the receptors, which is ~ 10^4.
Note: $V = 35*10^{-12}$ m^3 implies that length scale for the microfluidic chamber can be estimated as ~ $3*10^{-4}$ m = 0.3 mm

Appendix 4. Supplementary to Chapter 4

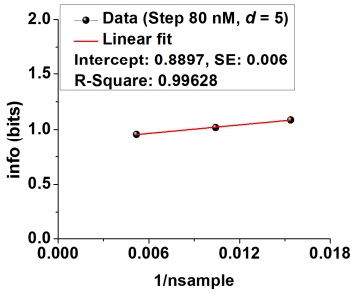

Fig. 4A.1. Information capacity is over-estimated with decreasing sample size. Our method (adapted from Selimkhanov *et al*, 2014) of estimating information using knn search algorithm for multi-point measurements over-estimates the information transfer. A linear extrapolation of the data can provide the estimate of an infinitely large sample size.

Appendix 5. Supplementary to Chapter 5

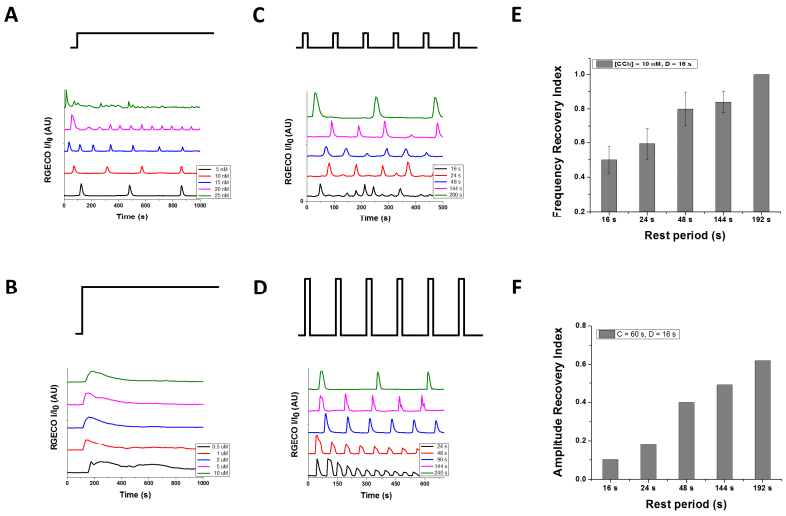

Fig. 5A.1. Pulsatile stimulation leads to phase-locked responses with distinct calcium features in low and high concentration regimes. A. Representative single traces of cytoplasmic calcium from single HEK293 cells stimulated with low concentrations of carbachol (5nm – 25nM) leads primarily to oscillatory response. B. At higher ligand concentrations (50 nM- 10 μM), the response is primarily peak-and-plateau type. C. Pulsatile stimulation in low concentration regime leads to complete recovery of the oscillation amplitude, but may lead to beat skipping. D. Pulsatile stimulation in high concentration regime leads to complete recovery beats, but may lead to amplitude decay. E. The extent of frequency recovery in low concentration regime increases with increase in the rest period between the pulses, as depicted by the increasing frequency recovery index. F. Similarly, the extent of amplitude recovery in high concentration regime increases with increase in the rest period between the pulses, as depicted by the increasing amplitude recovery index.

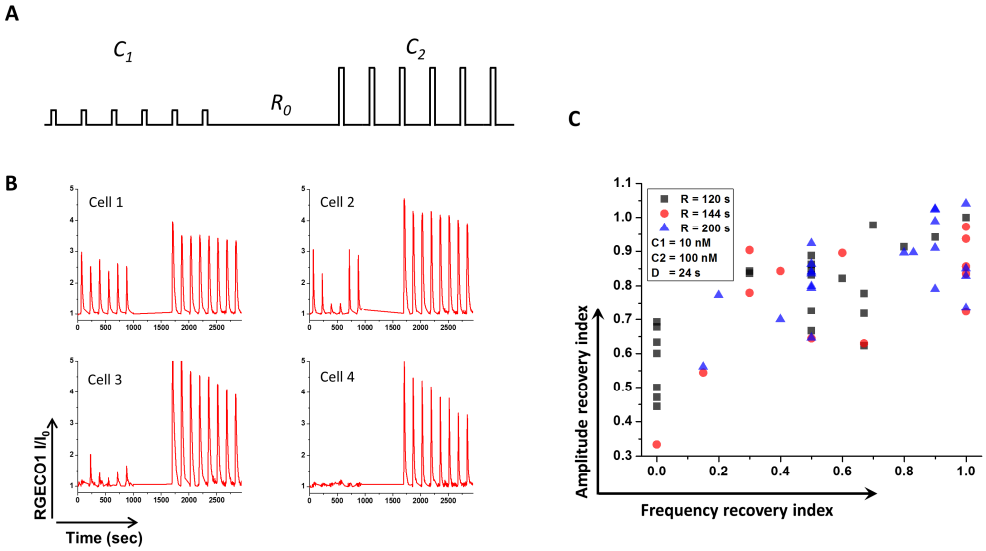

Fig. 5A.2. Two regime pulsed stimulation (TRePS) experiment. A. Microfluidic scheme of two-regime pulsatile stimulation in single cells (TRePS) wherein cells are stimulation by a set of low concentration pulses (C_1) followed by a sufficiently long rest period (R_0) which is followed by a set of high concentration pulses (C_2). B. Representative single cell traces from TRePS experiment shows that cells vary in their extent of frequency and amplitude recovery in the two regimes. C. High PLR in oscillatory regime also leads to high PRR in peak-and-plateau regime and vice versa.

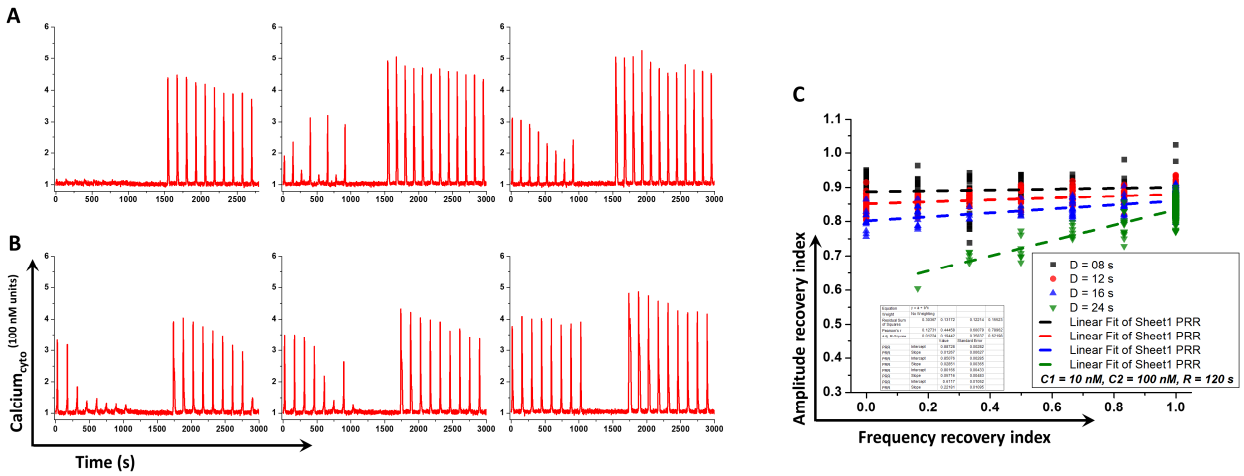

Fig. 5A.3. *In silico* two regime pulsed stimulation (TRePS) experiment. A-B. Representative single cell traces from *in silico* TRePS experiment shows that cells vary in their extent of frequency and amplitude recovery in the two regimes when the initial values of major nodes in the deterministic model sampled from a distribution. Data shown for two different duration 'D' periods: (A) 8s and (B) 24 s. C. Frequency and amplitude recovery indices show a positive correlation in the simulation with increasing D.

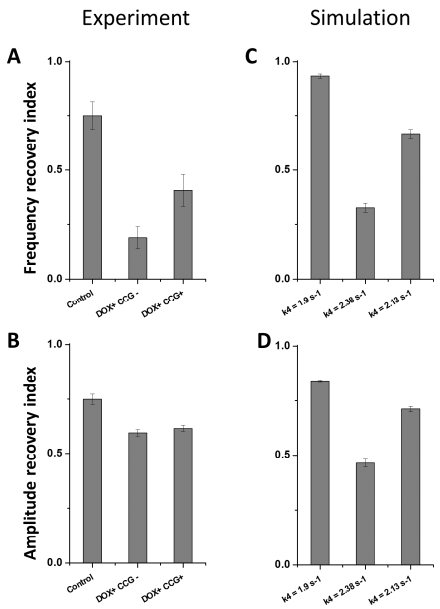

Fig. 5A.4. Population scale comparison of amplitude and frequency recovery indices in experiments and simulation. Both frequency and amplitude recovery indices are affected by RGS4 expression and subsequent CCG-769 drug treatment in experiment as well as in the simulation at population scale.

BIBLIOGRAPHY

Abboud FM, Harwani SC & Chapleau MW (2012) Autonomic neural regulation of the immune system: Implications for hypertension and cardiovascular disease. *Hypertension* **59:** 755–762

Adams J A, Omann GM & Linderman JJ (1998) A mathematical model for ligand/receptor/G-protein dynamics and actin polymerization in human neutrophils. *J. Theor. Biol.* **193:** 543–560

Aladjalova N A (1957) Infra-slow rhythmic oscillations of the steady potential of the cerebral cortex. *Nature* **179:** 957–959

Aldridge BB, Burke JM, Lauffenburger D a & Sorger PK (2006) Physicochemical modelling of cell signalling pathways. *Nat. Cell Biol.* **8:** 1195–203

Alfred J. Lotka (1925) Elements of Physical Biology. *Williams Wilkins Co.***:** 435

Altschuler SJ & Wu LF (2010) Essay Cellular Heterogeneity : Do Differences Make a Difference ? *Cell***:** 559–563

Aramburu J, Yaffe MB, López-Rodríguez C, Cantley LC, Hogan PG & Rao A (1999) Affinity-driven peptide selection of an NFAT inhibitor more selective than cyclosporin A. *Science* **285:** 2129–2133

Armstrong SP, Caunt CJ, Fowkes RC, Tsaneva-Atanasova K & McArdle C A (2009) Pulsatile and sustained gonadotropin-releasing hormone (GnRH) receptor signaling: does the Ca2+/NFAT signaling pathway decode GnRH pulse frequency? *J. Biol. Chem.* **284:** 35746–57

Ashall L, Horton C A, Nelson DE, Paszek P, Harper C V, Sillitoe K, Ryan S, Spiller DG, Unitt JF, Broomhead DS, Kell DB, Rand D a, Sée V & White MRH (2009) Timing and Specificity of NF-kB – Dependent Transcription. *Science.* **324:** 242–246

Aulehla A, Pourquié O, Aulehla A & Pourquie O (2009) Signaling Gradients during Paraxial Mesoderm Development.

Avraham R & Yarden Y (2011) Feedback regulation of EGFR signalling: decision making by early and delayed loops. *Nat. Rev. Mol. cell Biol.* **12:** 104–117

Behar M, Barken D, Werner SL & Hoffmann A (2013) XThe dynamics of signaling as a pharmacological target. *Cell* **155:** 448–461

Bergendahl M, Aloi JA, Iranmanesh A, Mulligan TM, Veldhuis JD, Bergendahl M, Aloi JA, Iranmanesh ALI, Mulligan TM & Veldhuis JD (1998) Fasting Suppresses Pulsatile Luteinizing Hormone (LH) Secretion and Enhances Orderliness of LH Release in Young but Not Older Men, *J. Clin. Endo. Met.* **83:** 1967–1975

Bhalla US & Iyengar R (1999) Emergent Properties of Networks of Biological Signalling Pathways. *Science.* **283:** 381–387

Bhatia SN & Ingber DE (2014) Microfluidic organs-on-chips. *Nat. Biotechnol.* **32:** 760–772

Bhola PD & Simon SM (2009) Determinism and divergence of apoptosis susceptibility in mammalian cells. *J. Cell Sci.* **122:** 4296–4302

Blazer LL, Storaska AJ, Jutkiewicz EM, Turner EM, Calcagno M, Wade SM, Wang Q, Huang X-P, Traynor JR, Husbands SM, Morari M & Neubig RR (2015) Selectivity and Anti-Parkinson's Potential of Thiadiazolidinone RGS4 Inhibitors. *ACS Chem. Neurosci.* **6:** 911–

919
Blower SM & Dowlatabadi H (1994) Sensitivity and uncertainty analysis of complex models of disease transmission: an HIV model, as an example. *Int. Stat. Rev. Int. Stat.* **62:** 229–243
Bodenstein J, Sunahara RK & Neubig RR (2007) N-terminal residues control proteasomal degradation of RGS2, RGS4, and RGS5 in human embryonic kidney 293 cells. *Mol. Pharmacol.* **71:** 1040–1050
Bowsher CGC & Swain PSP (2012) Identifying sources of variation and the flow of information in biochemical networks. *Proc. Natl. Acad. Sci.***109:** E1320–8
Bradley SJ & Challiss RAJ (2012) G protein-coupled receptor signalling in astrocytes in health and disease: A focus on metabotropic glutamate receptors. *Biochem. Pharmacol.* **84:** 249–259
Carcich B & Joseph J (2001) Letters To Nature. **413:** 396–400
Chappell PE, White RS & Mellon PL (2003) Circadian gene expression regulates pulsatile gonadotropin-releasing hormone (GnRH) secretory patterns in the hypothalamic GnRH-secreting GT1-7 cell line. *J. Neurosci.* **23:** 11202–13
Chay T & Lee Y (1995) Appearance of phase-locked Wenckebach-like rhythms, devil's staircase and universality in intracellular calcium spikes in non-excitable cell models. *J. Theor. Biol.***:** 21–44
Cheong R, Paliwal S & Levchenko A (2010) Models at the single cell level. *Wiley Interdiscip. Rev. Syst. Biol. Med.* **2:** 34–48
Cheong R, Rhee A., Wang CJ, Nemenman I & Levchenko a. (2011) Information Transduction Capacity of Noisy Biochemical Signaling Networks. *Science.* **334:** 354–358
Cilfone NA, Kirschner DE & Linderman JJ (2015) Strategies for Efficient Numerical Implementation of Hybrid Multi-scale Agent-Based Models to Describe Biological Systems. *Cell. Mol. Bioeng.* **8:** 119–136
Cohen-Saidon C, Cohen AA, Sigal A, Liron Y & Alon U (2009) Dynamics and Variability of ERK2 Response to EGF in Individual Living Cells. *Mol. Cell* **36:** 885–893
Collin T, Franconville R, Ehrlich BE & Llano I (2009) Activation of metabotropic glutamate receptors induces periodic burst firing and concomitant cytosolic Ca2+ oscillations in cerebellar interneurons. *J. Neurosci.* **29:** 9281–91
Cooling MT, Hunter P & Crampin EJ (2009) Sensitivity of NFAT Cycling to Cytosolic Calcium Concentration : Implications for Hypertrophic Signals in Cardiac Myocytes. *Biophysj* **96:** 2095–2104
Das J, Ho M, Zikherman J, Govern C, Yang M, Weiss A, Chakraborty AK & Roose JP (2009) Digital Signaling and Hysteresis Characterize Ras Activation in Lymphoid Cells. *Cell* **136:** 337–351
David F (2004) It 's a GPCR World. *Mod. Drug Discov.***:** 24–27
Dhumpa R, Truong TM, Wang X, Bertram R & Roper MG (2014) Negative feedback synchronizes islets of langerhans. *Biophys. J.* **106:** 2275–2282
Dhumpa R, Truong TM, Wang X & Roper MG (2015) Measurement of the entrainment window of islets of Langerhans by microfluidic delivery of a chirped glucose waveform. *Integr. Biol.* **7:** 1061–1067
Dolmetsch, Ricardo; Lewis, Richard; Goodnow, Christopher; Healy J (1997) Differential activation of transcriptional factors induced by Ca2+ response amplitude and duration. *Nature* **386:** 855– 858
Dolmetsch RE, Xu K & Lewis RS (1998) Calcium oscillations increase the efficiency and

specificity of gene expression. *Nature* **392:** 933–936
Dowling MR & Charlton SJ (2006) Quantifying the association and dissociation rates of unlabelled antagonists at the muscarinic M3 receptor. *Br. J. Pharmacol.* **148:** 927–937
Dunant Y, Jirounek P, Israël M, Lesbats B & Manaranche R (1974) Sustained oscillations of acetylcholine during nerve stimulation. *Nature* **252:** 485–6
Duncombe TA, Tentori AM & Herr AE (2015) Microfluidics: reframing biological enquiry. *Nat. Rev. Mol. Cell Biol.* **16:** 554–567
Dupont G, Combettes L, Bird GS & Putney JW (2011a) Calcium oscillations. *Cold Spring Harb. Perspect. Biol.* **3:** 1–18
Dupont G, Lokenye EFL & Challiss R A J (2011b) A model for Ca2+ oscillations stimulated by the type 5 metabotropic glutamate receptor: an unusual mechanism based on repetitive, reversible phosphorylation of the receptor. *Biochimie* **93:** 2132–8
Dyachok O, Isakov Y, Sagetorp J & Tengholm A (2006) Oscillations of cyclic AMP in hormone-stimulated insulin-secreting beta-cells. *Nature* **439:** 349–352
Elowitz MB, Levine AJ, Siggia ED & Swain PS (2002) Stochastic gene expression in a single cell. *Science* **297:** 1183–6
Fan H-Y (2003) Protein Kinase C and Mitogen-Activated Protein Kinase Cascade in Mouse Cumulus Cells: Cross Talk and Effect on Meiotic Resumption of Oocyte. *Biol. Reprod.* **70:** 1178–1187
Fisher WG, Yang P-C, Medikonduri RK & Jafri MS (2006) NFAT and NFkappaB activation in T lymphocytes: a model of differential activation of gene expression. *Ann. Biomed. Eng.* **34:** 1712–28
Frank T & Tay S (2015) Automated co-culture system for spatiotemporal analysis of cell-to-cell communication. *Lab Chip* **15:** 2192–2200
Freeman JLR, De La Cruz E, Pollard TD, Lefkowitz RJ & Pitcher JA (1998) Regulation of G protein-coupled receptor kinase 5. *J. Biol. Chem.* **273:** 20653–20657
French A R & Lauffenburger D A (1996) Intracellular receptor/ligand sorting based on endosomal retention components. *Biotechnol. Bioeng.* **51:** 281–97
Fujita K A, Toyoshima Y, Uda S, Ozaki Y, Kubota H & Kuroda S (2010) Decoupling of receptor and downstream signals in the Akt pathway by its low-pass filter characteristics. *Sci. Signal.* **3:** ra56
Futai N, Gu W, Song W & Takayama S (2006) Handheld recirculation system and customized media for microfluidic cell culture. *Lab Chip.* **6:** 149–154
Giri L, Patel AK, Karunarathne WKA, Kalyanaraman V, Venkatesh K V. & Gautam N (2014) A G-protein subunit translocation embedded network motif underlies GPCR regulation of calcium oscillations. *Biophys. J.* **107:** 242–254
Goldberg M, de Pittà M, Volman V, Berry H & Ben-Jacob E (2010) Nonlinear gap junctions enable long-distance propagation of pulsating calcium waves in astrocyte networks. *PLoS Comput. Biol.* **6:** e1000909
Goldbeter A (1996) Biochemical Oscillations and Cellular Rhythms. The Molecular Bases of Periodic and Chaotic Behaviour
Gu W, Zhu X, Futai N, Cho BS & Takayama S (2004) Computerized microfluidic cell culture using elastomeric channels and Braille displays. *Proc. Natl. Acad. Sci. U. S. A.* **101:** 15861–15866
Gubellini P, Saulle E, Centonze D, Costa C, Tropepi D, Bernardi G, Conquet F & Calabresi P (2003) Corticostriatal LTP requires combined mGluR1 and mGluR5 activation.

Neuropharmacology **44:** 8–16
Gurevich E V., Tesmer JJG, Mushegian A & Gurevich V V. (2012) G protein-coupled receptor kinases: More than just kinases and not only for GPCRs. *Pharmacol. Ther.* **133:** 40–69
Hansen AS, Hao N & Shea EKO (2015) High-throughput microfluidics to control and measure signaling dynamics in single yeast cells. *Nat. Protoc.* **10:** 1181–1197
Hao N, Budnik BA, Gunawardena J & O'Shea EK (2013) Tunable Signal Processing Through Modular Control of Transcription Factor Translocation. *Science.* **339:** 460–464
Hartley RVL (1928) Transmission of Information 1. *Bell Syst. Tech. J.* **7:** 535–563
He L, Kniss A, San-Miguel A, Rouse T, Kemp ML & Lu H (2015) An automated programmable platform enabling multiplex dynamic stimuli delivery and cellular response monitoring for high-throughput suspension single-cell signaling studies. *Lab Chip* **15:** 1497–1507
Hersen P, McClean MN, Mahadevan L & Ramanathan S (2008) Signal processing by the HOG MAP kinase pathway. *Proc. Natl. Acad. Sci. U. S. A.* **105:** 7165–7170
Hilioti Z, Sabbagh W, Paliwal S, Bergmann A, Goncalves MD, Bardwell L & Levchenko A (2008) Oscillatory Phosphorylation of Yeast Fus3 MAP Kinase Controls Periodic Gene Expression and Morphogenesis. *Curr. Biol.* **18:** 1700–1706
Hoffmann A, Levchenko A, Scott ML & Baltimore D (2002) The IkappaB-NF-kappaB signaling module: temporal control and selective gene activation. *Science* **298:** 1241–1245
Hsieh M, Thao K & Conti M (2011) Genetic dissection of epidermal growth factor receptor signaling during luteinizing hormone-induced oocyte maturation. *PLoS One* **6:**
Hughey JJ, Gutschow M V., Bajar BT & Covert MW (2014) Single-cell variation leads to population invariance in NF- B signaling dynamics. *Mol. Biol. Cell* **26:** 583–590
Isermann R & Münchhof M (2011) Identification of Dynamic Systems Berlin, Heidelberg: Springer Berlin Heidelberg
Jovic A, Howell B, Cote M, Wade SM, Mehta K, Miyawaki A, Neubig RR, Linderman JJ & Takayama S (2010) Phase-locked signals elucidate circuit architecture of an oscillatory pathway. *PLoS Comput. Biol.* **6:** e1001040
Jovic A, Wade SM, Miyawaki A, Neubig RR, Linderman JJ & Takayama S (2011) Hi-Fi transmission of periodic signals amid cell-to-cell variability. *Mol. Biosyst.* **7:** 2238–44
Jovic A, Wade SM, Neubig RR, Linderman JJ & Takayama S (2013) Microfluidic interrogation and mathematical modeling of multi-regime calcium signaling dynamics. *Integr. Biol. (Camb).* **5:** 932–9
Kar P & Parekh AB (2015) Distinct Spatial Ca^{2+} Signatures Selectively Activate Different NFAT Transcription Factor Isoforms. *Mol. Cell* **58:** 232–243
Kato S, Xu Y, Cho CE, Abbott LF & Bargmann CI (2014) Temporal Responses of C.elegans Chemosensory Neurons Are Preserved in Behavioral Dynamics. *Neuron* **81:** 616–628
Keenan DM, Alexander S, Irvine CHG, Clarke I, Scott C, Turner A, Tilbrook a J, Canny BJ & Veldhuis JD (2004) Reconstruction of in vivo time-evolving neuroendocrine dose-response properties unveils admixed deterministic and stochastic elements. *Proc. Natl. Acad. Sci. U. S. A.* **101:** 6740–5
Kellogg R A & Tay S (2015) Noise Facilitates Transcriptional Control under Dynamic Inputs. *Cell* **160:** 381–392
Kholodenko BN (2006) Cell-signalling dynamics in time and space. *Nat. Rev. Mol. Cell Biol.* **7:** 165–76
Kilinc D, Schwab J, Rampini S, Ikpekha OW, Thampi A, Blasiak A, Li P, Schwamborn R, Kolch W, Matallanas D & Lee GU (2015) A microfluidic dual gradient generator for conducting

cell-based drug combination assays. *Integr. Biol. (Camb).***:** 39–49
Kim TJ, Seong J, Ouyang M, Sun J, Lu S, Jun PH, Wang N & Wang Y (2009) Substrate rigidity regulates Ca2+ oscillation via RhoA pathway in stem cells. *J. Cell. Physiol.* **218:** 285–293
Kotlinska J & Bochenski M (2007) Comparison of the effects of mGluR1 and mGluR5 antagonists on the expression of behavioral sensitization to the locomotor effect of morphine and the morphine withdrawal jumping in mice. *Eur. J. Pharmacol.* **558:** 113–118
Kragl M & Lammert E (2012) Calcineurin/NFATc signaling: role in postnatal β cell development and diabetes mellitus. *Dev. Cell* **23:** 7–8
Kraskov A, Stragbauer H & Grassberger P (2004) Estimating mutual information. *Phys. Rev. E - Stat. Nonlinear, Soft Matter Phys.* **69:** 1–16
Kruse AC, Kobilka BK, Gautam D, Sexton PM, Christopoulos A & Wess J (2014) Muscarinic acetylcholine receptors: novel opportunities for drug development. *Nat. Rev. Drug Discov.* **13:** 549–60
Kupzig S, Walker S A & Cullen PJ (2005) The frequencies of calcium oscillations are optimized for efficient calcium-mediated activation of Ras and the ERK/MAPK cascade. *Proc. Natl. Acad. Sci. U. S. A.* **102:** 7577–82
Ladbury JE & Arold ST (2012) Noise in cellular signaling pathways: Causes and effects. *Trends Biochem. Sci.* **37:** 173–178
Lembong J, Sabass B, Sun B, Rogers ME & Stone HA (2015) Mechanics regulates ATP-stimulated collective calcium response in fibroblast cells. *J. R. Soc. Interface* **12:** 20150140
Levchenko A & Nemenman I (2014) Cellular noise and information transmission. *Curr. Opin. Biotechnol.* **28:** 156–164
Li W, Llopis J, Whitney M, Zlokarnik G & Tsien RY (1998) Cell-permeant caged InsP3 ester shows that Ca2+ spike frequency can optimize gene expression. *Nature* **392:** 936–41
Li Y & Goldbeter A (1992) Pulsatile signaling in intercellular communication. *Biophys. J.* **61:** 161–171
Lim W A., Lee CM & Tang C (2013) Design Principles of Regulatory Networks: Searching for the Molecular Algorithms of the Cell. *Mol. Cell* **49:** 202–212
Linderman JJ (2009) Modeling of G-protein-coupled Receptor Signaling Pathways. *J. Biol. Chem.* **284:** 5427–5431
Linderman JJ & Lauffenburger DA (1988) Analysis of intracellular receptor/ligand sorting in endosomes. *J. Theor. Biol.* **132:** 203–245
Linkenkaer-Hansen K, Nikouline V V, Palva JM & Ilmoniemi RJ (2001) Long-range temporal correlations and scaling behavior in human brain oscillations. *J. Neurosci.* **21:** 1370–1377
Liu H, Rhodes M, Wiest DL & Vignali D a (2000) On the dynamics of TCR:CD3 complex cell surface expression and downmodulation. *Immunity* **13:** 665–675
Lohse MJ & Hoffmann C (2014) Arrestins - Pharmacology and Therapeutic Potential Gurevich V V. (ed) Berlin, Heidelberg: Springer Berlin Heidelberg
Losick R & Desplan C (2008) Stochasticity and cell fate. *Science* **320:** 65–68
Luo J, Busillo J & Benovic J (2008) M3 muscarinic acetylcholine receptor-mediated signaling is regulated by distinct mechanisms. *Mol. Pharmacol.* **74:** 338–347
Mahama P A & Linderman JJ (1994a) A Monte Carlo study of the dynamics of G-protein activation. *Biophys. J.* **67:** 1345–57
Mahama PA & Linderman JJ (1994b) Calcium signaling in individual BC3H1 cells: Speed of calcium mobilization and heterogeneity. *Biotechnol. Prog.* **10:** 45–54
Mannaioni G, Marino MJ, Valenti O, Traynelis SF & Conn PJ (2001) Metabotropic glutamate

receptors 1 and 5 differentially regulate CA1 pyramidal cell function. *J.Neurosci* **21:** 5925–5934

Marino S, Hogue IB, Ray CJ & Kirschner DE (2008) A methodology for performing global uncertainty and sensitivity analysis in systems biology. *J. Theor. Biol.* **254:** 178–196

Marshall CJ (1995) Specificity of receptor tyrosine kinase signaling: Transient versus sustained extracellular signal-regulated kinase activation. *Cell* **80:** 179–185

Massagué J (2012) TGFβ signalling in context. *Nat. Rev. Mol. Cell Biol.* **13:** 616–30

Melin J & Quake SR (2007) Microfluidic Large-Scale Integration : The Evolution of Design Rules for Biological Automation.

Mitchell A, Wei P & Lim WA (2015) Oscillatory stress stimulation uncovers an Achilles' heel of the yeast MAPK signaling network. *Science.* **350:** 1379–1383

Mondragón-Palomino O, Danino T, Selimkhanov J, Tsimring L & Hasty J (2011) Entrainment of a population of synthetic genetic oscillators. *Science* **333:** 1315–1319

Monod J (1949) A Certain Number. *Annu. Rev. M* **3:** 371–394

Mosadegh B, Kuo C-H, Tung Y-C, Torisawa Y-S, Bersano-Begey T, Tavana H & Takayama S (2010) Integrated Elastomeric Components for Autonomous Regulation of Sequential and Oscillatory Flow Switching in Microfluidic Devices. *Nat. Phys.* **6:** 433–437

Neubig RR & Siderovski DP (2002) Regulators of G-Protein Signalling As New Central Nervous System Drug Targets. *Nat. Rev. Drug Discov.* **1:** 187–197

Newman JRS, Ghaemmaghami S, Ihmels J, Breslow DK, Noble M, DeRisi JL & Weissman JS (2006) Single-cell proteomic analysis of S. cerevisiae reveals the architecture of biological noise. *Nature* **441:** 840–846

Ni Q, Ganesan A, Aye-Han N-N, Gao X, Allen MD, Levchenko A & Zhang J (2011) Signaling diversity of PKA achieved via a Ca2+-cAMP-PKA oscillatory circuit. *Nat. Chem. Biol.* **7:** 34–40

Nilsson LM, Sun Z-W, Nilsson J, Nordström I, Chen Y-W, Molkentin JD, Wide-Swensson D, Hellstrand P, Lydrup M-L & Gomez MF (2007) Novel blocker of NFAT activation inhibits IL-6 production in human myometrial arteries and reduces vascular smooth muscle cell proliferation. *Am. J. Physiol. Cell Physiol.* **292:** C1167–C1178

Nobles KN, Xiao K, Ahn S, Shukla AK, Lam CM, Rajagopal S, Strachan RT, Huang T-Y, Bressler E A, Hara MR, Shenoy SK, Gygi SP & Lefkowitz RJ (2011) Distinct Phosphorylation Sites on the {beta}2-Adrenergic Receptor Establish a Barcode That Encodes Differential Functions of {beta}-Arrestin. *Sci. Signal.* **4:** ra51

Nyquist H (1924) Certain Factors Affecting Telegraph Speed 1. *Bell Syst. Tech. J.* **3:** 324–346

Omann GM, Swann WN, Oades ZG, Parkos CA, Jesaitis AJ & Sklar LA (1987) N-formylpeptide-receptor dynamics, cytoskeletal activation, and intracellular calcium response in human neutrophil cytoplasts. *J. Immunol.* **139:** 3447–55

Paliwal S, Wang CJ & Levchenko A (2008) Pulsing cells: how fast is too fast? *HFSP J.* **2:** 251–256

Palmer AE & Tsien RY (2006) Measuring calcium signaling using genetically targetable fluorescent indicators. *Nat. Protoc.* **1:** 1057–1065

Pietraszek M, Gravius A, Schäfer D, Weil T, Trifanova D & Danysz W (2005) mGluR5, but not mGluR1, antagonist modifies MK-801-induced locomotor activity and deficit of prepulse inhibition. *Neuropharmacology* **49:** 73–85

De Pittà M, Goldberg M, Volman V, Berry H & Ben-Jacob E (2009) Glutamate regulation of calcium and IP3 oscillating and pulsating dynamics in astrocytes. *J. Biol. Phys.* **35:** 383–411

Plaçais P-Y, Trannoy S, Isabel G, Aso Y, Siwanowicz I, Belliart-Guérin G, Vernier P, Birman S, Tanimoto H & Preat T (2012) Slow oscillations in two pairs of dopaminergic neurons gate long-term memory formation in Drosophila. *Nat. Neurosci.* **15:** 592–599

Politi A, Gaspers LD, Thomas AP & Höfer T (2006) Models of IP3 and Ca2+ oscillations: frequency encoding and identification of underlying feedbacks. *Biophys. J.* **90:** 3120–33

Prindle A, Selimkhanov J, Li H, Razinkov I, Tsimring LS & Hasty J (2014) Rapid and tunable post-translational coupling of genetic circuits. *Nature* **508:** 387–91

Purvis JE & Lahav G (2013) Encoding and decoding cellular information through signaling dynamics. *Cell* **152:** 945–56

Raser JM (2004) Control of Stochasticity in Eukaryotic Gene Expression. *Science (80-.).* **304:** 1811–1814

Rhee A, Cheong R & Levchenko A (2012) The application of information theory to biochemical signaling systems. *Phys. Biol.* **9:** 045011

Rhee A, Cheong R & Levchenko A (2014) Noise decomposition of intracellular biochemical signaling networks using nonequivalent reporters. *Proc. Natl. Acad. Sci.* **111:** 17330–17335

Robinson JW, Zhang M, Shuhaibar LC, Norris RP, Geerts A, Wunder F, Eppig JJ, Potter LR & Jaffe LA (2012) Luteinizing hormone reduces the activity of the NPR2 guanylyl cyclase in mouse ovarian follicles, contributing to the cyclic GMP decrease that promotes resumption of meiosis in oocytes. *Dev. Biol.* **366:** 308–316

Rodriguez-Diaz R, Dando R, Jacques-Silva MC, Fachado A, Molina J, Abdulreda MH, Ricordi C, Roper SD, Berggren P-O & Caicedo A (2011) Alpha cells secrete acetylcholine as a non-neuronal paracrine signal priming beta cell function in humans. *Nat. Med.* **17:** 888–892

Ruskin DN, Bergstrom D A, Kaneoke Y, Patel BN, Twery MJ & Walters JR (1999) Multisecond oscillations in firing rate in the basal ganglia: robust modulation by dopamine receptor activation and anesthesia. *J. Neurophysiol.* **81:** 2046–2055

Ryu H, Chung M, Dobrzyński M, Fey D, Blum Y, Lee SS, Peter M, Kholodenko BN, Jeon NL & Pertz O (2015) Frequency modulation of ERK activation dynamics rewires cell fate. *Mol. Syst. Biol.* **11:** 838

Saltelli A, Ratto M, Tarantola S & Campolongo F (2005) Sensitivity Analysis for Chemical Models. **14:**

Saltelli A, Tarantola S, Campolongo F & Ratto M (2002) Sensitivity Analysis in Practice Chichester, UK: John Wiley & Sons, Ltd

Santen RJ & Bardin CW (1973) Episodic Luteinizing Hormone Secretion in Man. *J. Clin. Investig. J. Clin. Investig.* **52:** 2617–2628

Schreiber G, Henis YI & Sokolovsky M (1985) Rate constants of agonist binding to muscarinic receptors in rat brain medulla. Evaluation by competition kinetics. *J. Biol. Chem.* **260:** 8795–8802

Scott M, Hwa T & Ingalls B (2007) Deterministic characterization of stochastic genetic circuits. *Proc. Natl. Acad. Sci. U. S. A.* **104:** 7402–7

Selimkhanov J, Taylor B, Yao J, Pilko A, Albeck J, Hoffmann A, Tsimring L & Wollman R (2014) Accurate information transmission through dynamic biochemical signaling networks. *Science* **346:** 1370–3

Sgro AE, Schwab DJ, Noorbakhsh J, Mestler T, Mehta P & Gregor T (2015) From intracellular signaling to population oscillations: bridging size- and time-scales in collective behavior. *Mol. Syst. Biol.* **11:** 779–779

Shankaran H, Wiley HS & Resat H (2007) Receptor downregulation and desensitization enhance

the information processing ability of signalling receptors. *BMC Syst. Biol.* **1:** 48
Shannon CE (1948) A mathematical theory of communication. *Bell Syst. Tech. J.* **27:** 379–423
Shannon CE (1998) Communication In The Presence Of Noise. *Proc. IEEE* **86:** 447–457
Sible JC & Tyson JJ (2007) Mathematical modeling as a tool for investigating cell cycle control networks. *Methods* **41:** 238–47
Siltanen C, Yaghoobi M, Haque A, You J, Lowen J, Soleimani M & Revzin A (2016) Microfluidic fabrication of bioactive microgels for rapid formation and enhanced differentiation of stem cell spheroids. *Acta Biomater.***:** 1–8
Sneppen K, Krishna S & Semsey S (2010) Simplified models of biological networks. *Annu. Rev. Biophys.* **39:** 43–59
Snijder B & Pelkmans L (2011) Origins of regulated cell-to-cell variability. *Nat. Rev. Mol. Cell Biol.* **12:** 119–125
Song S, Li J, Zhu L, Cai L, Xu Q, Ling C, Su Y & Hu Q (2012) Irregular Ca2+ oscillations regulate transcription via cumulative spike duration and spike amplitude. *J. Biol. Chem.* **287:** 40246–40255
Sorre B, Warmflash A, Brivanlou AH & Siggia E (2014) Encoding of temporal signals by the TGF-β Pathway and implications for embryonic patterning. *Dev. Cell* **30:** 334–342
Spencer SL, Cappell SD, Tsai FC, Overton KW, Wang CL & Meyer T (2013) XThe proliferation-quiescence decision is controlled by a bifurcation in CDK2 activity at mitotic exit. *Cell* **155:** 369–383
Spencer SL, Gaudet S, Albeck JG, Burke JM & Sorger PK (2009) Non-genetic origins of cell-to-cell variability in TRAIL-induced apoptosis. *Nature* **459:** 428–32
Sternberg EM (2006) Neural regulation of innate immunity: a coordinated nonspecific host response to pathogens. *Nat. Rev. Immunol.* **6:** 318–328
Storaska AJ, Mei JP, Wu M, Li M, Wade SM, Blazer LL, Sj??gren B, Hopkins CR, Lindsley CW, Lin Z, Babcock JJ, McManus OB & Neubig RR (2013) Reversible inhibitors of regulators of G-protein signaling identified in a high-throughput cell-based calcium signaling assay. *Cell. Signal.* **25:** 2848–2855
Sumit M, Neubig RR, Takayama S & Linderman JJ (2015) Band-pass processing in a GPCR signaling pathway selects for NFAT transcription factor activation. *Integr. Biol.* **7:** 1378–1386
Sun H & Neugebauer V (2011) mGluR1, but not mGluR5, activates feed-forward inhibition in the medial prefrontal cortex to impair decision making. *J. Neurophysiol.* **106:** 960–73
Sykes D A, Dowling MR & Charlton SJ (2009) Exploring the mechanism of agonist efficacy: a relationship between efficacy and agonist dissociation rate at the muscarinic M3 receptor. *Mol. Pharmacol.* **76:** 543–551
Takayama S, Ostuni E, LeDuc P, Naruse K, Ingber DE & Whitesides GM (2003) Selective Chemical Treatment of Cellular Microdomains Using Multiple Laminar Streams. *Chem. Biol.* **10:** 123–130
Tay S, Hughey JJ, Lee TK, Lipniacki T, Quake SR & Covert MW (2010) Single-cell NF-κB dynamics reveal digital activation and analogue information processing. *Nature* **466:** 267–271
Tengholm A & Gylfe E (2009) Oscillatory control of insulin secretion. *Mol. Cell. Endocrinol.* **297:** 58–72
Thomsen WJ & Neubig RR (1989) Rapid kinetics of alpha 2-adrenergic inhibition of adenylate cyclase. Evidence for a distal rate-limiting step. *Biochemistry* **28:** 8778–86

Thurley K, Tovey SC, Moenke G, Prince VL, Meena A, Thomas AP, Skupin A, Taylor CW & Falcke M (2014) Reliable encoding of stimulus intensities within random sequences of intracellular Ca2+ spikes. *Sci. Signal.* **7:** ra59

Toettcher JE, Weiner OD & Lim W A. (2013) Using optogenetics to interrogate the dynamic control of signal transmission by the Ras/Erk module. *Cell* **155:** 1422–1434

Tomida T, Hirose K, Takizawa A, Shibasaki F & Iino M (2003) NFAT functions as a working memory of Ca2+ signals in decoding Ca2+ oscillation. *EMBO J.* **22:** 3825–32

Tomida T, Oda S, Takekawa M, Iino Y & Saito H (2012) The Temporal Pattern of Stimulation Determines the Extent and Duration of MAPK Activation in a *Caenorhabditis elegans* Sensory Neuron. *Sci. Signal.* **5:** ra76–ra76

Tseng P, Weaver WM, Masaeli M, Owsley K & Carlo D Di (2014) Research highlights: microfluidics meets big data. *Lab Chip* **14:** 828–832

Tsimring L, Hasty J, Danino T, Mondrago O, Mondragón-Palomino O, Tsimring L & Hasty J (2010) A synchronized quorum of genetic clocks. *Nature* **463:** 326–330

Turing AM (1952) The Chemical Basis of Morphogenesis. *Philos. Trans. R. Soc. B Biol. Sci.* **237:** 37–72

Turner D A, Paszek P, Woodcock DJ, Nelson DE, Horton C a, Wang Y, Spiller DG, Rand D a, White MRH & Harper C V (2010) Physiological levels of TNFalpha stimulation induce stochastic dynamics of NF-kappaB responses in single living cells. *J. Cell Sci.* **123:** 2834–2843

Ullah M & Wolkenhauer O (2010) Stochastic approaches in systems biology. *Wiley Interdiscip. Rev. Syst. Biol. Med.* **2:** 385–397

Uri Alon (2007) An introduction to systems biology. *Hall/CRC*

Vayttaden SJ, Friedman J, Tran TM, Rich TC, Dessauer CW & Clark RB (2010) Quantitative Modeling of GRK-Mediated b 2AR Regulation. **6:** e1000647

Voliotis M, Perrett RM, McWilliams C, McArdle C a & Bowsher CG (2014) Information transfer by leaky, heterogeneous, protein kinase signaling systems. *Proc. Natl. Acad. Sci. U. S. A.* **111:** E326–33

Volterra V (1926) Variazioni e fluttuazioni del numero d'individui in specie animali conviventi. *Mem. della R. Accad. dei Lincei* **6:** 31–113

Walker JJ, Terry JR, Tsaneva-Atanasova K, Armstrong SP, McArdle C a & Lightman SL (2010) Encoding and decoding mechanisms of pulsatile hormone secretion. *J. Neuroendocrinol.* **22:** 1226–38

Warmflash A, Sorre B, Etoc F, Siggia ED & Brivanlou AH (2014) A method to recapitulate early embryonic spatial patterning in human embryonic stem cells. *Nat. Methods* **11:** 847–54

Warmflash A, Zhang Q, Sorre B, Vonica A, Siggia ED & Brivanlou AH (2012) Dynamics of TGF-β signaling reveal adaptive and pulsatile behaviors reflected in the nuclear localizationof transcription factor Smad4. *Proc. Natl. Acad. Sci. U. S. A.* **109:** E1947–56

Whitesides GM, Ostuni E, Jiang X & Ingber DE (2001) S Oft L Ithography in B Iology. *Annu. Rev. Biomed. Eng.* **3:** 335–73

Woods DC & Johnson AL (2007) Protein kinase C activity mediates LH-induced ErbB/Erk signaling in differentiated hen granulosa cells. *Reproduction* **133:** 733–741

Xu ZP, Song Y, Yang K, Zhou W, Hou LN, Zhu L, Chen HZ & Cui YY (2014) M3 mAChR-mediated IL-8 expression through PKC/NF-??B signaling pathways. *Inflamm. Res.* **63:** 463–473

Yissachar N, Sharar Fischler T, Cohen AA, Reich-Zeliger S, Russ D, Shifrut E, Porat Z &

Friedman N (2013) Dynamic Response Diversity of NFAT Isoforms in Individual Living Cells. *Mol. Cell* **49:** 322–330

Yum K, Hong SG, Healy KE & Lee LP (2014) Physiologically relevant organs on chips. *Biotechnol. J.* **9:** 16–27

Zak DE, Stelling J & Doyle FJ (2005) Sensitivity analysis of oscillatory (bio)chemical systems. *Comput. Chem. Eng.* **29:** 663–673

Zambrano S, Bianchi ME & Agresti A (2014a) High-throughput analysis of NF-κB dynamics in single cells reveals basal nuclear localization of NF-κB and spontaneous activation of oscillations. *PLoS One* **9:**

Zambrano S, Bianchi ME & Agresti A (2014b) A simple model of NF-kappaB dynamics reproduces experimental observations. *J. Theor. Biol.* **347:** 44–53

Zambrano S, De Toma I, Piffer A, Bianchi ME & Agresti A (2016) NF-κB oscillations translate into functionally related patterns of gene expression. *Elife* **5:** e09100

Zhang B, Shan H, Li D, Li ZR, Zhu KS, Jiang ZB & Huang MS (2012) Different methods of detaching adherent cells significantly affect the detection of TRAIL receptors. *Tumori* **98:** 800–803

Zhang X, Grimley A, Bertram R & Roper MG (2010) Microfluidic System for Generation of Sinusoidal Glucose Waveforms for Entrainment of Islets of Langerhans. *Anal. Chem.* **82:** 6704–6711

Zhang X, Stevens RC & Xu F (2015) The importance of ligands for G protein-coupled receptor stability. *Trends Biochem. Sci.* **40:** 79–87